

A PASSIVE SUSPENSION SYSTEM FOR A HYDROFOIL SUPPORTED CATAMARAN

by

Markus Köpke

*Thesis presented at the University of Stellenbosch
in partial fulfilment of the requirements for the
degree of*

Master of Science in Mechanical Engineering



Department of Mechanical and Mechatronic Engineering
University of Stellenbosch
Private Bag X1, 7602, Matieland, South Africa

Supervisors:

Prof Johannes L. van Niekerk
Dr Günther Migeotte

March 2008

DECLARATION

By submitting this thesis electronically, I declare that the entirety of the work contained therein is my own, original work, that I am the owner of the copyright thereof (unless to the extent explicitly otherwise stated) and that I have not previously in its entirety or in part submitted it for obtaining any qualification.

Signature:

MW Köpke

Date:



ABSTRACT

A Passive Suspension System for a Hydrofoil Supported Catamaran

M.W. Köpke

*Department of Mechanical and Mechatronic Engineering
University of Stellenbosch
Private Bag X1, 7602, Matieland, South Africa*

Thesis: MScEng (Mech)
March 2008

This study investigates practical passive methods to improve the seakeeping of a Hydrofoil Supported Catamaran (Hysucat). The Hysucat is a hybrid vessel combining hydrofoil efficiency with the stability of catamarans.

The seakeeping of the Hysucat was initially investigated experimentally to determine what seakeeping improvements are inherent to the Hysucat design. The results showed that the seakeeping is improved by 5-30%.

A passive suspension system for the main hydrofoil of the Hysucat was designed and tested. A concept development strategy was followed for the design of the suspension system as such a system had never been investigated previously. Detailed specifications for the design were developed and concepts that could satisfy the customer and engineering requirements were generated.

Numerical simulation models for the Hysucat and the final concepts were derived assuming a simplified 2nd order system to describe the seakeeping dynamics of the demi-hulls. Unknown parameters were determined using parameter estimation techniques. Representative parameter values were calculated from multiple towing tank experiments. Theory describing the motion of a hydrofoil in an orbital velocity wave field was combined with the hull model to simulate the Hysucat as well as the suspension system concepts.

The models indicated that the concept where the main hydrofoil was attached to a spring loaded arm, that was free to pivot in response to orbital waves, was the most feasible in damping out vertical transmitted accelerations. Experimental tests indicated that little improvement was achieved with the suspension system at low frequencies. At resonance the suspension system was effective in decreasing the heave of the vessel by up to 27%. The pitch and acceleration response results showed improvements at the higher encounter frequencies of up to 50%. The calm water resistance of the vessel increased by 10% over the Hysucat with rigidly attached hydrofoils; however was still 24% less than the hull without foils.

UITTREKSEL

'n Passiewe Suspensie Stelsel vir 'n Watervleuel Gesteunde Tweerompskuit

(" A Passive Suspension System for a Hydrofoil Supported Catamaran")

M.W Köpke

*Departement Meganiese en Megatroniese Ingenieurswese
Universiteit van Stellenbosch
Privaatsak X1, 7602, Matieland, Suid Afrika*

Tesis: MScIng (Meg)

Maart 2008

Hierdie studie ondersoek praktiese, passiewe metodes om die seehouvermoë van 'n watervleuel gesteunde tweerompskuit (Hysucat) te verbeter. Die Hysucat is 'n hibriede vaartuig wat die effektiwiteit van 'n watervleuel en die stabiliteit van 'n tweerompskuit saamvoeg.

Die seehouvermoë van die Hysucat was oorspronklik deur eksperimente ondersoek om te bepaal watter seehouvermoë verbetering is ingebou in die Hysucat ontwerp. Die uitslae toon dat die seehouvermoë verbeter is deur 5-30%.

'n Passiewe suspensie stelsel vir die hoof watervleuel van die Hysucat was ontwerp en getoets. 'n Konsep ontwikkeling strategie is gevolg vir die ontwerp van die suspensie stelsel want so 'n stelsel was nog nooit vroeër ondersoek nie. Breedvoerige spesifikasies vir die ontwerp is ontwikkel en konsepte wat die kliënt en konstruktuering vereistes kon bevredig was ontwikkel.

Numeriese modelle vir die Hysucat en die finale konsepte was ontwikkel deur 'n tweede orde stelsel aan te neem om die seehouvermoë dinamika van die twee rompe te beskryf. Onbekende parameters was bepaal deur die gebruik van parameter beraaming tegnieke. Verteenwoordige parameter waardes is bereken deur menige sleeptenk eksperimente. Teorie wat die beweging van 'n watervleuel in 'n snelheid golf veld beskryf was gekombineer met die romp model om die Hysucat asook die suspensie stelsel konsepte te simuleer.

Die modelleering het aangewys dat die konsep waar die hoof watervleuel geheg was aan 'n veer gelaaide arm, wat vry was om te draai in reaksie tot golwe, was die mees uitvoerbare in die demping van vertikaal oordraagbare versnellings. Eksperimentele toetse het aangewys dat min verbetering bereik was met die suspensie stelsel by lae frekwensies. By weerklank was die suspensie stelsel effektief in die verlaag van die vertikale beweging van die vaartuig met tot 27%. Die heil beweging en versnelling reaksie uitslae het verbetering getoon by die hoër frekwensies van tot 50%. Die kalm water weerstand van die vaartuig het verhoog met 10% oor die Hysucat met vaste watervleuels; maar was steeds 24% laer as die romp sonder watervleuels.

ACKNOWLEDGEMENTS

I would like thank the following people and organisations who have contributed to making this work possible:

Prof JL van Niekerk for his excellent leadership and guidance and providing the necessary support throughout the project duration.

Dr Günther Migeotte for insight on technical matters and analysis with marine engineering problems that were encountered.

Cobus Zietsmann, Ferdi Zietsman and the workshop staff who manufactured the parts and were willing to make changes on short notice.

The two towing trolley drivers, Peter Gordon and Christian Swart, for the endless hours that were spent in the towing tank, often in unbearable summer temperatures.

Finally, the Mechanical and Mechatronic Engineering department at the University of Stellenbosch for the use of their facilities to conduct the research.



TABLE OF CONTENTS

LIST OF FIGURES VI

LIST OF TABLES VIII

NOMENCLATURE IX

CHAPTER 1: INTRODUCTION 1

 1.1 Motivation and Background Information 1

 1.2 Objectives 2

 1.3 Structure of Thesis 2

CHAPTER 2: LITERATURE REVIEW 3

 2.1 Hydrofoils and Hydrofoil Craft 3

 2.2 Ship Hydrodynamic Theory 7

 2.2.1 Scaling Laws 7

 2.2.2 Planing Craft 8

 2.3 Seakeeping 9

 2.3.1 Waves and Seaways 9

 2.4 Human Comfort and Acceleration Exposure 12

 2.5 Passive Methods to Improve Seakeeping 13

 2.6 Vessel Modelling 15

 2.7 Conclusion 16

CHAPTER 3: SPECIFICATIONS AND CONCEPT GENERATION 18

 3.1 Identify Needs 18

 3.2 Plan for the Design Process 18

 3.3 Determine Customer Requirements and Engineering Specifications 18

 3.3.1 Customers and Customer Requirements 20

 3.3.2 Engineering Specifications 20

 3.3.3 Competition Evaluation 23

 3.4 Concept Generation 28

 3.5 Concept Evaluation 28

 3.5.1 Vertical Suspension System 28

 3.5.2 Torsional Suspension System 29

 3.6 Conclusion 30

CHAPTER 4: HYSUCAT SUSPENSION SYSTEM MODELLING 32

 4.1 Demi-hulls 32

 4.1.2 System Identification 34

 4.1.3 System Identification Inputs and Procedure 35

 4.1.4 System Identification Results 36

 4.2 Hysucat Model 40

 4.3 Vertical Suspension System 45

 4.3.1 Calm Water Analysis 46

 4.3.2 Seakeeping Analysis 47

4.4 Torsional Suspension System.....	49
4.4.1 Calm Water Operation	50
4.4.2 Seakeeping Analysis.....	52
4.5 Discussion and Conclusions	55
CHAPTER 5: DESIGN AND EXPERIMENTAL TESTING	57
5.1 Scale Model with Torsional Suspension System	57
5.2 Experimental Validation	58
5.2.1 Towing Setup	60
5.2.2 Wave Generation	61
5.3 Post Processing	62
5.4 Limitations	64
5.5 Experimental Results	64
5.5.1 Suspension System with Different Stiffness Configurations.....	64
5.5.2 Comparison with Hysucat with and without Foils	67
5.6 Full Scale Implementation.....	71
5.6.1 Environmental Conditions	71
5.6.2 Vessel Efficiency	72
5.6.3 Structural Considerations.....	72
5.7 Discussion and Conclusions	73
CHAPTER 6: CONCLUSIONS	76
6.1 Further Work	77
REFERENCES	79
APPENDIX A: HULL AND HYDROFOIL DIMENSIONS AND PARAMETERS.....	84
A.1 Model Hull Dimensions	84
A.2 Calculation of Moment of Inertia and Radius of Gyration	85
A.3 Hydrofoil Dimensions and Parameters	85
APPENDIX B: HYDROFOIL CALCULATIONS	88
B.1 Calm Water Hydrofoil Theory	88
B.2 Hysucat Calm Water Calculation	93
APPENDIX C: SPRING DESIGN	94
APPENDIX D: DATA.....	96
D.1 Atlantic Ocean Data.....	96

LIST OF FIGURES

Figure 1: Typical Hysucacat configuration	5
Figure 2: Lift to drag ratios of the Hysucacat compared to other	7
Figure 3: Hysucacat in wave crest encounter	14
Figure 4: Catamaran coordinate system	15
Figure 5: Quality Functional Deployment diagram	19
Figure 6: ITTC 1978 spectrum	21
Figure 7: Speed wave-height envelope	22
Figure 8: Heave RAO	25
Figure 9: Pitch RAO	26
Figure 10: Acceleration RAO	26
Figure 11: Added resistance RAO	27
Figure 12: Concept 1 - Vertical suspension system.....	28
Figure 13: Concept 2 – Torsional suspension system	29
Figure 14: Planing Hull Force Diagram.....	33
Figure 15: Estimated and experimental response results for heave and pitch	37
Figure 16: Estimated values for k_z , k_θ , b_z and b_θ	37
Figure 17: Estimated values for F_o and M_o	38
Figure 18: Comparison between simulated response and experimental data for demi-hulls.....	39
Figure 19: Hysucacat force diagram.....	40
Figure 20: Hydrofoil in orbital wave motion.....	41
Figure 21: Hysucacat simulation results	44
Figure 22: Concept 1: Vertical suspension system force diagram	45
Figure 23: Spring stiffness for various initial displacements	46
Figure 24: Vertical suspension system simulation results	48
Figure 25: Concept 2: Torsional suspension system	49
Figure 26: Foil lift for varying spring stiffness.....	51
Figure 27: Suspended hydrofoil in orbital velocity field.....	52
Figure 28: Hydrofoil lift for lumped mass model.....	53
Figure 29: Torsion suspension modelling results.....	54
Figure 30: Torsional suspension system for model Hysucacat.....	57
Figure 31: Towing tank and trolley used for testing	59
Figure 32: Scale model – Hys 1	60
Figure 33: Towing setup	61
Figure 34: Wave generator	61
Figure 35: PSD of experimental data	63
Figure 36: Heave RAO.....	65
Figure 37: Pitch RAO	65
Figure 38: Acceleration RAO	66
Figure 39: Added resistance RAO	66
Figure 40: Heave RAO comparison	68
Figure 41: Pitch RAO comparison	68
Figure 42: Acceleration RAO comparison.....	69
Figure 43: Added resistance RAO comparison.....	70

Figure 44: Calm water resistance comparison.....	70
Figure 45: Seakeeping comparison to hull without foils.....	74
Figure 46: Calm water resistance comparison.....	74
Figure A.1: Model dimensions – Hys 1	85
Figure A.2: Hysucat with suspension system model assembly.....	87
Figure C.1: Tension springs.....	94



LIST OF TABLES

Table 1: Acceleration limits	13
Table 2: Hull parameters for model and full scale hull	24
Table 3: Parameter estimation results	38
Table 4: Calculated natural frequencies and damping ratios	40
Table 5: Measurement sensor specifications.....	59
Table A.1: Hull model dimensions	85
Table A.2: Hydrofoil specifications	86
Table B.1: Hysucat calm water analysis	93
Table C.1: Tension spring calculation results	95
Table D.1: Atlantic Ocean seaway data	96



NOMENCLATURE**Constants**

g 9.814 m/s

Roman

A	Added mass matrix
A, B, C, D	State-space matrices
AR	Aspect ratio
B	Damping matrix
B	Beam
b	Damping coefficient
B_a	Chine half beam
c	Foil chord length
C_D	Drag coefficient
C_{Di}	Induced drag friction coefficient
C_{DP}	Skin friction coefficient
C_{DS}	Spray drag coefficient
C_{Dsep}	Separation drag coefficient
C_{DW}	Wave drag coefficient
C_f	Friction coefficient
C_L	Lift coefficient
C_{La}	Lift curve slope
c_w	Wave celerity
D	Hydrofoil drag
D'	Drag parallel to up-flow
d_{tw}	Tunnel width
E	Planform correction factor
F	Force vector
f	Hydrofoil camber
F_b	Damping force
F_c	Froude number based on chord length
F_e	Encounter frequency
F_k	Restoring force
Fn_{∇}	Displacement Froude number
f_n	Spring natural frequency
F_o	Wave excitation force gain
F_p	Planing force
F^v	Excitation force vector due to viscous effects
F_w	Vertical wave excitation force
F^w	Wave excitation force vector
H_s	Average height of the 1/3 highest waves
h	Hydrofoil submergence below the free surface
$h_{1/3}$	Significant wave height
h_b	Bow trim

NOMENCLATURE

h_s	Stern trim
I	Inertia
I_a	Added inertia
j	Counter
\mathbf{K}	Stiffness matrix
K	Lift loss due to pressure relief
k	Stiffness coefficient
k_a	Added mass coefficient
k_w	Wave number
k_ϕ	Lift curve slope correction factor
L	Hydrofoil lift
L'	Lift normal to up-flow
L_{ch}	Chine length
L_{OA}	Overall length
L_w	Waterline length
l_a	Pivot arm length
l_b	Distance from LCG to bow
l_{LCG}	Length from transom to LCG along chine
l_{mf}	Distance from main foil quarter chord to LCG on keel
l_s	Distance from LCG to stern
l_{tf}	Distance from trim foil quarter chord to LCG on keel
l_{VCG}	Distance from keel to vertical centre of gravity
l_{wh}	Distance from LCG to wave height sensor
\mathbf{M}	Mass matrix
m	Mass
M_b	Damping moment
M_k	Restoring moment
M_o	Wave excitation moment gain
M_w	Moment on hull as result of waves
m_a	Added mass
m_p	Empirical correction factor
n_a	Added mass coefficient
P	Depth correction factor
q	Reduced frequency
R_{av}	Added resistance
Rn	Reynolds number
R_T	Total resistance
r_g	Radius of gyration
S	Planform area
T	Temperature
t	Time
T_k	Spring Torque
T_l	Reciprocal of the true average wave frequency
T_o	Modal wave frequency
t_f	Maximum hydrofoil thickness
U	Resultant velocity relative to the hydrofoil
u_o	Hydrofoil velocity

NOMENCLATURE

u_w	Horizontal wave velocity
u_w	Local horizontal wave velocity
V	Velocity vector
V	Vessel velocity
v_w	Local vertical wave velocity
W_h	Hull weight
W_w	Weight of foil and appropriate portion of pivot arm
X, Y, Z	Global Cartesian coordinates
x, y, z	Local Cartesian coordinates

Greek Symbols

α	Hydrofoil angle of attack
α_o	Zero lift angle of attack
β	Hydrofoil inclination angle, deadrise angle
Δ	Weight
Γ	Dihedral angle
ζ	Damping coefficient, wave height
ζ_o	Wave amplitude
η	Load coefficient
θ	Pitch angle
κ	Free surface correction factor
λ	Scale factor, eigenvalue
Λ	Sweep angle
μ	Wave encounter angle
ξ	Hull coordinate
ρ	Density
σ	Prandtl's finite-span biplane factor
τ_h	Calm water trim angle
φ	Up-flow angle, Velocity potential
χ	Pivot arm displacement
ψ	Up-flow angle
Ω	Free surface wave lift loss
ω	Wave circular frequency
ω_d	Damped natural frequency
ω_e	Encounter circular frequency
ω_n	Natural frequency

Other Symbols

∇	Displacement volume
----------	---------------------

Subscripts

f	Hydrofoil
h	Hull
mf	Main hydrofoil

NOMENCLATURE

<i>tf</i>	Trim hydrofoil
<i>vs</i>	Vertical suspension
<i>ts</i>	Torsional suspension

Abbreviations

HSC	High Speed Craft
Hysucat	HYdrofoil SUported CATamaran
IMS	International Maritime Organization
ISO	International Standards Organization
ITTC	International Towing Tank Convention
LCG	Longitudinal Centre of Gravity
LTI	Linear Time Invariant
RAO	Response Amplitude Operator
rms	Root mean square



CHAPTER 1: INTRODUCTION

1.1 Motivation and Background Information

The design for seakeeping is becoming more important as the demand for High Speed Craft (HSC) increases. Traditionally the design of vessels has been limited to calm water with an allowance being made for rough water power requirements. According to Couser (undated), greater attention is being given to the seakeeping of marine craft due to:

- the proliferation of high speed semi-displacement passenger vessels;
- an increasing demand for passenger comfort;
- the deployment of ever increasing sophisticated systems on ever smaller naval vessels;
- greater pressure from regulatory bodies and the public for safer and more comfortable vessels;
- advancements in desktop computing power;
- new developments in analysis and prediction tools;
- increasing demand for higher speeds in rough water, especially for military vessels.

The analysis and modelling of vessel seakeeping is often challenging and requires a large amount of computing power. There have been great advancements in the analysis of traditional displacement hulls; however the analysis of HSC poses more of a challenge as their dynamics are highly non-linear with wave motion. Aspects such as slamming, deck wash and air-water flow are almost impossible to simulate with current models with most boat designers relying on empirical and semi-empirical methods to account for such aspects in their design. Seakeeping analysis is generally limited to the vertical motions (heave, pitch and acceleration) as well as the added resistance of the vessel in waves.

This thesis focuses on improving the seakeeping of a HSC known as the Hysucat. The Hysucat is a hybrid between a planing catamaran and a hydrofoil vessel. Most of the research that has been done on this type of craft has concentrated on resistance, hull optimisation and propulsion. For further details see Hoppe (1989, 1990, 1995, 2001) and Migeotte (2002).

Pienaar and Roos (1991) performed an introductory analysis on the seakeeping of the Hysucat, however they did not attempt to model its seakeeping. Milandri (2006) investigated various active control strategies for the Hysucat in order to improve the seakeeping of the vessel which included a LQR and bang-bang controller using the trim foil as an actuator. A simple linearised state-space model was developed to simulate the control strategies. Model tests were completed and improvements in the seakeeping of the vessel of up to 50% were achieved.

CHAPTER 1: Introduction

Most methods used to improve the seakeeping of HSC, especially hydrofoil craft, are active and require electronic sensors and actuators to control the motion of the vessel. Active methods have to be carefully evaluated to ensure the safety of passengers, crew and the vessel itself. It is thus more difficult to have active controllers certified and they require extensive testing to obtain operational certification. The cost of such active methods also makes them unfeasible for many designs thus it would be useful to investigate passive methods to improve the seakeeping of the Hysucat. Passive methods are much easier to implement thus reducing the cost of the overall design.

This thesis investigates passive methods to improve the seakeeping of the Hysucat as well as modelling strategies used to simulate the vessel dynamics. The model could then be used as an aid for the design of the passive suspension system.

1.2 Objectives

The principle objectives for this study are given below:

1. Develop and validate a numerical simulation model for the Hysucat that includes the dynamics of a passive suspension system in regular waves.
2. Design and manufacture a suspension system for a Hysucat scale model and refine the design using experimental techniques.
3. Determine the effects of the main hydrofoil suspension system on the seakeeping of the vessel by analysing aspects such as the heave, pitch and acceleration Response Amplitude Operators (RAOs).
4. Complete a preliminary analysis on the feasibility of a suspension system for a full scale Hysucat.

1.3 Structure of Thesis

This thesis is divided into 6 chapters. Chapter 2 gives a brief overview of the literature that was studied for the research. Chapter 3 discusses the specifications and concepts that were generated for the design. The two most feasible concepts were modelled in chapter 4 in order to assess and compare the two concepts.

Chapter 5 discusses the experimental methods and equipment that was used to analyse the various hull and Hysucat configurations as well the techniques used to process the experimental data. The feasibility of implementing the system on a full scale Hysucat is also investigated. Chapter 6 concludes with a discussion of the results of the experimental testing and modelling. Recommendations for further research in this field are also given.

CHAPTER 2: LITERATURE REVIEW

This chapter gives an overview of the literature that was studied for this research. Numerous concepts and theory were reviewed and thus the literary study is necessarily broad to cover all the relevant topics.

Topics that are covered include hydrofoils and the development of hydrofoil craft, the Hysucat, which forms the basis for the research, as well as hydrodynamic theory which was fundamental to this thesis. Methods used to analyse the vessel seakeeping and modelling techniques of planing craft are also included in the study.

2.1 Hydrofoils and Hydrofoil Craft

Hydrofoils, like aerofoils, produce lift when moving through a liquid as a result of pressure gradients between the top and the bottom surfaces of the hydrofoil. According to Daskovsky (2000), hydrofoils differ from aerofoils in three important ways:

1. Hydrofoils operate in proximity to a free surface.
2. Hydrofoils operate in a liquid where cavitation can occur if the pressure drops below a critical level.
3. Hydrofoils operate in a different Reynolds number range than aerofoils.

These effects result in a reduction in the lift curve from the idealistic value used in classical aerofoil theory.

Two main types of hydrofoils that are used are fully-submerged and surface piercing hydrofoils. Fully submerged hydrofoils provide good ride quality and speed performance because they are not influenced by the free surface waves however require a control system to maintain the correct submergence below the free surface. (Kim and Yamoto, 2004). Surface piercing foils do not require an active control system as the foils provide automatic control and stability owing to the changing surface area and submergence of the foils below the water surface.

The lift and drag of a hydrofoil profile is described by equations 2.1 and 2.2 respectively.

$$L = \frac{1}{2} \rho u_o^2 S C_L \quad (2.1)$$

$$D = \frac{1}{2} \rho u_o^2 S C_D \quad (2.2)$$

Where:

- L is the foil lift;
- ρ is the fluid density;
- u_o is the hydrofoil velocity;
- S is the planform area;
- D is the drag force;

CHAPTER 2: Literature Review

- C_L the lift coefficient;
- C_D the drag coefficient.

Equation 2.1 and 2.2 from Du Cane (1972) are for a hydrofoil in an ideal, unbounded fluid. C_L is the lift coefficient which varies with angle of attack over a certain operating range depending on the foil profile. According to Du Cane (1972), estimating the lift of a practical hydrofoil is a process of accounting for various influences that reduce the lift curve slope from the ideal value of 2π .

The dynamics of a hydrofoil in a seaway is complicated even when not considering the influence of the hulls on the foil lift and drag. The availability of theoretical equations for a hydrofoil in a seaway is limited. Most of the literature is for motions predicted by time domain programs, the details of which are regarded as proprietary by the authors and their employers (Payne, 1997).

According to Matveev and Duncan (2006), techniques used for modelling hydrofoils in waves include vortex-lattice methods, but the complexity of this technique makes it unsuitable for parametric design. Even if we restrict the model to two degrees of freedom in an idealised orbital velocity wave field, it is still extremely difficult to model due to non-linearities such as the surface effect and foil broaching. Payne (1997) uses a quasi-static approach to model a hydrofoil in an orbital velocity wave field. If we confine the analysis to small angles and high speeds then the lift of the foil can be shown to be:

$$L = \frac{1}{2} \rho u_o^2 S C_{La} \left[\theta_f + \frac{v_w - \dot{z}_f}{u_o} \right] \quad (2.3)$$

Where:

- C_{La} is the lift curve slope;
- θ_f the foil angle of attack;
- v_w the local vertical wave velocity;
- \dot{z}_f the vertical velocity of the hydrofoil.

The quasi-static lift is multiplied with an appropriate lift deficiency function to allow for changes in its induced velocity due to the hydrofoil's wake of vorticity. Payne (1997) uses a Theodorsen function to model the transient effects. The Theodorsen function is given by equation 2.4.

$$\frac{\text{Actual lift}}{\text{Quasi - static lift}} = C(q) = F(q) + iG(q) \quad (2.4)$$

Where:

- $C(q)$ is the Theodorsen function;
- $F(q)$ and $G(q)$ are Bessel functions of the first and second kind of order q ;
- q is the reduced frequency.

CHAPTER 2: Literature Review

More details on hydrofoils operating in an orbital velocity wave field are given in chapter 4 when the modelling of the Hysucacat is discussed.

Hydrofoil craft utilise hydrofoils to partially or fully support the craft weight. According to Matveev and Duncan (2006), hydrofoil craft are characterised by the highest lift to drag ratios of any marine craft.

During the second half of the twentieth century there was a significant upsurge in the development of hydrofoil craft. However they were displaced from a dominant position in the ferry market due to the emergence of simpler and lower maintenance semi-displacement and semi-planing catamarans. A planing vessel is a craft where a significant portion of the lift is created by hydrodynamic forces generated by the vessel's forward velocity.

Hydrofoil craft saw a re-emergence in the 1980's and 1990's with the development of retrofitting existing catamarans with hydrofoils and building new hydrofoil assisted hulls. According to Matveev and Duncan (2006), the development of this type of technology has been limited due to the relatively complicated development process of robust, efficient and inexpensive hydrofoil systems.

The most successful configuration is the Hysucacat that was developed in the late 1980's by Prof. KG Hoppe at the University of Stellenbosch. The Hysucacat forms the focus of this research thesis. A typical layout of the Hysucacat configuration is given in figure 1.

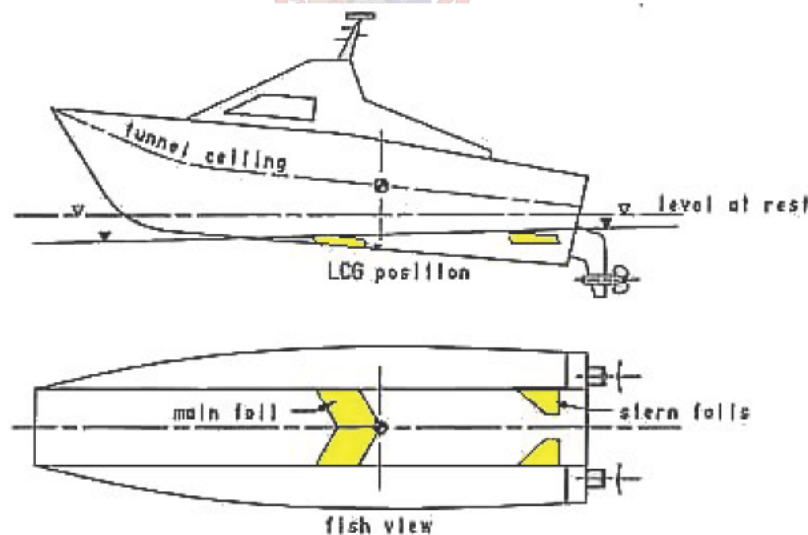


Figure 1: Typical Hysucacat configuration (Hoppe, 1989)

Hysucacat is an acronym for Hydrofoil Supported CATamaran and is a hybrid between a planing catamaran and hydrofoil craft with hydrofoils spanned in the tunnel between the demi-hulls. As the craft's velocity increases the foils create lift, partially lifting the hulls out of the water and thus increasing the overall efficiency of the vessel.

CHAPTER 2: Literature Review

The fixed hydrofoil system, which consists of a main foil slightly forward of the centre of gravity and the two trim foils near the two transoms, provides dynamic trim stabilisation through the hydrofoil surface effect. The foil lift is reduced gradually when the hydrofoil approaches the water surface from beneath at increased speeds. This so-called hydrofoil surface effect prevents the hydrofoil from “popping” out of the water at excessive speeds. The foil runs at a certain submergence depth, in which the lift forces and planing forces combine to balance the total craft weight.

According to Hoppe (1989) and Milandri (2006), Hysucats have the following advantages over planing hulls:

- An increase in vessel speed.
- An increased load carrying capacity.
- Improved seakeeping. The hydrofoils provide damping of the hull vertical motions.
- A reduction in friction and wavemaking due to the hull being partially lifted out of the water.
- Improved fuel efficiency due to the reduction in drag.
- Improved manoeuvring.
- A decrease in crew fatigue.
- Less wake behind the vessel.

The Hysucat was extensively tested using towing tank tests with different hulls and foil configurations. The tests showed that a reduction in drag of up to 50% could be achieved. Figure 2 shows the lift to drag ratios of various types of hulls. The figure indicates the efficiency improvement obtained with the Hysucat configuration over conventional hulls for various Froude numbers. For $Fn_v > 2.5$ hydrofoil craft have superior efficiency over planing and displacement hulls. The Froude number is discussed in section 2.2.1.

Other hydrofoil systems that were developed are the so-called Canard-hydrofoil arrangement that has advantages to Hysucats at the lower Froude numbers (Gerdson *et al*, 1986). In this arrangement, the smaller trim foils are forward of the longitudinal centre of gravity (LCG) and the main foil aft of it.

Migeotte (1997) discusses a hydrofoil system for semi-displacement craft similar to the Canard system described by Gerdson *et al*. (1986) based on the Hysucat principle. The system is generically referred to as the Hysuwac system which is an acronym for Hydrofoil Supported Watercraft. The system has been fitted to numerous ferries.

CHAPTER 2: Literature Review

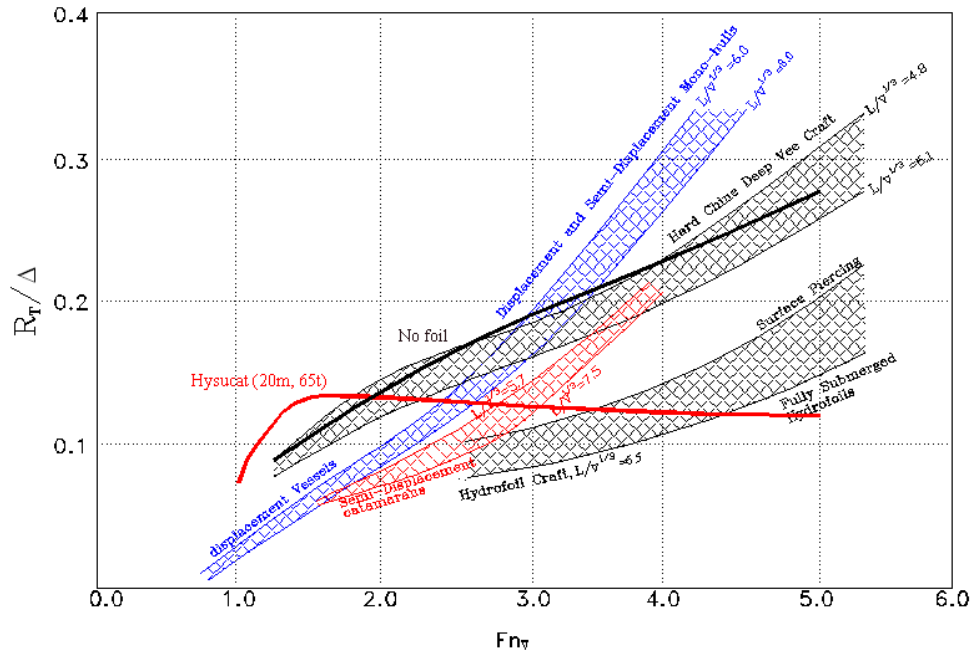
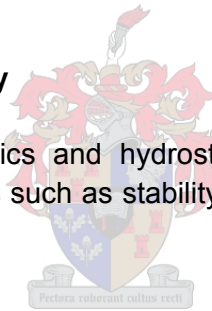


Figure 2: Lift to drag ratios of the Hysucat compared to other HSC (Migeotte, 2002)

2.2 Ship Hydrodynamic Theory

Fundamental ship hydrodynamics and hydrostatics essential to the research was studied. These included aspects such as stability, modelling methods and scaling laws used in model towing tank tests.



2.2.1 Scaling Laws

In scale model tests, dynamic similarity is achieved by maintaining the same Froude number between model and full scale hull. For planing vessels the displacement Froude number is used and is described by equation 2.5.

$$Fn_v = \frac{V}{\sqrt{g \nabla^{1/3}}} \tag{2.5}$$

Where:

- V the vessel velocity;
- g the gravitational acceleration;
- ∇ the vessel displacement volume.

All towing tank experiments are done according to the International Towing Tank Convention (ITTC) guidelines, ITTC – Recommended Procedures, High Speed Marine Vehicles, 7.5-02-05.

CHAPTER 2: Literature Review

2.2.2 Planing Craft

Planing vessels are a type of HSC and are characterised by hull lift due to dynamic forces acting on the hull. The analysis of planing vessels is complex. Savitsky (1964) gives a detailed calm water analysis of planing craft.

Planing craft are characterised by three main operating regions. The characteristics of each region are dependent on the Froude number at which the craft is operating. The three main regions, according to Migeotte (2002), are:

1. **Semi - Displacement:** [$1.5 < Fn_v < 2.5$] In this regime buoyancy forces dominate and theory used to analyse displacement hulls is applicable.
2. **Semi - planing:** [$2.5 < Fn_v < 4$] This area of operation forms a transition between fully displacement and fully planing operation. Buoyancy as well as dynamic forces dominate in this regime.
3. **Full planing:** [$Fn_v > 4$] Buoyancy effects are negligible and any forces acting on the hull are almost completely dynamic planing forces.

Planing hulls differ from displacement hulls in that they have hard chines in order to successfully operate at higher Froude numbers. According to Rosén (2004), for planing hulls to work flow separation needs to occur at the transom and positive dynamic pressures need to occur on the bottom of the hull. Savitsky (2003) gives a good overview of the hull requirements depending on the operating regime defined by the Froude number.

An important aspect of planing hulls is the concept of added mass. It is used in manoeuvring, seakeeping and planing calculations. Added mass theory treats the resistance to acceleration of a body in a fluid as an increase in the mass of the body itself. For a body moving through water Newton's second law of motion is given by equation 2.6.

$$F = \frac{d}{dt} [(m + m_a)V] \quad (2.6)$$

Where:

- F is the resultant force;
- m is the mass of the body;
- m_a is the added mass;
- V is the hull velocity.

The added mass varies with the shape and size of the hull. Payne (1988) gives empirical values for various hull shapes.

According to Milandri (2006), added mass is used to describe the impact type motion of the craft when viewed from a fixed inertial reference frame. This accounts for the added

CHAPTER 2: Literature Review

lift acting on a body when moving through water as well as other forces such as dynamic suction, transom drag and impact of the hull on the water. The dynamic suction, transom drag and water impact were not used in seakeeping calculations in this research and are not discussed any further.

2.3 Seakeeping

The seakeeping analysis of marine vessels has usually been left until late in the design process as naval architects have concentrated on aspects such as resistance and tonnage requirements. However with the development of advanced computing techniques and the increasing demands from passengers for better comfort, the role of seakeeping analysis in the design process has increased. Couser (undated) states that seakeeping analysis is generally a three part process:

1. The estimation of the likely environmental conditions that will be experienced by the vessel.
2. The prediction of the response characteristics of the vessel.
3. The specification of the criteria used to assess the vessel's seakeeping behaviour.

Bertram (2000) gives a good overview of the main computational methods used in seakeeping analysis namely: strip theory, unified theory, high speed strip theory, Green function method and the Rankine singularity method. The methods use potential flow strategies to obtain detail time domain simulations of the hull motions.

Strip methods are the most popular of these methods as they are quick and easily implemented. (Akers, 1999). Two main approaches that have been used in the analysis of planing hulls are 2-D and 2½-D strip methods. The former examines each transverse section independently and then integrates over the hull length on each time step. 2½-D methods, often referred to as High Speed Strip Theory (HSST), are similar to 2-D methods however take into account the effects of the upstream sections.

Zarnick (1978) combined theory to predict resistance, motions in waves and resultant hull pressures of planing craft. The 2-D method involves dividing the hulls into a number of transverse sections and then calculating the hydrodynamic flow for each section using relevant boundary conditions. The concept has successfully been implemented for planing hulls and commercial packages such as Powersea® are available.

2.3.1 Waves and Seaways

It is important that one is able to model waves and seaways accurately when analysing the seakeeping of vessels. Waves are usually generated as regular 'airy' head waves in towing tanks. An excellent description of regular waves is given by Bhattacharyya (1978) and Bertram (1999). According to Bertram (1999) the velocity potential for deepwater waves for the standard coordinate system is described by equation 2.7.

CHAPTER 2: Literature Review

$$\varphi = \text{Re} \left(-i c_w \zeta_o e^{-k_w z} e^{i(\omega t - k_w x)} \right) \quad (2.7)$$

Where:

- φ is the velocity potential;
- c_w the wave celerity;
- ζ_o the wave amplitude;
- ω the wave circular frequency;
- k_w the wave number.

The local wave velocity in the vertical and horizontal directions is given by equation 2.8 and 2.9 respectively.

$$v_w = \frac{\delta\varphi}{\delta x} = \text{Re} \left(-\omega \zeta_o e^{-k_w z} e^{i(\omega t - k_w x)} \right) \quad (2.8)$$

$$u_w = \frac{\delta\varphi}{\delta z} = \text{Re} \left(i \omega \zeta_o e^{-k_w z} e^{i(\omega t - k_w x)} \right) \quad (2.9)$$

Where:

- u_w the local horizontal wave velocity;
- v_w the local vertical wave velocity.

The waves are modelled using their wavelength, amplitude, frequency and celerity. The parameters are combined into a single describing parameter k_w which is given by equation 2.10.

$$k_w = \frac{\omega^2}{g} \quad (2.10)$$

The frequency at which the boat encounters waves will not be the same as the wave frequency observed from an inertial reference frame but differs with vessel speed as well as the encounter angle. This is known as the encounter frequency and is described by equation 2.11.

$$\omega_e = \omega + \frac{\omega^2 V}{g} \cos(\mu) \quad (2.11)$$

Where:

- ω_e is the encounter angular frequency;
- μ is the vessel wave encounter angle.

These formulas are applicable to regular head waves in a towing tank, but do not describe waves encountered on natural open water seaways. Irregular waves are modelled as a combination of regular waves with varying amplitude and frequency.

CHAPTER 2: Literature Review

Michel (1999) gives a detailed explanation of seaway modelling. The variance of wave height with frequency is described by an energy spectrum. Typical energy spectrums that are used are the ISSC, ITTC, Jonswap and Pierson-Moskowitz spectrum. Seaway statistics for global seas used in the sea spectra are given by Söding (2001).

The ITTC spectrum is ideal for fully developed seas and is used in this thesis as it is the most widely used. The ITTC wave spectrum, from Michel (1999), is given by equation 2.12.

$$S(\omega) = 173 H_s^2 T_l^{-4} \omega^{-5} e^{-691(T_l \omega)^4} \quad (2.12)$$

Where:

- H_s is the average height of the 1/3 highest waves.

And

$$T_l = \frac{T_o}{\left(\frac{5}{4}\right)^{1/4} \Gamma\left(\frac{3}{4}\right)} \quad (2.13)$$

Where:

- T_l is the reciprocal of the true average frequency;
- T_o is the modal wave period;
- Γ is the gamma function.

The seakeeping of planing craft, as well as displacement vessels, is analysed using Response Amplitude Operators (RAO) for pitch, heave, roll, acceleration and added resistance. The RAOs are the normalised amplitudes of the four motions non-dimensionalised over the entire operating frequency range. Only heave, pitch, acceleration and added resistance were considered in this research. The RAOs for the above parameters are given by equations 2.14-2.17.

$$RAO_h = \frac{z_h \text{ rms}}{\zeta_{rms}} \quad RAO_p = \frac{\theta_h \text{ rms}}{\zeta_{rms} k_w} \quad (2.14-2.17)$$

$$RAO_a = \frac{\ddot{z}_h \text{ rms}}{\zeta_{rms} g} \quad RAO_{rw} = \frac{R_{aw}}{2 \zeta_{rms}^2 \rho g B^2 / L_w}$$

Where:

- z_h is the heave of the vessel;
- θ_h the vessel pitch;
- \ddot{z}_h is the acceleration in the vertical direction;
- R_{aw} the added resistance in waves;
- ρ the density of water;
- B the chine beam.

CHAPTER 2: Literature Review

The RAOs give an indication of the natural frequency of the craft as well as the damping in the system. RAOs represent a method to compare the seakeeping of various craft over a certain frequency range and are obtained using the methods described in section 2.3 or experimental techniques such as towing tank tests.

2.4 Human Comfort and Acceleration Exposure

The response of humans to accelerations plays a critical role in the design of any marine craft, especially craft designed to carry passengers not accustomed to marine transportation. The limiting values for the safe operation of a vessel have been set by organisations such as the International Maritime Organisation who have defined the HSC code.

The final sets of limiting values are those for vessel passengers and crew. According to Savitsky and Koelbel (1993) there is no point designing a craft to withstand accelerations higher than what the passengers can tolerate. Milandri (2006) reports that the primary human factor reasons to control vessel motions are to reduce the motion sickness of passengers, reduce motion induced interruptions in crew work and reduce the fatigue of passengers due to the constant need to compensate for the vessels motions.

Sea sickness is quantified in a Motion Sickness Incidence (MSI) (Griffin, 1990) which is used to quantify motion sickness and is based on experimental work. According to O'Hanlon and MacCauley (1974), most motion sickness occurs with vertical movement at a frequency of 0.2 Hz. For this study motion sickness is not considered and thus will not be discussed further as the encounter frequency of planing craft is usually above 0.2 Hz and therefore the effect is negligible.

The focus of this research is to improve the heave and pitch motions as well as the transmitted accelerations to the passengers onboard the vessel. Savitsky and Koelbel (1993) give fatigue reduced Proficiency Limits for whole body vibration for vertical and transverse accelerations. These graphs are calculated using the ISO 2631 standard for whole body vibration. Savitsky and Koelbel (1993) give acceleration limiting values that can be used as a design guideline and are presented in table 1.

CHAPTER 2: Literature Review

Table 1: Acceleration limits

Acceleration [g]	Effect on Personnel	Application
0.6	Minor discomfort	Craft for fare paying passengers
1	Maximum for military function over 4 hrs	
1.5	Maximum for military function short duration	
2		Patrol boat crew, average owners
3	Extreme discomfort	Test crew, long races
4		Medium length races
5	physical injury	
6		Military crew under fire

The above values were used to calculate some of the specifications for the design discussed in chapter 3.

2.5 Passive Methods to Improve Seakeeping

Active methods to improve the seakeeping of hydrofoil craft are widely used in industry and are fundamental to the design of any fully supported hydrofoil craft. The use of active control systems is well described in the literature. See Kim and Yamoto (2005) and Du Cane (1972). Milandri (2006) investigated various control strategies to improve the seakeeping of the Hysucat. Reductions of up to 50% in the heave and pitch motions were obtained with a LQR and bang-bang controller.

This thesis investigates passive methods to improve the seakeeping of the Hysucat. The literature available on passive methods to improve the seakeeping of hydrofoil craft is limited. Welnicki (1998 and 1998a) investigated the effect of various hydrofoil configurations and types of foils on the seakeeping characteristics of catamarans. A comparison was made between resistances, accelerations, heave and pitch in irregular head waves with and without fitted foils. Welnicki (1998 and 1998a) investigated the following:

- The position of a single foil between the catamaran hulls in three positions;
- T - foils at the bow of the catamaran;
- Variations in angles of attack of the above foils.

The results showed that the foils should be located at the bow to decrease the resistance of the vessel. Hydrofoils located near the LCG damp out vertical accelerations the best; however are ineffective for pitch motions. The work also showed that the full foil, spanned between the demi-hulls, had better overall motion

CHAPTER 2: Literature Review

reduction than the T- foil at the bow. Reductions of 20-75% of peak accelerations were obtained at the forward point and LCG. Welnicki (1998 and 1998a) also showed that the variation in angle of attack has no real improvement on the seakeeping of the vessel. The added resistance increased for various configurations by 10-19%.

Payne (1997) discusses the development of a passive suspension system for a fully supported catamaran. The system was known as the Dynafoil and damped out vertical accelerations between the fully submerged hydrofoil and the hull. Payne showed with the Dynafoil concept that if the foil support struts are hinged, inclined aft and resiliently supported, so that the hydrofoil can swing about the struts and pivot in response to changes in local water velocity, then vertical accelerations to the hull can be reduced by an order of magnitude. The Dynafoil never went into production and the project was terminated.

Hoppe (1989) reported that with the Hysucat hydrofoil system significant seakeeping improvements over conventional catamarans can be achieved. The foil system gives a strong damping effect of the vertical and pitch motions which results in improved seakeeping in rough water which is non-existent on monohulls or catamarans.

Figure 3, from Hoppe (undated), illustrates the damping effect of the Hysucat. If the Hysucat runs into a wave crest the demi-hulls will be submerged deeper with a larger uplift force which pushes the bow upwards.

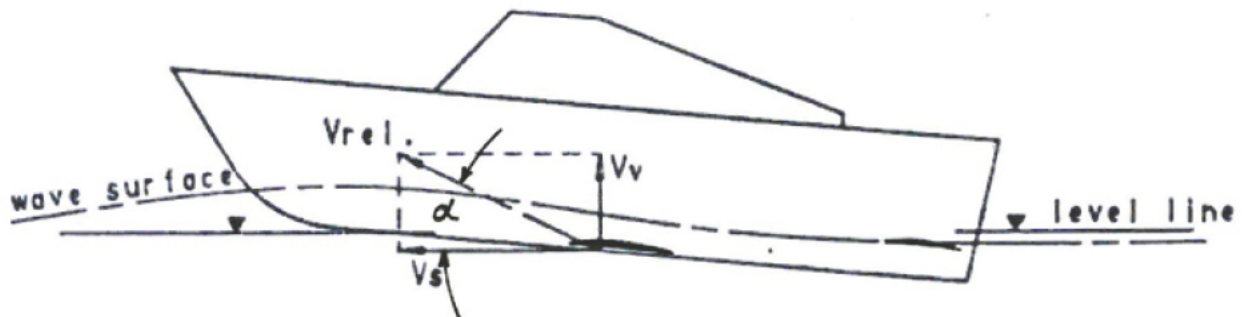


Figure 3: Hysucat in wave crest encounter

According to Hoppe (undated), this creates a change in the relative inflow angle (α) towards the mainfoil with a smaller or even negative attack angle of attack which reduces the foil forces momentarily. The hull forces are increased and the foil forces are reduced when running into waves thus creating less lift improving the ride quality of the vessel. When running through a wave trough similar force variations exist, so that the total wave running behaviour gives a much softer ride. The extreme and hard pitch motions of fast planing craft in rough water are absent on Hysucats.

CHAPTER 2: Literature Review

However no systematic experiments were conducted to investigate this behaviour thus this thesis would be used to investigate the seakeeping improvements of the Hysucat foil system using experimental techniques.

2.6 Vessel Modelling

It is necessary to develop an appropriate model that describes the dynamics of the Hysucat in order to effectively design a suspension system for the craft. The modelling of planing vessels presents more of a challenge than displacement hulls as planing vessel motions are extremely non-linear with wave height as reported by Savitsky and Koelbel (1993). Most literature attempts to linearise the non-linear equations of motion around some operating point.

The most common method used to describe the motion of a vessel is by the simplified 6-dof Euler equations that describe a rigid body. As in aeronautical theory they are divided into longitudinal motions (heave, pitch and surge) and lateral motions (yaw, sway and roll).

In the vertical direction the equations of motion are described by two coupled, second order, differential equations of motion shown by equation 2.18 from Fang *et al.* (1996 and 1997) as defined from the inertial reference coordinate system given in figure 4.

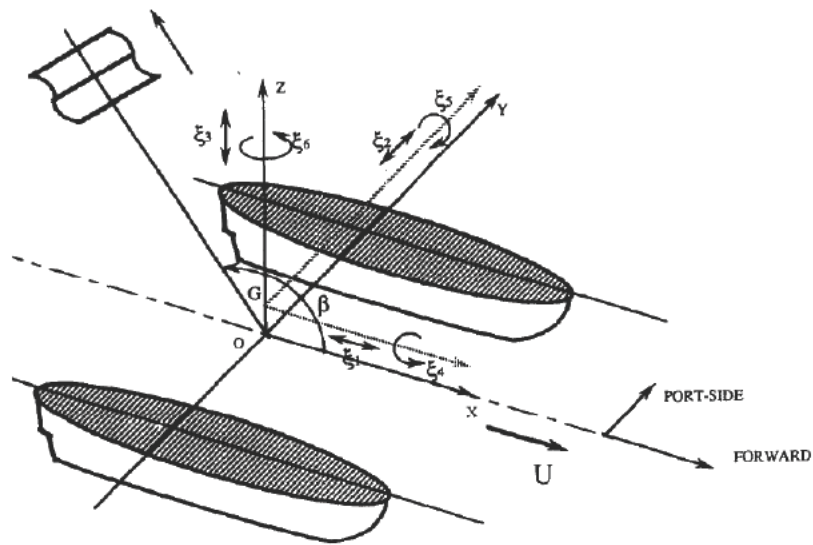


Figure 4: Catamaran coordinate system (Fang, 1996)

$$\sum_{k=1}^6 \left\{ (M_{jk} + A_{jk}) \ddot{\xi}_k + B_{jk} \dot{\xi}_k + K_{jk} \xi_k \right\} = F_j^W + F_j^V \quad j=1,2...6 \quad (2.18)$$

Where:

- *M* is the mass matrix;
- *A* the added mass matrix;

CHAPTER 2: Literature Review

- B the damping coefficient matrix;
- K the restoring coefficient matrix;
- F^w the wave excitation force vector;
- F^v the excitation force due to viscous effects.;
- ξ is the hull coordinate.

The equations of motion for pitch and heave are given by equation 2.19. The viscous effects have been neglected.

$$\begin{bmatrix} (m_{33}+a_{33}) & a_{35} \\ a_{53} & (I_{55}+a_{55}) \end{bmatrix} \begin{bmatrix} \ddot{\xi}_3 \\ \ddot{\xi}_5 \end{bmatrix} + \begin{bmatrix} b_{33} & b_{35} \\ b_{53} & b_{55} \end{bmatrix} \begin{bmatrix} \dot{\xi}_3 \\ \dot{\xi}_5 \end{bmatrix} + \begin{bmatrix} k_{33} & k_{35} \\ k_{53} & k_{55} \end{bmatrix} \begin{bmatrix} \xi_3 \\ \xi_5 \end{bmatrix} = \begin{bmatrix} F_3^w \\ F_5^w \end{bmatrix} \quad (2.19)$$

The above equations do not describe hydrofoil craft. Modelling equations for fully supported hydrofoil craft are described in Kim and Yamoto (2004 and 2004a). The modelling of planing hulls with hydrofoils, according to Matveev and Duncan (2006), is complicated and optimisation of their performance requires complex analysis.

The added effect of the motion of hydrofoils in an orbital velocity field adds to the complexity of the modelling problem. Dyachkov and Makov (2005) developed a method for the calculation of fast displacement catamaran with fin stabilisers which included speed factors, hull interference as well as stabilisation factors. The results achieved represented good comparison to model tests in irregular head waves. The complex equations are described in detail in Dyachkov and Makov (2005). The equations are only valid however for displacement speeds thus for Froude numbers less than 2. The equations were not validated for higher Froude numbers.

Milandri (2006) used system identification and parameter estimation to obtain the model for a Hysucat with rigid foils in waves. Milandri used system identification software that utilised experimental data together with optimisation algorithms to identify unknown parameters of his model. According to Milne (2000), system identification refers to the derivation of mathematical models of dynamic systems from observed data. The foil forces were modelled theoretically and unknown vessel parameters such as damping and stiffness were determined using the optimisation software.

The use of such an experimentally based approach is common and has been widely used in the design of robust controllers and workable models. Haddara and Xu (1999) used a neural network approach combined with a parameter estimation technique to identify a model for the vessel. The non-linearities were modelled using the neural network function. A Markov process theory approach was used to determine the form of the function. The results compared well to experimental data if the system was lightly damped.

2.7 Conclusion

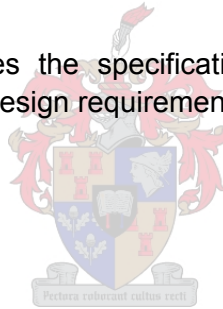
This literature study outlined the information required to understand the dynamics of the Hysucat as well as methods to improve the vertical motions of the hull.

CHAPTER 2: Literature Review

The main conclusions from the study are:

- There is no clear method to model the Hysucat. Strip methods are the most suited for planing hulls but attempts to model the Hysucat with strip methods have proven to be unsuccessful. Milandri (2006) showed that a simple LTI model could be developed to capture the majority of the Hysucat dynamics by using experimental data to determine values for unknown coefficients used in the model.
- The seakeeping of the Hysucat has not been experimentally investigated previously thus it is difficult to determine what seakeeping improvements are inherent to the Hysucat design. Sea trials show that improvements in the seakeeping of the Hysucat are achieved when compared to conventional catamarans due to the hydrofoil damping effect.
- Most methods used to improve the seakeeping of Hydrofoil vessels are active and are complicated and expensive to implement. The use of passive methods has been limited. The torsional suspension system that was developed by Payne (1997) was successful in damping out the transmitted accelerations of a fully submerged hydrofoil vessel.

The following section describes the specifications for the design as well as the concepts that could satisfy the design requirements.



CHAPTER 3: SPECIFICATIONS AND CONCEPT GENERATION

This chapter presents an overview of the specification development as well as the concepts that were generated for the Hysucat suspension system. The mechanical design process, as proposed by Ullman (1997), was followed for the design of the suspension system. The various steps in the design process are discussed in the following sections.

3.1 Identify Needs

The first step was to determine if a need for a passive suspension system for the Hysucat exists. According to Savitsky and Koelbel (1993), the limiting factor for any ocean going vessel is the level of accelerations that the crew and passengers can tolerate. If a suspension system can damp out these effects then the vessel can operate at higher speeds in rougher seas. This is especially important to military vessels and work boats where crews operate in rough seas. Military vessels require smoother seakeeping characteristics so as to support weapons platforms at fast speeds and to reduce crew fatigue. (Taunton, 2001)

The Hysucat system increases the efficiency over conventional catamarans as reported by Hoppe (1989, 1990, 2001) and Migeotte (2002); however a passive suspension system would improve the seakeeping of the craft whilst maintaining the same levels of efficiency.

3.2 Plan for the Design Process

The second step was to plan for the design process. A detailed time schedule for the project was determined and the problem statement and objectives were formulated. Further details can be found in Köpke (2006).

3.3 Determine Customer Requirements and Engineering Specifications

The third step was to develop the customer requirements and engineering specifications for the design. This was an important step as the specifications would form a basis with which the final design and concepts would be evaluated. The engineering specifications were summarised in a Quality Functional Deployment (QFD) diagram as proposed by Ullman (1997).

The QFD is a useful tool in quantifying and developing engineering specifications. It serves as a means for comparing the customer requirements with the engineering specifications and makes a comparison with competitors already on the market. Target values for the design are calculated with relevant upper and lower bounds. The QFD for the design of the suspension system is shown in figure 5.

CHAPTER 3: Specifications and Concept Generation

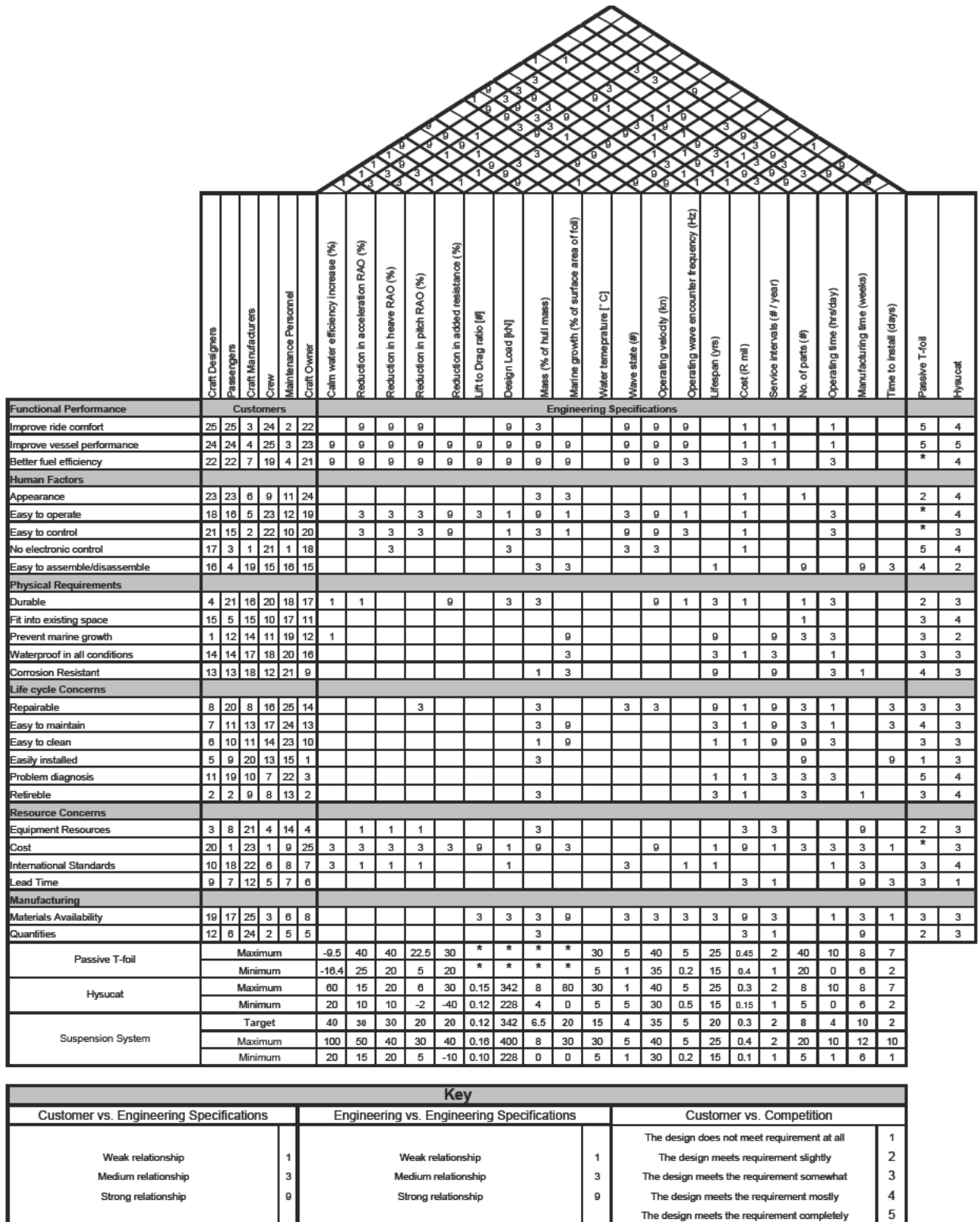


Figure 5: Quality Functional Deployment diagram

CHAPTER 3: Specifications and Concept Generation

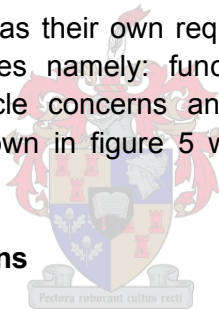
The customer requirements are listed in the left-hand column with the order of importance from 1 to 25 for each customer with 25 being the most important. The engineering specifications are listed horizontally at the top of the figure with the centre of the figure indicating the relationship between the customer requirements and the engineering specifications. The degree to which the competition satisfies the customer requirements is shown in the right-hand column. The engineering specification values are shown in the bottom section of the diagram for the competition as well as the target values for the suspension system design. Finally the 'roof' of the diagram shows the strength of the relationship between the various engineering specifications.

The following section explains how various aspects of the QFD were determined.

3.3.1 Customers and Customer Requirements

An important step was identifying the customers and their requirements. The main customers were craft designers, passengers, crew, maintenance personnel and vessel owners. The target craft is craft utilised in passenger transport and for leisure purposes. Large vessels for freight transport were not considered and their requirements were thus not determined.

Each of the above customers has their own requirements and preferences. They are grouped into 6 main categories namely: functional performance, human factors, physical requirements, life cycle concerns and manufacturing requirements. The customer requirements are shown in figure 5 with the order of importance to each customer.



3.3.2 Engineering Specifications

Engineering Specifications were developed from the customer requirements. According to Ullman (1997), these specifications are the restatement of the design problem in terms of parameters that can be measured and have target values.

Seakeeping Specifications

The engineering criteria with which the seakeeping of the Hysucat with suspension system was evaluated are the heave, pitch, acceleration and added resistance RAOs as defined in section 2.3. The RAOs were evaluated as a percentage reduction in the RAO when compared to the hull without foils.

Operating Conditions

The environmental conditions that the Hysucat with suspension system would operate in had to be determined in order to generate some of the engineering specifications.

The Atlantic Ocean was chosen as the sea for which the suspension system would be designed. Data for the Atlantic Ocean, from Chapman (1967), was used to determine the most common sea conditions that the vessel would encounter. The data is given in

CHAPTER 3: Specifications and Concept Generation

appendix D. Statistics for the Atlantic Ocean indicates that the most prevalent sea state is sea state 4. The data was used with the ITTC 1978 sea spectrum, as presented by Michel (1999), to calculate the wave energy spectrum for the Atlantic Ocean for the stationary condition as well as the design velocity of 16.6 m/s (32 knots). The hull utilised for the research, as well as the choice of the design velocity is discussed in section 3.3.3.

The sea spectrum, $S(\omega)$, is converted with the encounter frequency using equation 3.1 from Chapman (1967).

$$S(\omega_e) = \frac{S(\omega)}{1 + \frac{2\omega V}{g} \cos(\mu)} \quad (3.1)$$

The ITTC 1978 spectrum for Atlantic sea state 4 is shown in figure 6.

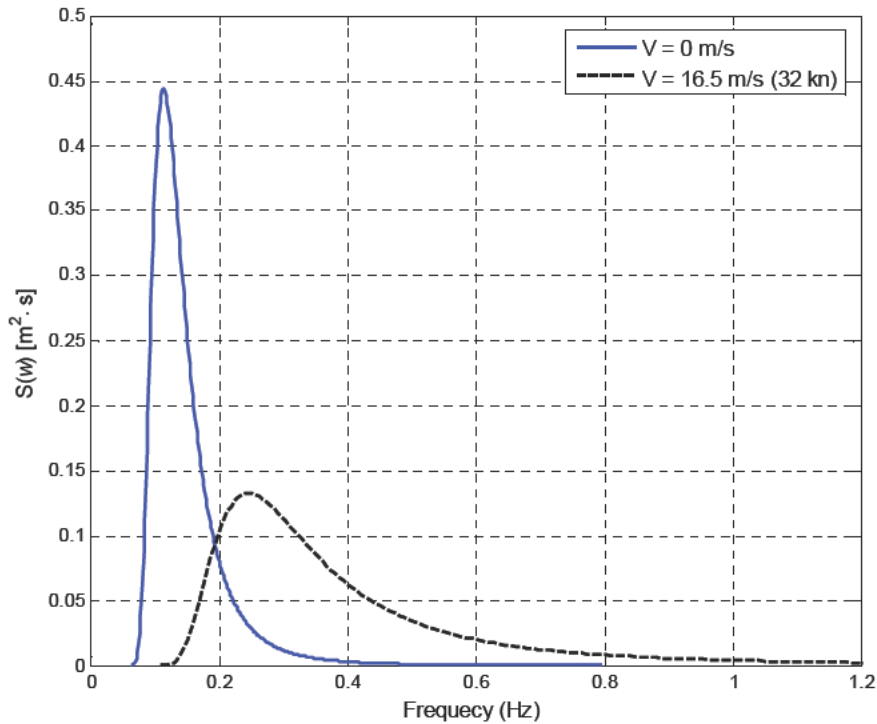


Figure 6: ITTC 1978 spectrum

It is evident from figure 6 that the modal frequency for the Atlantic Ocean sea state 4 is 0.11 Hz. The energy spectrum changes considerable when it is converted with encounter frequency. The total energy stays constant but is spread over a wider range of frequencies. The peak shifts with an increase in vessel velocity. According to Savitsky and Koelbel (1993), resonance on HSC can be avoided by changing the encounter frequency, either by changing the vessel speed or changing the hull heading into the waves.

CHAPTER 3: Specifications and Concept Generation

Values for the other operating conditions such as water temperature and operating time were determined from standard industry norms. Factors such as prevalent winds and atmospheric temperature were not considered.

The maximum accelerations that the suspension system would encounter were determined using the data presented in table 1, section 2.4. It is common practice to design the hull to only withstand the maximum accelerations that the human body can tolerate. (Savitsky and Koelbel, 1993)

The maximum wave height that the vessel would operate in is dependent on the speed at which the craft is operating. The maximum operating wave height as a function of the impact acceleration was calculated using an equation from Savitsky and Koelbel (1993). The equation is obtained from empirical data. The speed wave-height envelope was plotted using the maximum recommended accelerations from table 1.

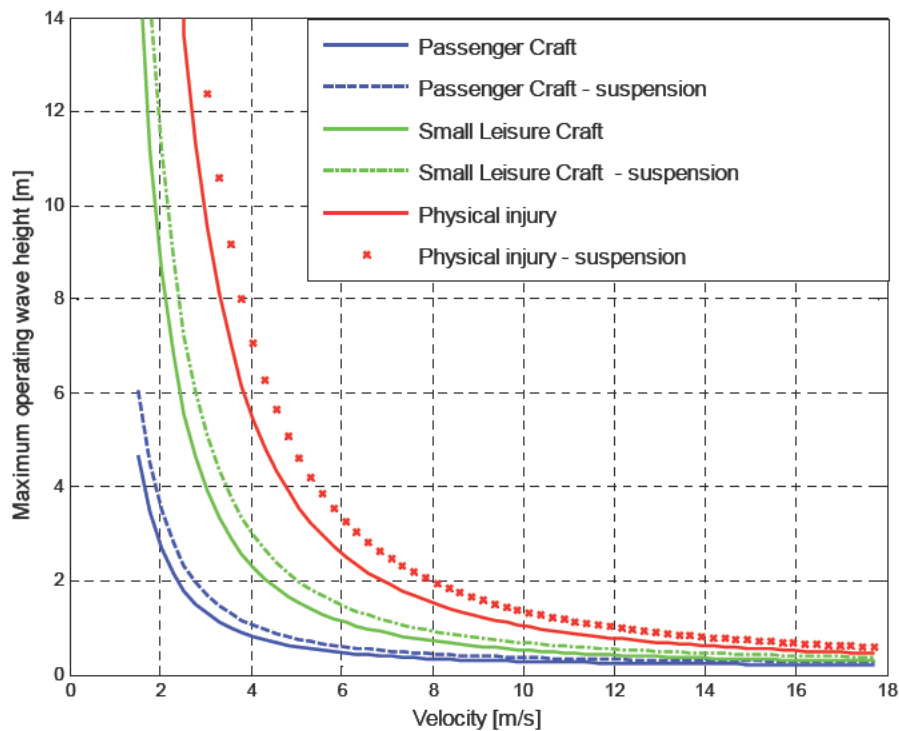


Figure 7: Speed wave-height envelope

The curves at low speed, high sea state, are less defined and more difficult to quantify than at high-speed, low sea state. However they still give a good indication of the conditions the vessel will operate in.

The target value for the Hysucat with suspension system was to damp transmitted accelerations by at least 30%. This would allow the vessel to negotiate higher sea states at the same velocity. The corresponding curves for the Hysucat with suspension system were also plotted in figure 7. It is evident from the speed wave-height envelope

CHAPTER 3: Specifications and Concept Generation

that the wave height that vessels can negotiate decays exponentially with velocity. At the design speed of 16.6 m/s (32 knots) the wave height is approximately 0.3 m. This corresponds to a scale wave height of 0.0375 m which is available in the towing tank at the University of Stellenbosch.

Manufacturing and Maintenance

The manufacturing specifications were determined by consultation with craft designers and manufacturers as well as artisans using the parameters of the existing hull and foil specifications discussed in section 3.3.3.

Maintenance requirements were based on standard industry practices and the size of the hull for which the suspension system would be designed.

3.3.3 Competition Evaluation

When designing a new product it is important to evaluate the competition and other products available on the market. At the moment there is no suspension system fitted to any hydrofoil craft that the author is aware of. The Dynafoil project (discussed in section 2.5) was terminated in the late 1990's.

The main competitors of the Hysucat craft with suspension system are the Hysucat with rigidly attached foils and passive T-foils. T-foils are attached underneath the two demi-hulls and provide damping in waves. Welnicki (1998 and 1998a) ran a systematic series of tests for different positions of T-foils on catamarans. The results obtained were used in the QFD to make a quantifiable comparison as to what seakeeping improvements can be achieved with passive T-foils.

It should be noted that only direct competition to passive motion damping systems was considered. Thus fully supported hydrofoil systems, catamarans and monohulls without hydrofoils were not considered. The results obtained by Milandri (2006) for an active trim-foil controller, discussed in section 2.5, were not included. The catamaran with no foils was used as a benchmark to compare the effectiveness of the competition and to set the target values for the suspension system design.

Most of the data available for Hysucats is for calm water and figures for improved efficiency over other HSC are readily available (See Hoppe, 1989 and Migeotte, 2002). Comparison with regards to seakeeping has not been evaluated and seakeeping analysis has been based on perceptions and not measured data. Hoppe (1989) briefly discusses the Hysucat seakeeping.

Hysucat Seakeeping

The towing tank at the University of Stellenbosch was used to run experiments for the comparison of the seakeeping of the Hysucat with and without foils in order to evaluate any seakeeping improvement achieved with the fitted hydrofoils. Seakeeping

CHAPTER 3: Specifications and Concept Generation

parameters that were evaluated were heave, pitch, acceleration and added resistance. The experimental procedure and equipment are discussed in chapter 5.

A catamaran hull with existing scale model and foil system was chosen for the research in order to save time and money. The same hull would also be used to test the suspension system design. This would be useful for establishing the feasibility of retrofitting an existing hydrofoil system should the suspension system be successful. Comparison could then be made between the experimental results obtained with the various hydrofoil configurations.

The existing model, designated Hys1, was measured up on a measuring table. The main hull parameters are given in table 2.

Table 2: Hull parameters for model and full scale hull

Parameter	Unit	MODEL	FULL SCALE
Scale factor [λ]		1	8
Hull mass [m_h]	[kg]	23.2	11878.4
Radius of gyration [r_G]	[m]	0.402	0.402
Moment of inertia [I_h]	[kg·m ²]	3.74	1919.6
Displacement volume [∇]	[m ³]	0.0226	11.61
Length overall [L_{OA}]	[m]	1.5	12
Chine length [L_{ch}]	[m]	1.29	10.32
Longitudinal Centre of Gravity [LCG]	[%]	43	43
Tunnel width [d]	[m]	0.26	2.08
Deadrise angle [β]	[degrees]	24	24
Chine beam [B]	[m]	0.155	1.24

Hull drawings, dimensions and parameters are given in appendix A. The hull had the standard Hysucat hydrofoil system with a main foil at the LCG spanned between the two demi-hulls and two trim foils at the stern. The hydrofoils are circular arc profile foils with flat bottoms. The foil dimensions and parameters are given in appendix A.

The experiments were run at the full range of frequencies available in the towing tank. Three velocities were tested namely: 4, 5 and 6 m/s which correspond to displacement Froude numbers of 2.4, 3 and 3.6 respectively. The Froude numbers correspond to full scale velocities of 11.3, 14.2 and 16.6 m/s (22, 28 and 32 knots) respectively. Only the final results are given. The expression $\omega_e \sqrt{L_w/g}$ is used to normalise the encounter frequency with hull length, L_w . The experimental results are shown in figures 8 to 11.

CHAPTER 3: Specifications and Concept Generation

RAO_h is obtained by dividing the heave response by the Root Mean Square (RMS) of the wave amplitude and is shown in figure 8. The heave response for the tested velocities tends to unity at the lower normalised encounter frequencies and zero at the higher encounter frequencies. This is to be expected because at the lower frequencies the wavelengths are long relative to the hull length. The model thus follows the wave contours. The heave motion increases relative to the wave height as the frequency increases. At the natural frequency the wavelength is approximately equal to the hull length. This is consistent with the literature. (Savitsky and Koelbel, 1993 and Akers, 1999)

At the higher frequencies the wave lengths are shorter than the hull length. The hull thus experiences more than one wave at a time. The hull rides on top of the waves and thus the heave motion is less than unity and tends to zero.

The results also show that there is an improvement in the heave motion of the Hysucat over the hull without foils. This is apparent at all the tested velocities. An improvement in the heave of approximately 10-20% is achieved with the Hysucat configuration. The figures show that the reduction is at the resonant frequency. At the higher and lower frequency the results are almost identical. The reduction confirms the seakeeping improvement of the Hysucat configuration reported by Hoppe (1989).

Figure 9 shows the RAO_p comparison between the Hysucat with and without foils.

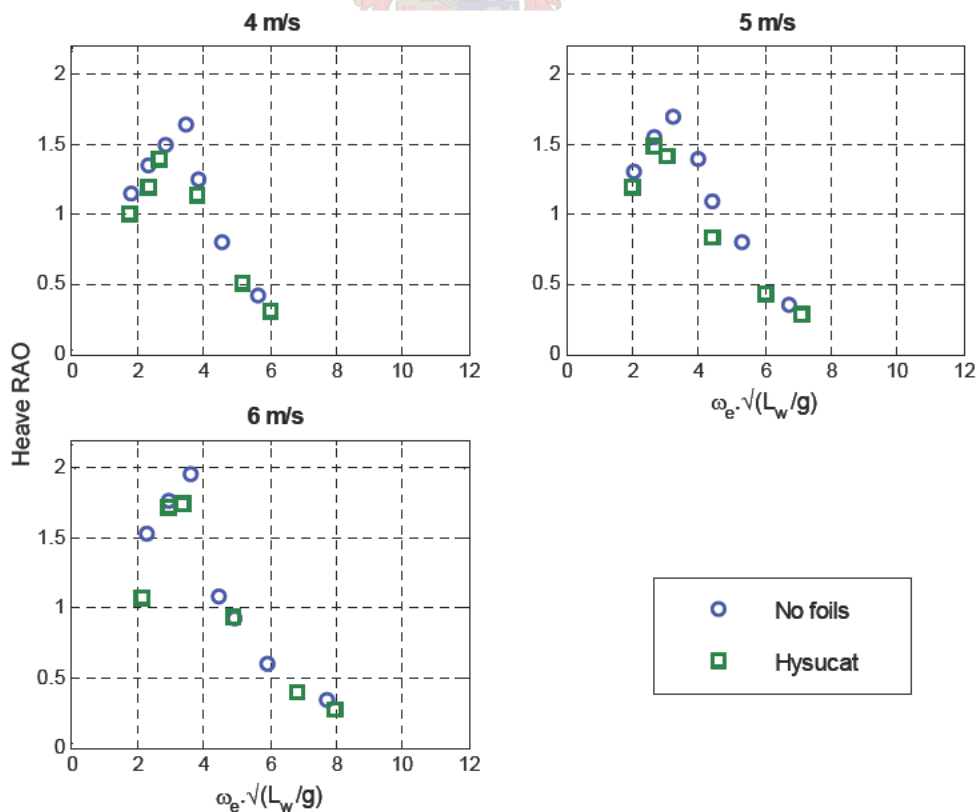


Figure 8: Heave RAO

CHAPTER 3: Specifications and Concept Generation

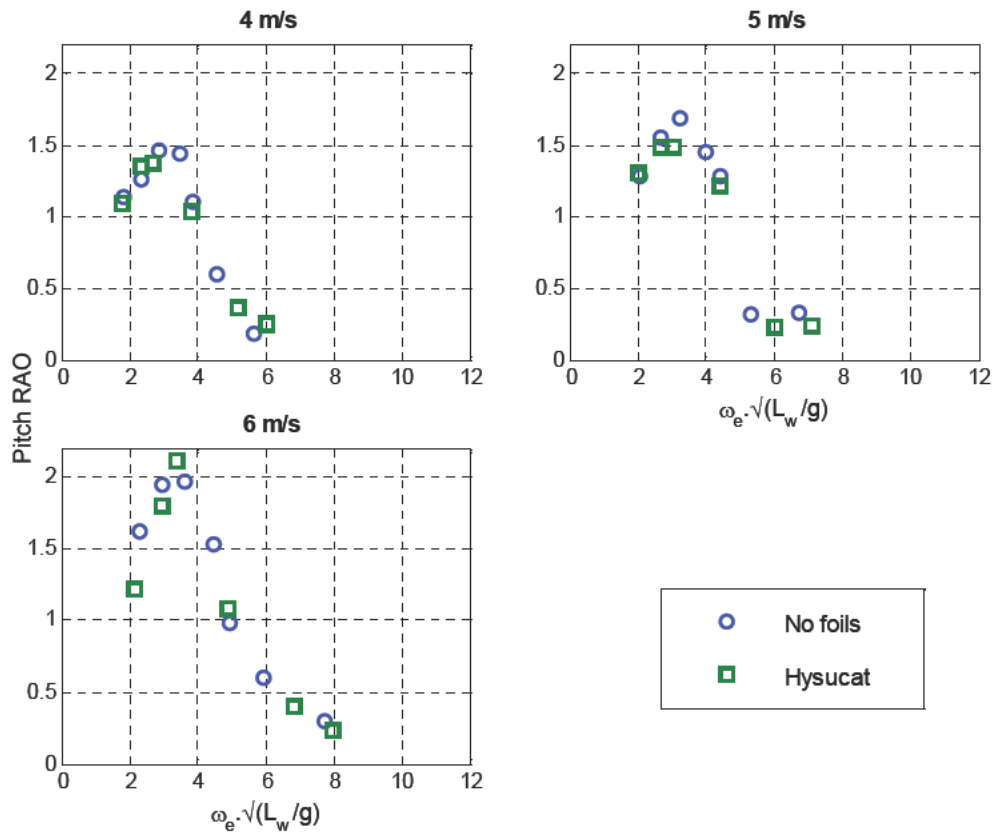


Figure 9: Pitch RAO

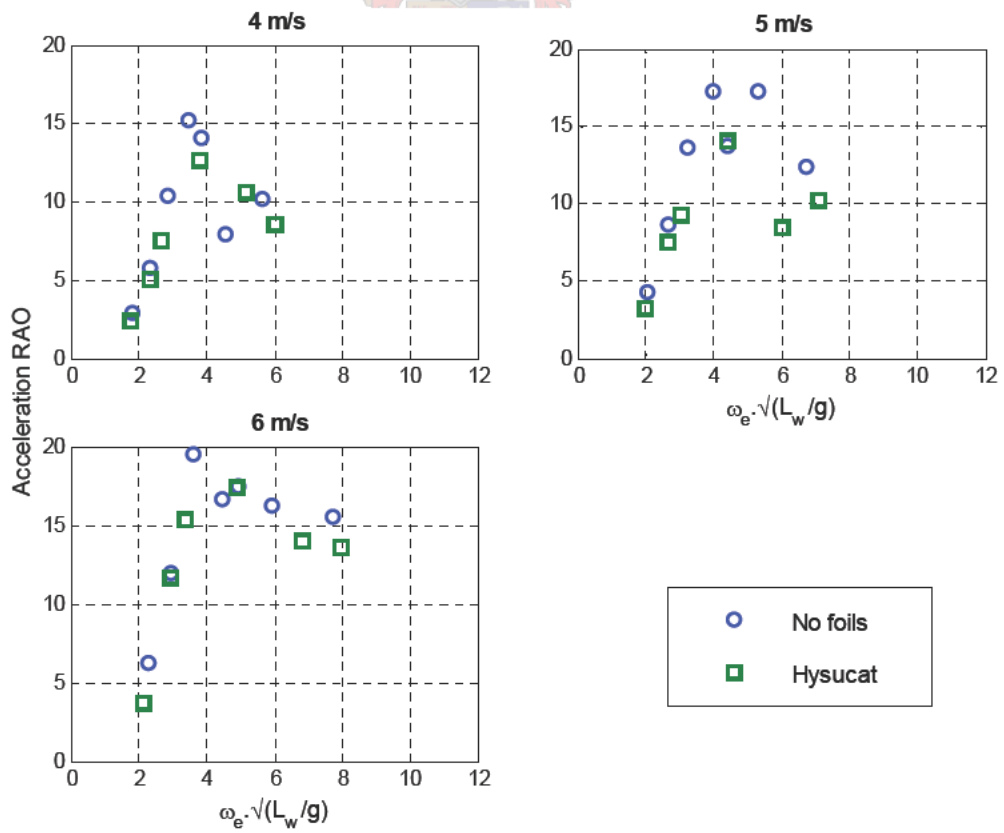


Figure 10: Acceleration RAO

CHAPTER 3: Specifications and Concept Generation

The pitch RAO shows the same tendencies that were obtained for the heave results. The maximum values increase with increase in speed which is to be expected.

At the lower frequencies the hull follows the wave and thus the RAO tends to unity. At 4 and 5 m/s there is a decrease in the pitch motions of approximately 6%. At 6 m/s the Hysucat result shows a slightly higher pitch RAO than the hull without foils. The results show that the hydrofoils have less influence on the pitch when compared to the heave results. This is due to the location of the main foil near the Longitudinal Centre of Gravity (LCG) and the pitch motion pivoting around the LCG. The trim foils have less lift than the main hydrofoil but still have some influence on the pitch motions.

The acceleration RAO results are shown in figure 10. The RAOs are obtained by dividing the RMS of the vertical acceleration by the gravitational acceleration as well as the RMS of the wave amplitude. The acceleration response RAO tends to zero at the lower frequencies. This is due to the hull following the contours of the wave. The results also show that there is a decrease in the vertical accelerations of the Hysucat at 4 and 5 m/s. The decrease in acceleration varies by 10-15%. The results show good comparison to the speed wave-height envelope discussed in section 3.3.2.

The results surprisingly show that there is no significant reduction in transmitted acceleration at 6 m/s. This would be one of the main purposes for fitting a suspension system to the Hysucat.

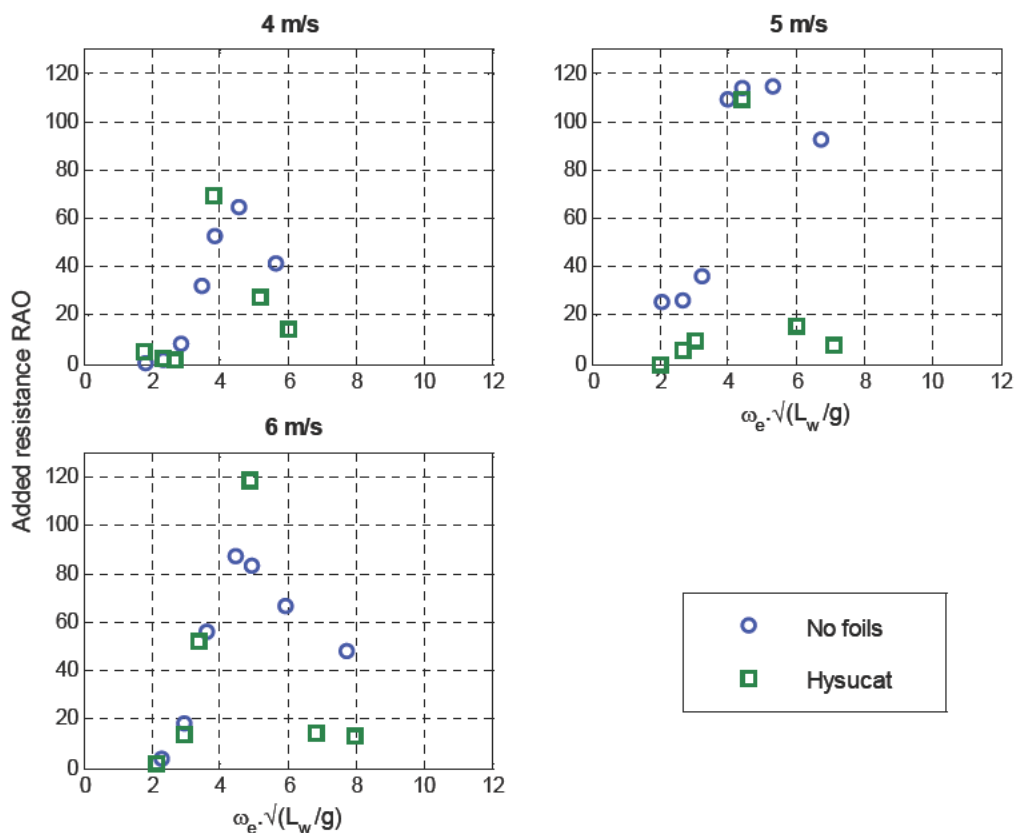


Figure 11: Added resistance RAO

CHAPTER 3: Specifications and Concept Generation

The added resistance RAO is an indication of how much the mean resistance of the hull increases in waves. The added resistance RAO is shown in figure 11. The added resistance for the Hysucat is the same for the hull without foils at 4 and 5 m/s. At 6 m/s the Hysucat shows an increase in added resistance of approximately 35%. This increase is only evident at the resonant frequency. The results indicate that the added resistance decreases sharply at encounter frequencies higher than the resonant frequency.

The results obtained from the experiments were used in the evaluation of the competition in the QFD presented in figure 5. The next step in the design process, once the specifications and customer requirements had been determined, was to generate concepts that would satisfy the customer requirements. The concept generation is discussed in the following section.

3.4 Concept Generation

Concepts that could satisfy the design requirements were generated. The concepts were generated using the techniques proposed by Ullman (1997), namely by researching previous work that had been done in the field, product patents and implementing the 6-3-5 method as proposed by Ullman (1997). Approximately 30 concepts were generated. The concepts differed with respect to kinematics, location as well as suspension type.

3.5 Concept Evaluation

One of the main deciding factors in choosing the most feasible concepts, besides satisfying the engineering requirements, was simplicity and ease of implementation. The concepts that were obviously unfeasible were discarded. The remaining concepts were evaluated using a decision matrix as proposed by Ullman (1997).

Two concepts that could satisfy the requirements remained and are described in the following section.

3.5.1 Vertical Suspension System

The first concept was a vertical suspension system. The concept is shown in figure 12.

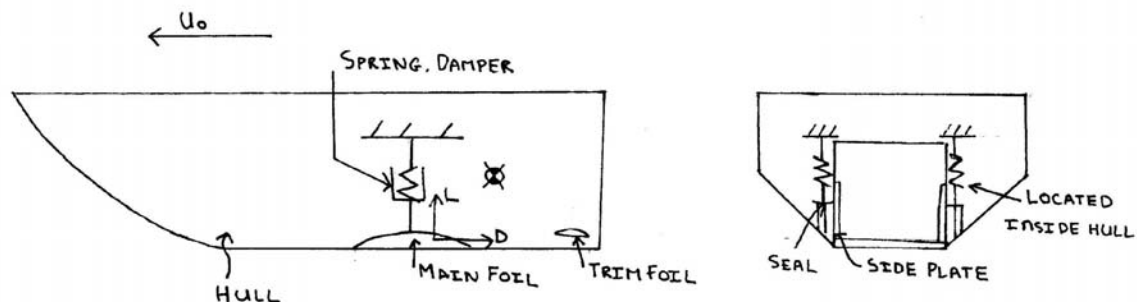


Figure 12: Concept 1 - Vertical suspension system

CHAPTER 3: Specifications and Concept Generation

The main foil is located slightly forward of the LCG and moves perpendicular to the forward motion of the hull in response to wave and impact disturbances. The vertical transmitted forces from the hydrofoil to the hull are damped out by a spring-damper system that is located in the tunnel wall and roof. The hydrofoil is attached to push rods that move through a sealed hole in the hull roof. Sided plates attached to the hydrofoil move up and down with the hydrofoil and direct the water flow over the rods to prevent flow separation which would result in loss of hydrofoil lift.

The advantages and disadvantages of the suspension system are listed below.

Advantages:

- The motion of the hydrofoil is in the direction of the foil lift.
- Transmitted forces are damped during hydrofoil broaching and impact when re-entering the water.
- The spring and damper are located inside the hull away from the water and corrosive environment.
- Transmitted forces are damped if the hydrofoil hits any floating objects in the water.

Disadvantages:

- It is difficult to waterproof the suspension system if there are moving components that penetrate the hull near or in the water.
- There is a limited amount of stroke available for the movement of the hydrofoil and is one of the major constraints placed on the system.
- Flow separation with the foil movement may occur which would result in lift loss.
- The mechanism would be subject to fatigue and corrosion would be a major problem.

The second concept is a torsional suspension system and is discussed in the following section.

3.5.2 Torsional Suspension System

The torsional suspension system was the second feasible concept and is shown in figure 13.

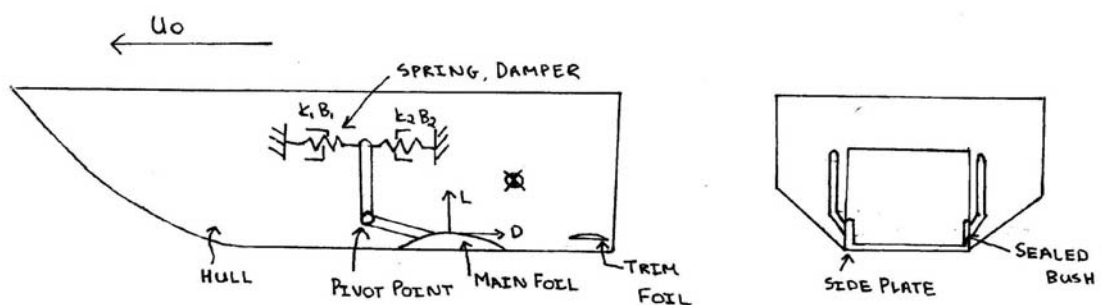


Figure 13: Concept 2 – Torsional suspension system

CHAPTER 3: Specifications and Concept Generation

The foil moves in the horizontal and angular direction around a pivot point in response to changes in the lift and drag force acting on the hydrofoil. The concept is shown here with two coil springs and dampers attached to a pivot rod. However the system could also consist of a torsional spring and damper at the pivot point. This concept is similar to the Dynafoil suspension system that was developed by Payne (1997) for a fully supported hydrofoil vessel. A reduction in vertically transmitted forces is achieved through variations in the angle of attack and vertical motion of the hydrofoil in response to orbital wave motions. Payne (1997) was able to achieve reductions in transmitted accelerations of an order of magnitude using a similar system.

The advantages and disadvantages of the concept are listed below.

Advantages:

- The system is easier to implement than concept 1.
- The foil lift would be reduced with relatively small variation in angle of attack of the hydrofoil.
- The pivot point would be located outside of the fluid flow and thus would not obstruct the flow over the foil.
- The suspension system would not be directly exposed to the corrosive environment.

Disadvantages:

- It will be difficult to waterproof the suspension system if there are moving components that penetrate the hull near the water.
- The concept is difficult to model and thus the dynamics are more unpredictable.
- The component count would increase and thus the assembly time would be longer.
- The calm water operating condition would have to be carefully determined in order to ensure optimal performance of the system.

It is important that the two concepts presented do not decrease the calm water efficiency of the hull as this would make them unfeasible to implement on a Hysucat.

3.6 Conclusion

The design methodology that was used in determining the specifications as well as the concepts that could satisfy the requirements for the suspension system were discussed. The QFD provided a means to evaluate the customer requirements against the engineering specifications. The two main competitors that would compete with the suspension system were the passive T-foils and the Hysucat with rigidly attached hydrofoils.

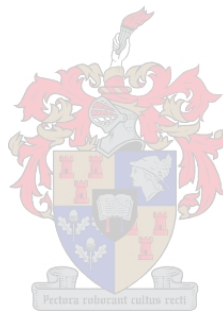
Experimental results indicated that an improvement in the seakeeping of 6-60% is achieved with the Hysucat over the hull without foils. The results indicated that there is not a significant improvement with the pitch motions, however there is an improvement

CHAPTER 3: Specifications and Concept Generation

with the heave and acceleration and added resistance RAOs. It is important to note that the results are for the specific hull that was tested and cannot be used to describe Hysucats in general.

The two final concepts that could possibly satisfy the design requirements were shown. The major problem with both concepts is that they would be operating in a corrosive environment and would add mass to the system. The suspension system would also have an effect on the calm water hydrodynamics of the vessel itself.

Analytical models for the two concepts had to be determined so that the dynamics of each concept could be investigated. The models would then be used to analyse each concept and to design the suspension system with the aid of experimental testing. The modelling strategies for the suspension system are described in chapter 4.



CHAPTER 4: HYSUCAT SUSPENSION SYSTEM MODELLING

The specifications for the suspension system design and the two concepts that could satisfy the customer requirements were discussed in the previous chapter. Simulation models were required to investigate the dynamics and feasibility of the concepts. The purpose of the models is to analyse the seakeeping response of the concepts and to use as a design tool in the design of the suspension system.

Matveev (2006) suggested that a catamaran hull model be superimposed with a hydrofoil model to capture the seakeeping dynamics in waves. The Hysucat with rigidly attached hydrofoils was modelled first in order to determine the accuracy of combining a hull model with a hydrofoil model.

4.1 Demi-hulls

The modelling of planing craft is different to displacement vessels as the motion is non-linear with wave height. Strip methods used to analyse displacement hulls cannot be used for planing hulls due to the non-linearities in motion. Detailed time-dependent hydrodynamic analysis would be required to accurately capture the hull's motion in waves. Such models are computationally intensive and clumsy to work with.

Milandri (2006) attempted to combine 2-D strip methods developed by Zarnick (1978) with hydrofoils using Powersea® (commercial software used to analyse planing hulls) but inaccurate results were obtained. Therefore an experimentally based approach, similar to the method followed by Milandri (2006), was attempted. Milandri (2006) used a linear, time invariant model to develop a state-space model for the Hysucat. The variable trim foil angle was an input to the system whilst the wave forces were modelled as disturbance forces.

A similar approach was used to model the catamaran demi-hulls' motion in waves. The physical dynamics of the system would be represented with appropriate coefficients of a state-space model. The running trim of the vessel was taken as the equilibrium point and the waves forces were modelled as inputs into the system. The force diagram for the planing hull is shown in figure 14.

The two degree of freedom system is free to heave in the vertical direction and pivot around the LCG. The motion is treated as a second-order spring-mass-damper system. F_k , F_w and F_b are the restoring force, wave excitation force and damping force in the vertical direction respectively, whilst M_k , M_w and M_b are the restoring moment, wave excitation moment and damping moment in the angular direction. According to Fang *et al.* (1997), the wave forces are proportional to the wave height.

CHAPTER 4: Hysucat Suspension System Modelling

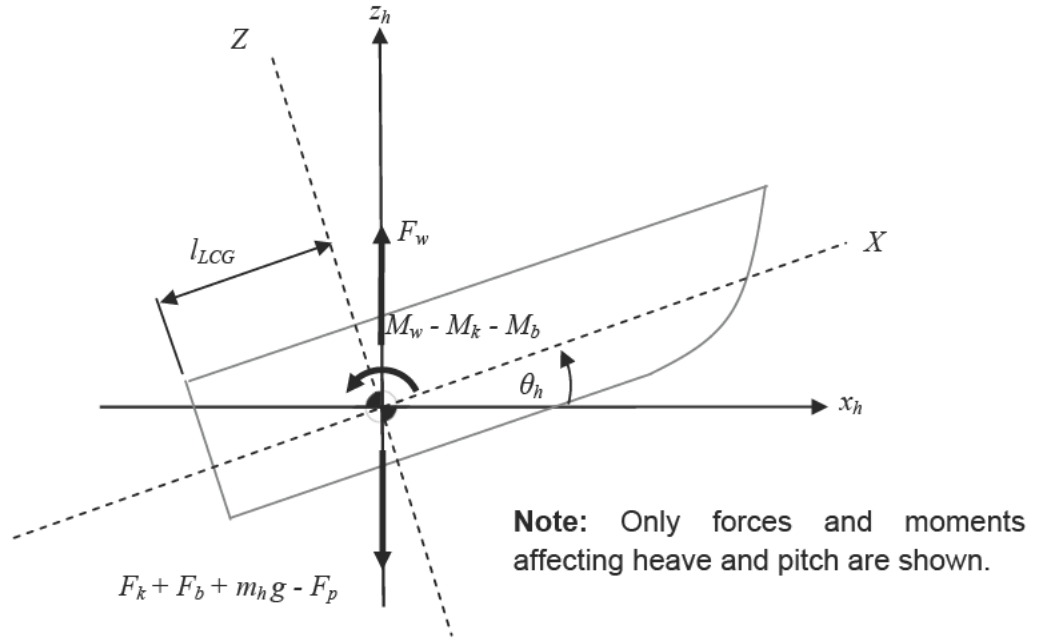


Figure 14: Planing Hull Force Diagram

The equations for heave and pitch are derived using Newton's second law of motion. The heave and pitch motions are shown by equation 4.1 and 4.2 respectively.

$$F_o \zeta_o \sin(\omega_e t) - b_z (\dot{z}_h - \dot{z}_{h0}) - k_z (z_h - z_{h0}) - m_h g + F_p = (m_h + m_a) \ddot{z}_h \quad (4.1)$$

$$M_o \zeta_o \sin(\omega_e t) - b_\theta (\dot{\theta}_h - \dot{\theta}_{h0}) - k_\theta (\theta_h - \theta_{h0}) = (I_h + I_a) \ddot{\theta}_h \quad (4.2)$$

Where:

- F_o is the wave excitation force gain;
- M_o is the wave exciting moment gain;
- F_p is the calm water planing force;
- ζ_o is the wave amplitude;
- k_θ is the equivalent torsional stiffness;
- k_z is the equivalent vertical stiffness;
- b_θ is the torsional damping;
- b_z is the vertical damping;
- m_h is the hull mass;
- m_a is the added mass;
- I_h the mass moment of inertia around the LCG;
- I_a the added moment of inertia around the LCG.

The subscript 0 represents the steady state running trim of the vessel. If we only consider the dynamics of the demi-hulls around the steady-state planing condition, so that $z_{h0} = \dot{z}_{h0} = \theta_{h0} = \dot{\theta}_{h0} = 0$, then the equilibrium values can be subtracted from equation 4.1 and 4.2 and rewritten in standard form shown by equation 4.3 and 4.4.

CHAPTER 4: Hysucat Suspension System Modelling

$$(m_h + m_a)\ddot{z}_h + b_z \dot{z}_h + k_z z_h = F_o \zeta_o \sin(\omega_e t) \quad (4.3)$$

$$(I_h + I_a)\ddot{\theta}_h + b_\theta \dot{\theta}_h + k_\theta \theta_h = M_o \zeta_o \sin(\omega_e t) \quad (4.4)$$

The full system can thus be described by a fourth order, state-space system. The state-space model for the hull motion in an orbital wave field is represented by equation 4.5 and 4.6.

$$\begin{bmatrix} \dot{z}_h \\ \ddot{z}_h \\ \dot{\theta}_h \\ \ddot{\theta}_h \end{bmatrix} = \underbrace{\begin{bmatrix} 0 & 1 & 0 & 0 \\ \frac{-k_z}{(m_h + m_a)} & \frac{-b_z}{(m_h + m_a)} & 0 & 0 \\ 0 & 0 & 0 & 1 \\ 0 & 0 & \frac{-k_\theta}{(I_h + I_a)} & \frac{-b_\theta}{(I_h + I_a)} \end{bmatrix}}_{\mathbf{A}} \begin{bmatrix} z_h \\ \dot{z}_h \\ \theta_h \\ \dot{\theta}_h \end{bmatrix} + \underbrace{\begin{bmatrix} 0 \\ \frac{F_o}{(m_h + m_a)} \\ 0 \\ \frac{M_o}{(I_h + I_a)} \end{bmatrix}}_{\mathbf{B}} \zeta_o \sin(\omega_e t) \quad (4.5)$$

$$\begin{bmatrix} z_h \\ \ddot{z}_h \\ \theta_h \end{bmatrix} = \underbrace{\begin{bmatrix} 1 & 0 & 0 & 0 \\ \frac{-k_z}{(m_h + m_a)} & \frac{-b_z}{(m_h + m_a)} & 0 & 0 \\ 0 & 0 & 1 & 0 \end{bmatrix}}_{\mathbf{C}} \begin{bmatrix} z_h \\ \dot{z}_h \\ \theta_h \\ \dot{\theta}_h \end{bmatrix} + \underbrace{\begin{bmatrix} 0 \\ \frac{F_o}{(m_h + m_a)} \\ 0 \end{bmatrix}}_{\mathbf{D}} \zeta_o \sin(\omega_e t) \quad (4.6)$$

A, **B**, **C** and **D** are the representative state-space matrices.

The values for the restoring coefficients, hull damping and wave excitation force gains could not be calculated analytically with current methods. A system identification approach was used to determine the values using experimental data and is discussed in the following section.

4.1.2 System Identification

The coefficients of the assumed model, described by equation 4.5 and 4.6, had to be determined.

The vessel mass was determined in the specification development. An experimental procedure was used to obtain the radius of gyration of the hull using swinging pendulum experiments as done by Zarnick and Turner (1981) and Milandri (2006). The experimental procedure and calculations are presented in appendix A. The added mass is calculated as if it were an impacting wedge as described by Akers (1999). The sectional added mass is calculated using equation 4.7.

CHAPTER 4: Hysucat Suspension System Modelling

$$m_a = \int_{L_{ch}} n_a \frac{\pi}{2} \rho B_a^2 dl \quad (4.7)$$

Where:

- n_a is the added mass coefficient;
- B_a is the chine half beam;
- L_{ch} is the wetted chine length.

Zarnick (1978) used an added mass coefficient of 1. Vorus (1996) suggested an added mass coefficient that is dependent on the deadrise angle of the hull. A value of 0.6 was selected according to graphical data presented in Akers (1999). The sectional added mass was integrated over the chine length. The added inertia is obtained using the radius of gyration for the model with equation A.3, presented in appendix A, using the added mass calculated using equation 4.7.

Parameter estimation was used to find the rest of the coefficients namely: k_z , k_θ , b_z , b_θ , F_o and M_o . According to Milandri (2006), parameter estimation is a frequently used technique, especially in the aircraft industry. Maine and Iliff (1986) give a thorough overview of the field with practical methods to implement the various techniques.

Parameter estimation involves stimulating the system with a known input and then measuring the output states. The inputs, as well as the measured output states, are sent to a representative LTI model for the system. Optimization algorithms then fit simulation values to the unknown parameters of the system to minimize the error between the model and the measured data.

MMLE, a system identification toolbox for Matlab, was used to perform the identification task. The toolbox is discussed in Milne (2000). The software uses the Newton, Levenberg-Marquardt and constrained-Newton optimization algorithms to estimate the unknown parameters, Cramer-Rao bounds, as well as the experimental measurement noise.

Systematic towing tank tests at 4, 5 and 6 m/s with the demi-hulls, described in chapter 3, were performed to obtain the experimental data required for the parameter estimation. The test velocities correspond to full scale velocities of 11.3, 14.2 and 16.6 m/s (22, 28 and 32 knots) respectively. The measured wave height was the input into the system. Experiments were run over 5 wave frequencies namely 0.35, 0.4, 0.49, 0.57 and 0.61 Hz. The LTI parameters were then estimated for each run. The experimental setup for the parameter estimation is described in chapter 5.

4.1.3 System Identification Inputs and Procedure

The parameters for the assumed LTI system were determined using the system identification toolbox. The program requires that numerous parameters be set by the user.

CHAPTER 4: Hysucat Suspension System Modelling

Starting values: The starting values of the unknown parameters had to be assigned before the simulation commenced. The starting values were determined by inspecting the results obtained by Milandri (2006) and the experimental results. The input values were adjusted until convergence was achieved.

Initial Conditions: The initial conditions of all the state variables were set to zero. This was done as the model described by equation 4.5 and 4.6 only deals with dynamic changes around the steady-state planing condition.

Control Parameters: The software required that numerous control parameters be set before estimation could commence namely, maximum number of iterations, relative change to indicate convergence and the cut-off frequency. The values were 100, 0.0001 and 5 Hz respectively.

The software used the time data obtained for the state variables of the system and assigned values to the unknown parameters so to minimise the error between the simulation and experimental results.

4.1.4 System Identification Results

The parameter identification results represented the measured data to varying degrees. Figure 15 shows the estimated response and the measured response with the input wave signal shown at the top of the figure. There was a tendency for the wave height sensor to produce voltage spikes. These were filtered with software using a fourth order, low pass, Butterworth filter. The filtered and unfiltered signals are shown in figure 15. The estimated response shows good correlation to the experimental data.

The estimated results for the unknown parameters are shown in figures 16 and 17. The results show some scatter at various frequencies. There are two reasons why this occurs.

1. The wave height in the towing tank is dependent on the operating wave frequency and therefore cannot be set independently. As we have assumed a LTI model, non-linearity will have an effect at larger wave amplitudes.
2. At low wave amplitudes the signal noise was prominent. The large signal to noise ratio affected the convergence of the system.

The median of each of the estimated parameters for each of the tested velocities was calculated. The LTI system, represented by equations 4.5 and 4.6, was then plotted with the experimental data. The response did not match as closely as was anticipated. The wave input force and moment were adjusted heuristically until the simulated data was best represented. The final values for the unknown parameters are shown in table 3 for the model design velocity of 6 m/s.

CHAPTER 4: Hysucat Suspension System Modelling

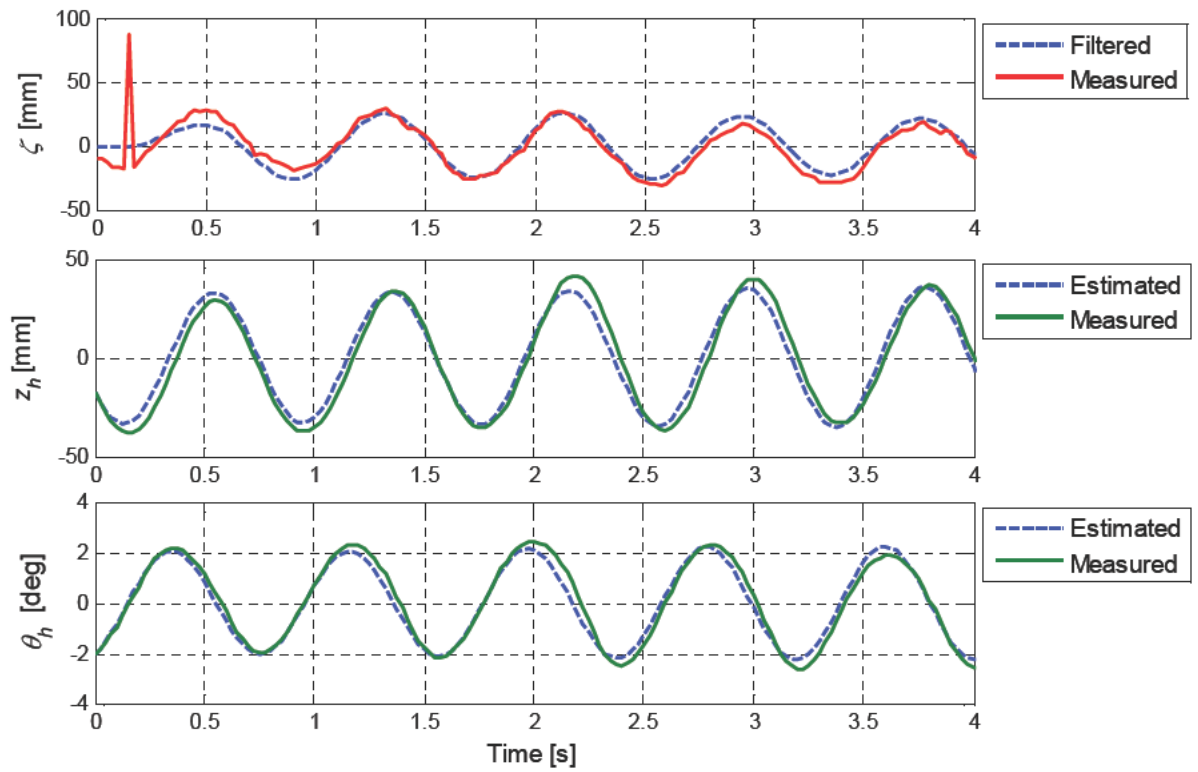


Figure 15: Estimated and experimental response results for heave and pitch

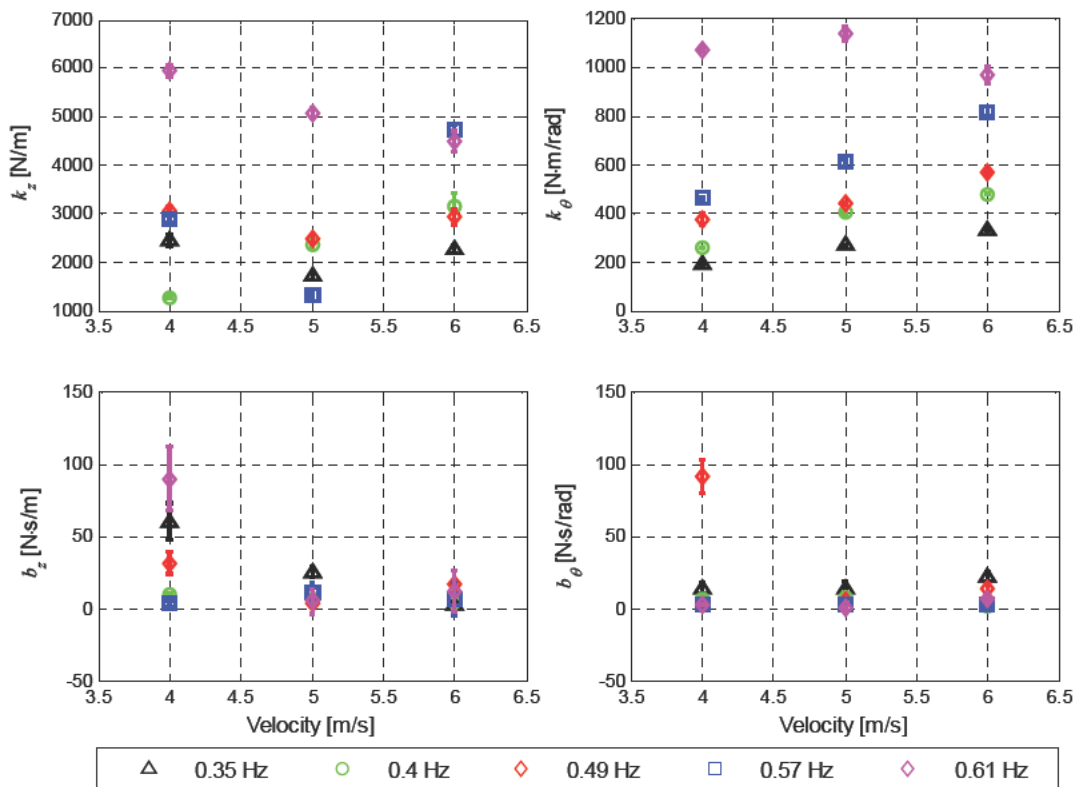


Figure 16: Estimated values for k_z , k_θ , b_z and b_θ

CHAPTER 4: Hysucat Suspension System Modelling

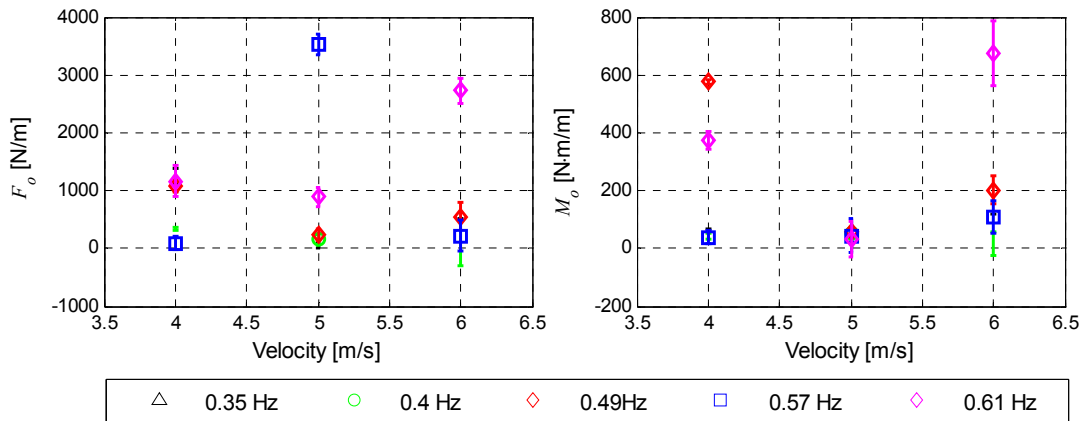

 Figure 17: Estimated values for F_o and M_o

Table 3: Parameter estimation results

Hull Parameters									
m [kg]	m_a [kg]	I [kg·m ²]	I_a [kg·m ²]	k_z [N/m]	b_z [N·s/m]	k_θ [N·m/rad]	b_θ [N·m·s/rad]	F_o [N/m]	M_o [N·m/rad]
23.2	22.7	3.712	3.632	5143	224	850	43.5	4695	938

The model parameter values shown in table 3 were used with equation 4.5 and 4.6 to simulate the hull seakeeping response shown in figure 18. The simulation results show good comparison for the heave and pitch RAO at the higher frequencies. It is expected that the simulation results would match the experimental data as the simulation model was adjusted heuristically until satisfactory results were obtained.

Where there is some discrepancy is with the pitch RAO at lower frequencies and the vertical acceleration RAO at the higher frequencies. The pitch response should tend to unity at the lower frequency; however the model tends towards infinity. This discrepancy in modelling of pitch at lower frequencies has been reported by Akers (1999) and Milandri (2006). The problem arises because the wave number k_w tends to zero faster than the numerator and thus the response grows rather than approach unity.

CHAPTER 4: Hysucat Suspension System Modelling

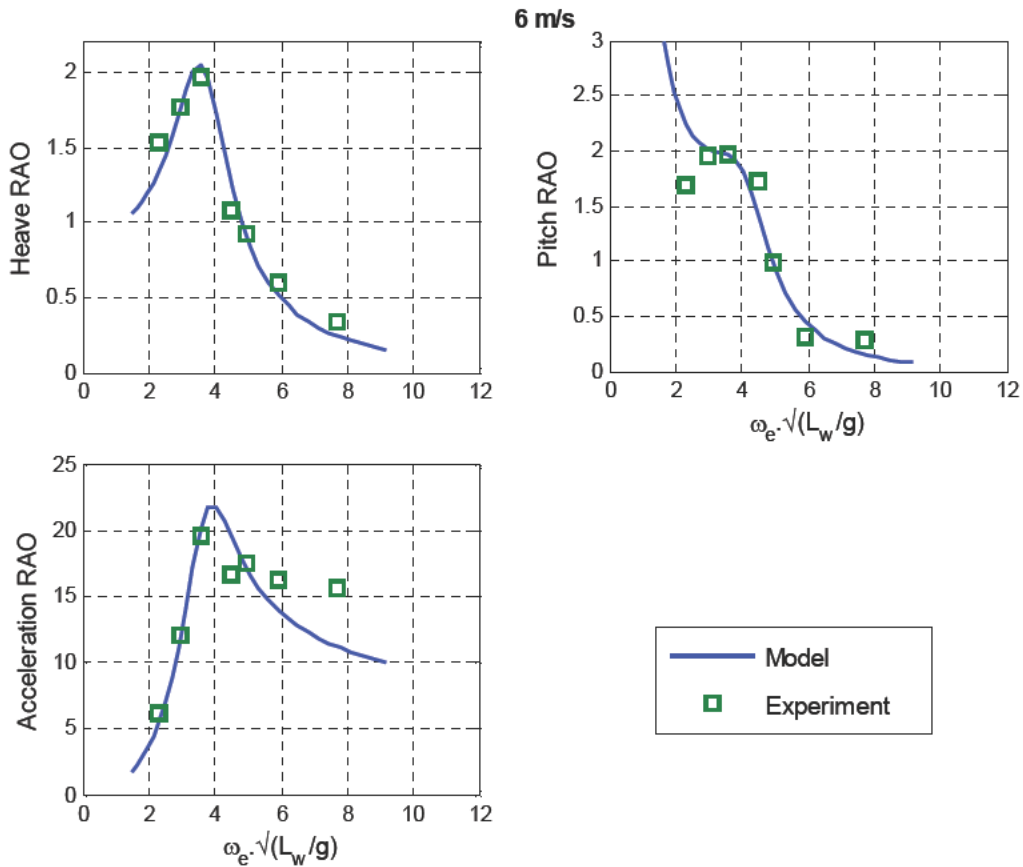


Figure 18: Comparison between simulated response and experimental data for demi-hulls

It is useful to calculate the model damping as well as the natural frequencies of the system. This is done using the eigenvalues of the system as described by Meirovitch (2001) as well as the representative system coefficients at 6 m/s. Savitsky and Koelbel (1993) used the same approach of fitting a response of known damping to a frequency response curve. The eigenvalues of matrix \mathbf{A} were calculated. The following is applicable for each of the eigenvalues.

$$\omega_{n_j} = \|\lambda_j\| = \sqrt{\text{Re}(\lambda_j)^2 + \text{Im}(\lambda_j)^2} \quad \text{for } j = 1, 2, 3, 4 \quad (4.9)$$

$$\zeta_j = -\frac{\text{Re}(\lambda_j)}{\omega_{n_j}} \quad \text{for } j = 1, 2, 3, 4 \quad (4.10)$$

The damped natural frequency is represented by equation 4.11

$$\omega_{d_j} = \omega_{n_j} \sqrt{1 - \zeta_j^2} \quad \text{for } j = 1, 2, 3, 4 \quad (4.11)$$

The results of the above calculations are presented in table 4.

CHAPTER 4: Hysucat Suspension System Modelling

Table 4: Calculated natural frequencies and damping ratios

Model Response Parameters							
ω_{nz} [rad/s]	$\omega_{n\theta}$ [rad/s]	ζ_z	ζ_θ	ω_{dz} [rad/s]	$\omega_{d\theta}$ [rad/s]	$\omega_{dz}\sqrt{L/g}$	$\omega_{d\theta}\sqrt{L/g}$
10.25	11.59	0.3824	0.2528	9.474	11.216	3.448	4.08

The vibration analysis for the heave and pitch motions show good comparison to the experimental results presented in figure 18. The damping ratios indicate that the response is under-damped. This is what is also reported in the results obtained by Savitsky and Koelbel (1993).

The next step was to obtain a model for the Hysucat with rigidly attached hydrofoils. This was done by combining a theoretical hydrofoil model with the model obtained for the demi-hulls.

4.2. Hysucat Model

Hydrofoil theory was combined with the catamaran demi-hull model to simulate the Hysucat seakeeping. The specifications for the hydrofoil suspension system determined that the hydrofoil would be operating in the sub-cavitation region therefore only the theory for sub-cavitating hydrofoils was used in the analysis.

The dynamics of the Hysucat had to be determined in order to design the suspension system for the vessel. A force diagram of a Hysucat in an orbital velocity wave field is shown in figure 19.

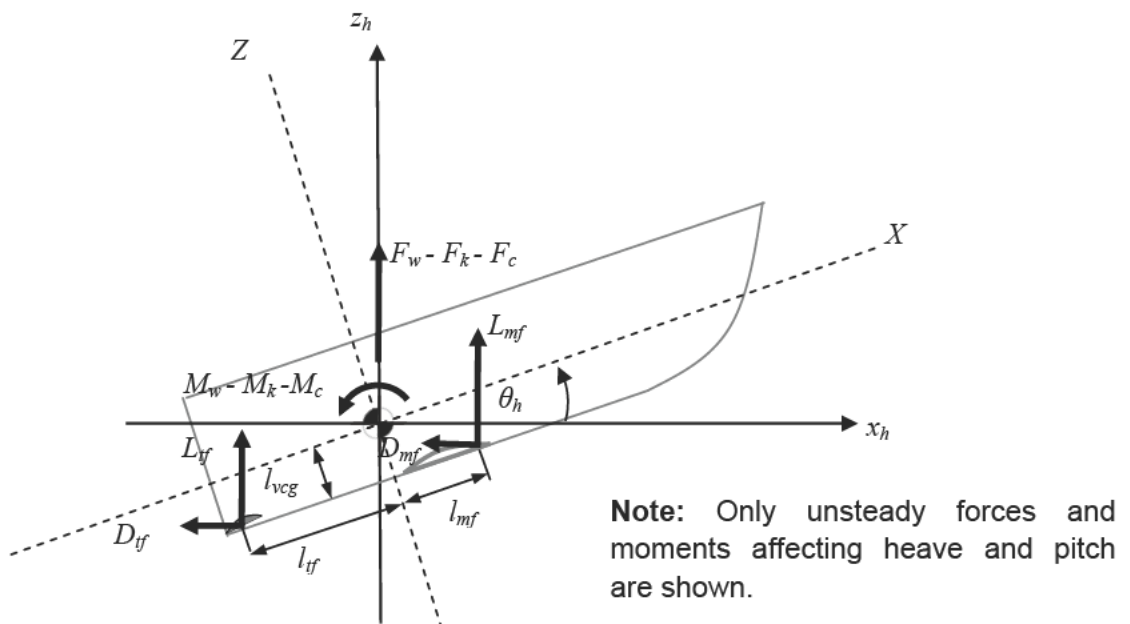


Figure 19: Hysucat force diagram

CHAPTER 4: Hysucat Suspension System Modelling

The forces, L_{mf} and L_{tf} , are the lift of the main and trim hydrofoils respectively, whilst D_{mf} and D_{tf} are the drag forces. Figure 20 shows a typical hydrofoil in an orbital velocity wave field and the velocity vectors experienced by the foil.

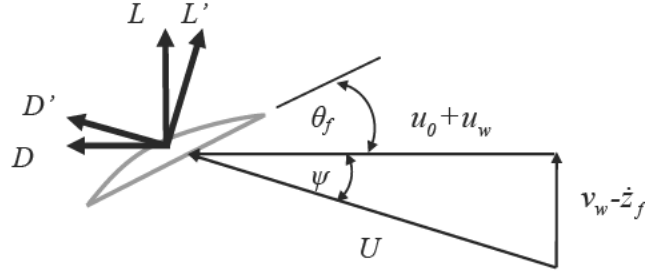


Figure 20: Hydrofoil in orbital wave motion

Where:

- L' is the hydrofoil lift normal to the up-flow;
- D' is the hydrofoil drag parallel to the up-flow;
- L is the hydrofoil lift in the vertical direction;
- D is the hydrofoil drag in the horizontal direction;
- U is the resultant velocity relative to the foil;
- u_w is the local horizontal wave velocity;
- v_w is the local vertical wave velocity;
- \dot{z}_f is the vertical velocity of the foil;
- θ_f the foil pitch angle;
- ψ the up-flow angle.

The resultant velocity of the water approaching the hydrofoil is a combination of the forward velocity of the hydrofoil as well as the orbital motion of the waves. The resultant velocity and up-flow angle are calculated using equations 4.12 and 4.13 respectively.

$$U^2 = (u_o + u_w)^2 + (v_w - \dot{z}_f)^2 \quad (4.12)$$

$$\psi = \text{atan} \left(\frac{v_w - \dot{z}_f}{u_o + u_w} \right) \quad (4.13)$$

The vertical and horizontal wave velocity components are represented by equation 4.14 and 4.15 respectively.

$$v_w = \omega \zeta_o \cos(\omega_e t + k_w x) \quad (4.14)$$

$$u_w = \omega \zeta_o \sin(\omega_e t + k_w x) \quad (4.15)$$

CHAPTER 4: Hysucat Suspension System Modelling

The pitch velocity of the hull has to be taken into account when calculating the vertical velocities at the main and trim foils due to the centre of lift of the hydrofoils being located away from the LCG.

In order to determine the lift-curve slope, calm water hydrofoil theory was used. The theory is presented in appendix B. The unsteady lift coefficient is calculated using the lift curve slope multiplied with the angle of incidence and the up-flow angle of the hydrofoil.

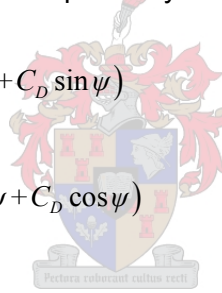
$$C_L = C_{L\alpha} (\theta_f + \psi) \quad (4.16)$$

A constant submergence ratio was assumed. Payne (1997) made the same assumption due to the difficulty in quantifying the affect of the free surface on the lift and drag of a hydrofoil whilst moving in an orbital velocity wave field. A constant submergence ratio of 0.3835, which was determined from calm water analysis, was used in the calculation.

The drag coefficient is calculated using foil theory given in appendix B. The resultant lift and drag in the vertical and horizontal direction in an orbital velocity wave field is shown by equation 4.17 and 4.18 respectively.

$$L = \frac{1}{2} \rho U^2 S F(q) (C_L \cos \psi + C_D \sin \psi) \quad (4.17)$$

$$D = \frac{1}{2} \rho U^2 S F(q) (-C_L \sin \psi + C_D \cos \psi) \quad (4.18)$$



Where:

- $F(q)$ is the lift deficiency function to account for the unsteady wake of vorticity proposed by Payne (1997) and described in section 2.1.

q is the reduced frequency defined by equation 4.19.

$$q = \omega_e c_w / 2u_o \quad (4.19)$$

The equations of motion for the Hysucat are derived from Newton's second law of motion by summing the forces in the vertical direction as well as the moments around the LCG. Only the dynamics of the hull around the steady-state planing condition are shown for brevity.

Equation 4.20 represents the equation of motion of the Hysucat in the vertical direction.

$$F_o \zeta_o \sin(\omega_e t) - k_z z_h - b_z \dot{z}_h + \frac{1}{2} \rho S_{mf} F(q) U_{mf}^2 [C_{L_{mf}} \cos \psi_{mf} + C_{D_{mf}} \sin \psi_{mf}] + \frac{1}{2} \rho S_{tf} F(q) U_{tf}^2 [C_{L_{tf}} \cos \psi_{tf} + C_{D_{tf}} \sin \psi_{tf}] = (m_h + m_a) \ddot{z}_h \quad (4.20)$$

CHAPTER 4: Hysucat Suspension System Modelling

The equation of motion for pitch is obtained by summing the moments around the LCG.

$$\begin{aligned}
 M_o \zeta_o \sin(\omega_e t) - b_\theta \dot{\theta}_h - k_\theta \theta_h + \frac{1}{2} \rho S_{mf} F(q) U_{mf}^2 l_{mf} [C_{Lmf} \cos \psi_{mf} \cos \theta_h + C_{Dmf} \sin \psi_{mf} \cos \theta_h] + \\
 \frac{1}{2} \rho S_{mf} F(q) U_{mf}^2 (l_{mf} \sin \theta_h + l_{VCG} \cos \theta_h) [-C_{Lmf} \sin \psi_{mf} + C_{Dmf} \cos \psi_{mf}] - \\
 \frac{1}{2} \rho S_{tf} F(q) U_{tf}^2 l_{tf} [C_{Ltf} \cos \psi_{tf} \cos \theta_h + C_{Dtf} \sin \psi_{tf} \cos \theta_h] - \\
 \frac{1}{2} \rho S_{tf} F(q) U_{tf}^2 (l_{tf} \sin \theta_h + l_{VCG} \cos \theta_h) [-C_{Ltf} \sin \psi_{tf} + C_{Dtf} \cos \psi_{tf}] = (I_h + I_a) \ddot{\theta}_h
 \end{aligned} \tag{4.21}$$

The subscripts *mf* and *tf* represent the main and trim hydrofoils respectively.

Equation 4.20 and 4.21 are non-linear equations which make them cumbersome to work with. A simpler model was derived by making the following assumptions.

- The lift has a much greater influence on the dynamics of the vessel in heave and pitch. The model is simplified by ignoring the drag forces.
- Using the small angle approximations for the cosine and sine terms. This is valid for normal vessel operation.
- The main foil force acts through the LCG and thus does not influence the pitch of the vessel.
- The unsteady wake of vorticity has little influence on lift, thus the lift deficiency function can be ignored.
- The relative velocity of the hydrofoil in water is mainly dependent on the forward velocity of the hydrofoil and vertical orbital velocity component of the waves and therefore the horizontal wave velocity can be ignored.

The lift of the foil was modelled according to Payne (1997) and is represented by equation 4.22.

$$L = \frac{1}{2} \rho u_o^2 S C_{L\alpha} \left[\theta_f + \frac{v_w - \dot{z}_f}{u_o} \right] \tag{4.22}$$

The constant η is defined by equation 4.23.

$$\eta = \frac{1}{2} \rho u_o S C_{L\alpha} \tag{4.23}$$

By making the above assumptions and simplifications, an LTI state-space model, given by equations 4.24 and 4.25, is derived. The non-linear equations, as well as the LTI model, were simulated in Matlab. The results with the experimental data are shown in figure 21.

CHAPTER 4: Hysucat Suspension System Modelling

$$\begin{pmatrix} \dot{z}_h \\ \ddot{z}_h \\ \dot{\theta}_h \\ \ddot{\theta}_h \end{pmatrix} = \underbrace{\begin{pmatrix} 0 & 1 & 0 & 0 \\ \frac{-k_z}{m_h+m_a} & \frac{-b_z-\eta_{mf}-\eta_{ff}}{m_h+m_a} & \frac{\eta_{mf}u_o+\eta_{ff}u_o}{m_h+m_a} & \frac{\eta_{ff}l_{ff}}{m_h+m_a} \\ 0 & 0 & 0 & 1 \\ 0 & \frac{\eta_{ff}l_{ff}}{I_h+I_a} & \frac{-k_\theta-\eta_{ff}u_o l_{ff}}{I_h+I_a} & \frac{-b_\theta-\eta_{ff}l_{ff}^2}{I_h+I_a} \end{pmatrix}}_{\mathbf{A}} \begin{pmatrix} z_h \\ \dot{z}_h \\ \theta_h \\ \dot{\theta}_h \end{pmatrix} + \underbrace{\begin{pmatrix} 0 & 0 & 0 \\ \frac{F_o}{m_h+m_a} & \frac{\eta_{mf}}{m_h+m_a} & \frac{\eta_{ff}}{m_h+m_a} \\ 0 & 0 & 0 \\ \frac{M_o}{I_h+I_a} & 0 & \frac{-\eta_{ff}l_{ff}}{I_h+I_a} \end{pmatrix}}_{\mathbf{B}} \begin{pmatrix} \zeta_o \sin(\omega_e t) \\ \omega \zeta_o \cos(\omega_e t) \\ \omega \zeta_o \cos(\omega_e t - k_w l_{ff}) \end{pmatrix} \quad (4.24)$$

$$\begin{pmatrix} z_h \\ \dot{z}_h \\ \theta_h \end{pmatrix} = \underbrace{\begin{pmatrix} 1 & 0 & 0 & 0 \\ \frac{-k_z}{m_h+m_a} & \frac{-b_z-\eta_{mf}-\eta_{ff}}{m_h+m_a} & \frac{\eta_{mf}u_o+\eta_{ff}u_o}{m_h+m_a} & \frac{\eta_{ff}l_{ff}}{m_h+m_a} \\ 0 & 0 & 1 & 0 \end{pmatrix}}_{\mathbf{C}} \begin{pmatrix} z_h \\ \dot{z}_h \\ \theta_h \end{pmatrix} + \underbrace{\begin{pmatrix} 0 & 0 & 0 \\ \frac{F_o}{m_h+m_a} & \frac{\eta_{mf}}{m_h+m_a} & \frac{\eta_{ff}}{m_h+m_a} \\ 0 & 0 & 0 \end{pmatrix}}_{\mathbf{D}} \begin{pmatrix} \zeta_o \sin(\omega_e t) \\ \omega \zeta_o \cos(\omega_e t) \\ \omega \zeta_o \cos(\omega_e t - k_w l_{ff}) \end{pmatrix} \quad (4.25)$$

Where A, B, C, D are the state-space representations.

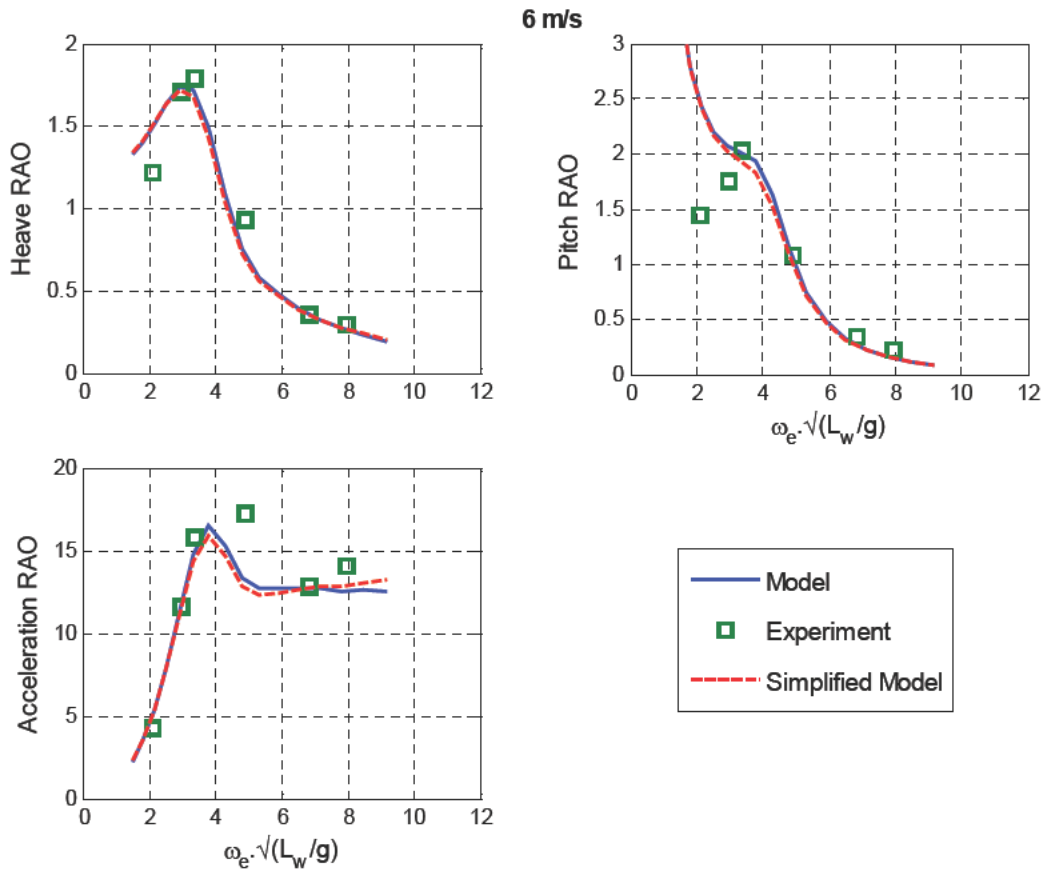


Figure 21: Hysucat simulation results

CHAPTER 4: Hysucat Suspension System Modelling

The model shows good correlation with the experimental results, especially for the heave and pitch at the higher normalised encounter frequencies. There is discrepancy between the simulation results and the acceleration RAO at the resonant frequency. The model overestimates the damping in the system. The same error obtained with the hull model, for the pitch RAO at low frequencies, is observed. The cause of this error was explained in the previous section.

The purpose of the Hysucat model was to investigate the accuracy of the modelling technique and to determine if such a model could be derived for the suspension system concepts. The results show that the model is good enough to represent the dynamics of the Hysucat.

The final two concepts, discussed in section 3.4, had to be modelled to investigate their dynamics and feasibility. Their modelling is discussed in the following section.

4.3 Vertical Suspension System

The first concept was the vertical suspension system with a spring-damper mounted in the tunnel wall of the Hysucat hull. A similar approach used for the Hysucat was used to model the seakeeping dynamics of the concept. The force diagram is shown in figure 22.

The foil moves up and down in response to the orbital wave motion. The forces transmitted to the hull are damped out by the spring-damper system.

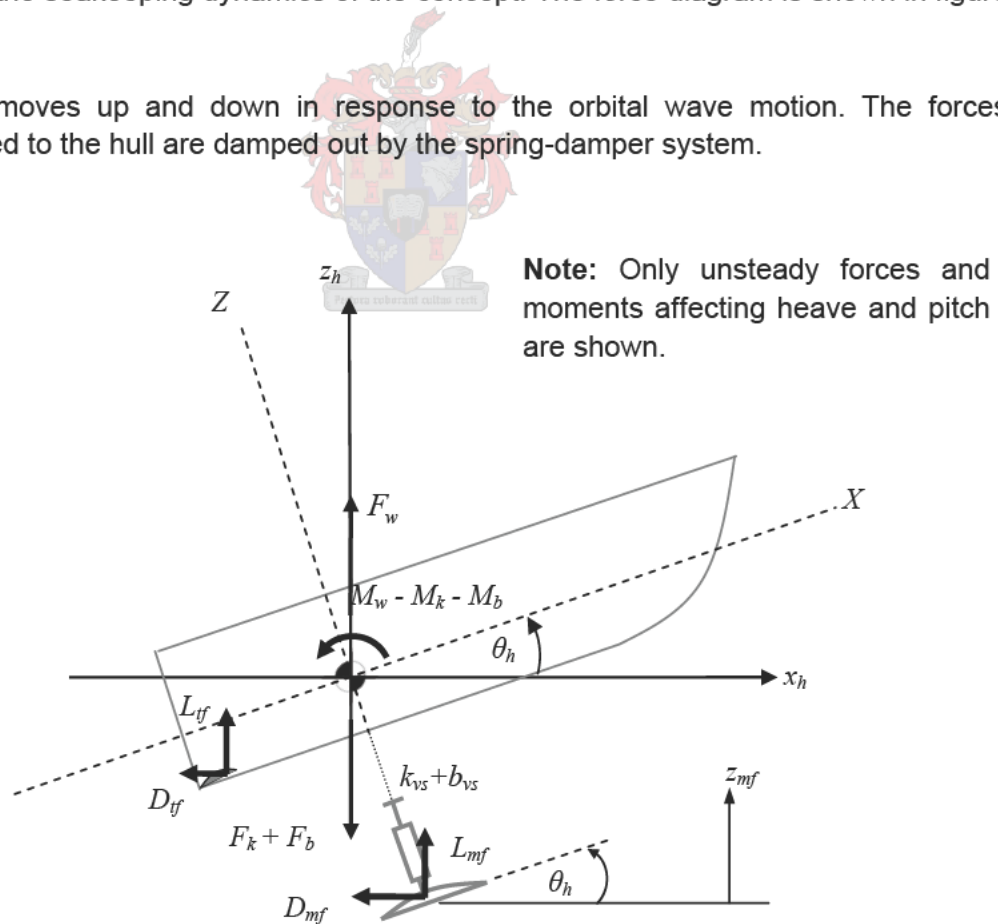


Figure 22: Concept 1: Vertical suspension system force diagram

CHAPTER 4: Hysucat Suspension System Modelling

An important aspect is the stroke of the spring and damper as well as the initial displacement of the suspension system limited by the calm water operating conditions. The calm water analysis is discussed in the following section.

4.3.1 Calm Water Analysis

The hydrofoil will initially have to be located below the keel. As the velocity of the vessel increases, the lift on the hydrofoil will increase and the hydrofoil will start moving up towards the keel. This will result in an increase in drag of the entire system.

The position of the hydrofoil at the design speed will be the same as the hydrofoil on the Hysucat with rigidly attached hydrofoils. Migeotte (2007) performed analysis using proprietary software to determine the calm water operating values for the full scale hull at the design speed of 16.6 m/s (32 knots). The calm water results are shown in appendix C. The calm water operating parameters were then combined with hydrofoil theory presented in appendix B to calculate the calm water lift and drag coefficients.

Figure 23 shows spring stiffness as a function of the initial displacement of the hydrofoil below the keel line. The stiffness has an allowable range depending on the initial displacement of the hydrofoil.

The analysis was done for initial displacements of between 0 and 0.08 m. The initial displacement had to be minimised to reduce the drag of the overall system.

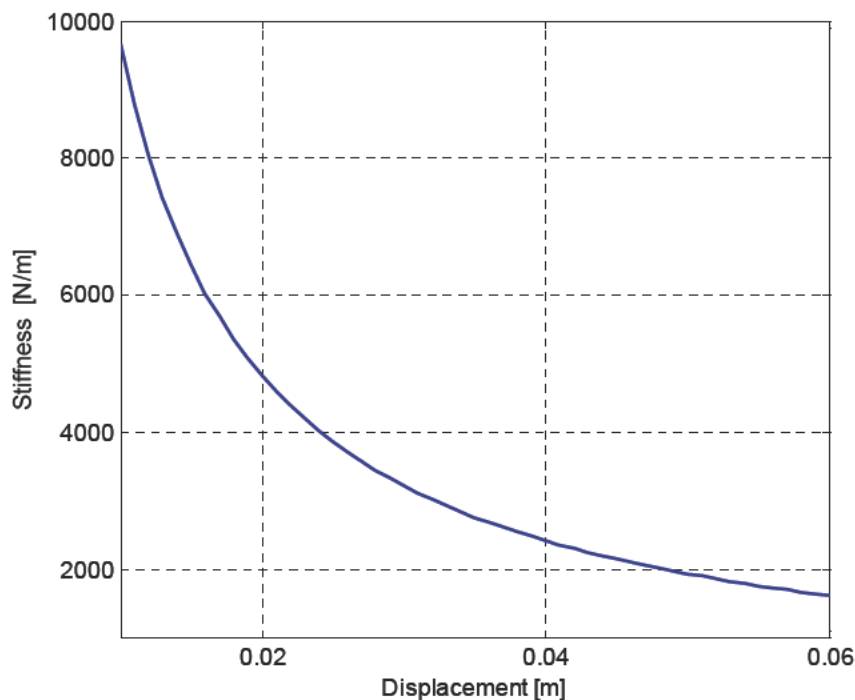


Figure 23: Spring stiffness for various initial displacements

CHAPTER 4: Hysucat Suspension System Modelling

Figure 23 indicates that there is an inverse relationship between the spring stiffness and the initial displacement of the spring. The range of spring stiffness that is available for the design is between 2 and 8 kN/m. The dynamics of the suspension system in an orbital velocity wave field are evaluated in the following section.

4.3.2 Seakeeping Analysis

The lift and drag forces acting on the hydrofoil are calculated using equations 4.17 and 4.18 respectively. The equations of motion for the concept were derived using Newton's second law of motion.

Equation 4.26 describes the motion of the Hysucat with the vertical suspension system.

$$F_o \zeta_o \sin(\omega_e t) - k_z z_h - b_z \dot{z}_h + k_{vs} (z_{mf} - z_h) (\cos \theta_h)^2 + b_{vs} (\dot{z}_{mf} - \dot{z}_h) (\cos \theta_h)^2 + \frac{1}{2} \rho S_{yf} F(q) U_{yf}^2 [C_{L_{yf}} \cos \psi_{yf} + C_{D_{yf}} \sin \psi_{yf}] = (m_h + m_a) \ddot{z}_h \quad (4.26)$$

Where:

- b_{vs} is the damping coefficient of the suspension system;
- k_{vs} is the spring stiffness coefficient of the suspension system.

The pitch motion of the vessel is described by equation 4.27.

$$M_o \zeta_o \sin(\omega_e t) - b_\theta \dot{\theta}_h - k_\theta \theta_h - \frac{I}{2} \rho S_{yf} F(q) U_{yf}^2 l_{yf} [C_{L_{yf}} \cos \psi_{yf} \cos \theta_h + C_{D_{yf}} \sin \psi_{yf} \cos \theta_h] - \frac{I}{2} \rho S_{yf} F(q) U_{yf}^2 (l_{yf} \sin \theta_h + l_{VCG} \cos \theta_h) [-C_{L_{yf}} \sin \psi_{yf} + C_{D_{yf}} \cos \psi_{yf}] = (I_h + I_a) \ddot{\theta}_h \quad (4.27)$$

The vertical motion of the hydrofoil is described by equation 4.28.

$$\frac{1}{2} \rho S_{mf} F(q) U_{mf}^2 [C_{L_{mf}} \cos \psi_{mf} + C_{D_{mf}} \sin \psi_{mf}] - k_{vs} (z_{mf} - z_h) - b_{vs} (\dot{z}_{mf} - \dot{z}_h) = (m_{mf} + m_{a_{mf}}) \ddot{z}_{mf} \quad (4.28)$$

The above equations were simplified using the same assumptions from section 4.2. The simplified state-space equations are represented by equation 4.29 and 4.30.

CHAPTER 4: Hysucat Suspension System Modelling

$$\begin{pmatrix} \dot{z}_h \\ \ddot{z}_h \\ \dot{z}_{mf} \\ \ddot{z}_{mf} \\ \dot{\theta}_h \\ \ddot{\theta}_h \end{pmatrix} = \begin{matrix} \text{A} \\ \begin{pmatrix} 0 & 1 & 0 & 0 & 0 & 0 \\ \frac{-k_z - k_{vs}}{m_h + m_a} & \frac{-b_z - b_{vs} - \eta_{vf}}{m_h + m_a} & \frac{k_{vs}}{m_h + m_a} & \frac{b_{vs}}{m_h + m_a} & \frac{\eta_{vf} u_o}{m_h + m_a} & \frac{\eta_{vf} l_{vf}}{m_h + m_a} \\ 0 & 0 & 0 & 1 & 0 & 0 \\ \frac{k_{vs}}{m_{mf}} & \frac{b_{vs}}{m_{mf}} & \frac{-k_{vs}}{m_{mf}} & \frac{-b_{vs} - \eta_{mf}}{m_{mf}} & \frac{\eta_{mf} u_o}{m_{mf}} & \frac{k_{vs}}{m_{mf}} \\ 0 & 0 & 0 & 0 & 0 & 1 \\ 0 & \frac{\eta_{vf} l_{vf}}{I_h + I_a} & 0 & 0 & \frac{-k_\theta - \eta_{vf} u_o l_{vf}}{I_h + I_a} & \frac{-b_\theta - \eta_{vf} l_{vf}^2}{I_h + I_a} \end{pmatrix} \end{matrix} \begin{matrix} \text{B} \\ \begin{pmatrix} 0 & 0 & 0 \\ \frac{F_o}{m_h + m_a} & 0 & \frac{\eta_{vf}}{m_h + m_a} \\ 0 & 0 & 0 \\ 0 & \frac{\eta_{vf}}{m_{mf}} & 0 \\ 0 & 0 & 0 \\ \frac{M_o}{I_h + I_a} & 0 & \frac{-\eta_{vf} l_{vf}}{I_h + I_a} \end{pmatrix} \end{matrix} \begin{pmatrix} z_h \\ \dot{z}_h \\ z_{mf} \\ \dot{z}_{mf} \\ \theta_h \\ \dot{\theta}_h \end{pmatrix} + \begin{pmatrix} \zeta_o \sin(\omega_e t) \\ \omega \zeta_o \cos(\omega_e t) \\ \omega \zeta_o \cos(\omega_e t - k_w l_{vf}) \end{pmatrix} \tag{4.29}$$

$$\begin{pmatrix} z_h \\ \dot{z}_h \\ z_{mf} \\ \dot{z}_{mf} \\ \theta_h \\ \dot{\theta}_h \end{pmatrix} = \begin{matrix} \text{C} \\ \begin{pmatrix} 1 & 0 & 0 & 0 & 0 & 0 \\ \frac{-k_z - k_{vs}}{m_h + m_a} & \frac{-b_z - b_{vs} - \eta_{vf}}{m_h + m_a} & \frac{k_{vs}}{m_h + m_a} & \frac{b_{vs}}{m_h + m_a} & \frac{\eta_{vf} u_o}{m_h + m_a} & \frac{\eta_{vf} l_{vf}}{m_h + m_a} \\ 0 & 0 & 0 & 0 & 1 & 0 \end{pmatrix} \end{matrix} \begin{matrix} \text{D} \\ \begin{pmatrix} 0 & 0 & 0 \\ \frac{F_o}{m_h + m_a} & 0 & \frac{\eta_{vf}}{m_h + m_a} \\ 0 & 0 & 0 \end{pmatrix} \end{matrix} \begin{pmatrix} z_h \\ \dot{z}_h \\ z_{mf} \\ \dot{z}_{mf} \\ \theta_h \\ \dot{\theta}_h \end{pmatrix} + \begin{pmatrix} \zeta_o \sin(\omega_e t) \\ \omega \zeta_o \cos(\omega_e t) \\ \omega \zeta_o \cos(\omega_e t - k_w l_{vf}) \end{pmatrix} \tag{4.30}$$

The above equations were implemented in Matlab. The results of the simulations are shown in figure 24.

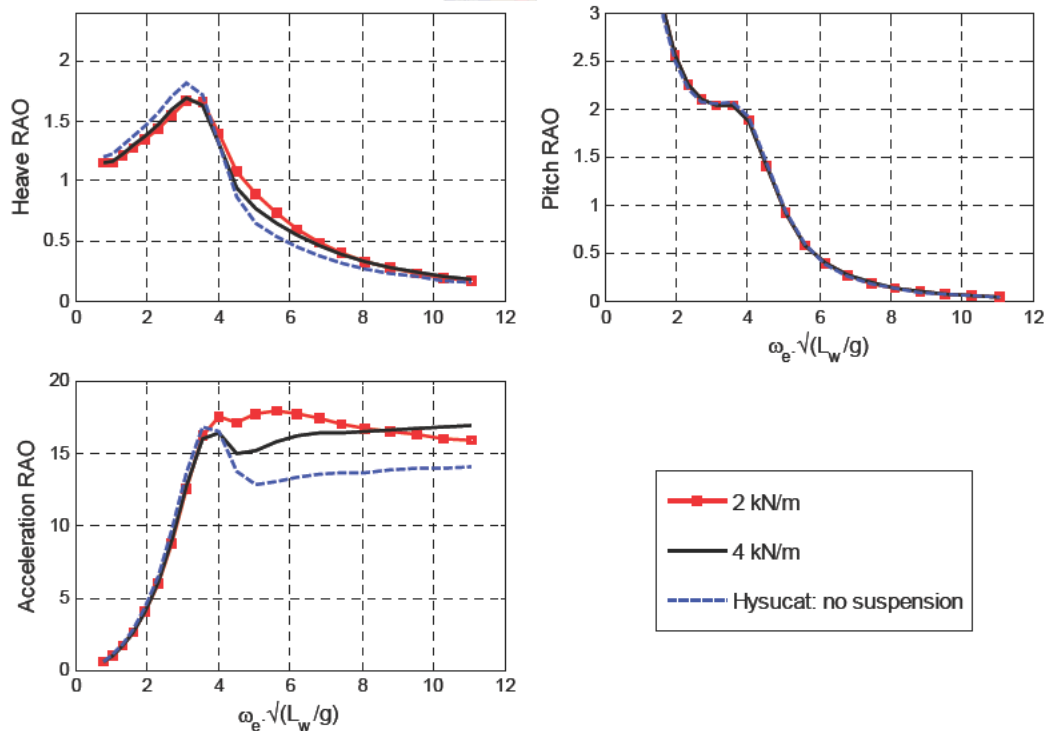


Figure 24: Simulation results with different spring stiffness

CHAPTER 4: Hysucat Suspension System Modelling

The results show that there is an reduction in the peak heave response with the suspension system. The vertical acceleration is the same as for the Hysucat up to the resonant frequency after which it is considerably worse.

The simulation model indicated that there would not be enough stroke available to effectively damp out any of the vertical accelerations. Various damping values were simulated and no real improvement was obtained with the results.

The modelling of the torsional suspension system is discussed in the following section.

4.4 Torsional Suspension System

The second concept that was generated was the torsional suspension system that utilised variation in the angle of attack and vertical motion of the main hydrofoil to dampen out the transmitted forces to the demi-hulls of the Hysucat. The hydrofoil is located at the end of a spring loaded arm that pivots in response to orbital wave motion. A force diagram of the torsional suspension system concept is shown in figure 25.

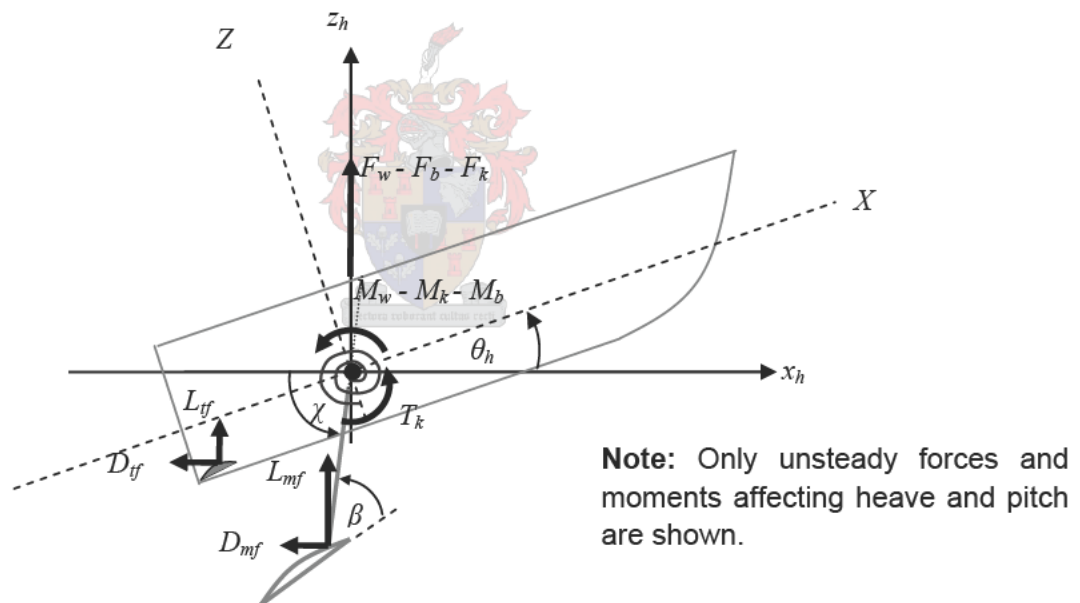


Figure 25: Concept 2: Torsional suspension system

The concept is modelled as a hydrofoil attached to the LCG of the hull with a spring loaded pivot arm. The variations in hydrofoil lift and drag cause the hydrofoil to pivot around the LCG changing the relative angle of attack.

The concept had to satisfy the calm water operating conditions. The foil lift will increase with increase in velocity. The pivot arm's inclination angle χ will decrease and the arm will move up in line with the keel as the velocity of the vessel increases. The following section analyses the calm water operating conditions for the torsional suspension system concept.

CHAPTER 4: Hysucat Suspension System Modelling

4.4.1 Calm Water Operation

An important aspect in the design of the torsional suspension system was the calm water operating conditions of the Hysucat. The optimal configuration for the suspension system in waves might not be the best in calm water.

The stiffness of the spring had to satisfy the calm water running conditions of the craft for the entire speed range. The lift and drag forces acting on the hydrofoil are dependent on the velocity of the vessel as well as the angle of attack of the foil. Changing the stiffness would thus affect the angle of attack of the hydrofoil, depending on the vessel speed. The suspension system configuration allows for a large angle of attack at low speeds which decreases as the Hysucat velocity increases due to the variation in lift.

In calm water the hydrofoil should have the same angle of attack as for the rigid Hysucat system at the design speed. The suspension system would then operate around this point in waves. The Hysucat calm water operating conditions were calculated by Migeotte (2007). If we ignore the effects of the orbital waves the steady-state lift for the hydrofoil system in figure 25 is calculated using equation 4.31.

$$L_{mf} = \frac{l}{2} \rho u_o^2 S_{mf} C_{L\alpha} (\chi - \beta - \alpha_o + \Delta\alpha_o) \quad (4.31)$$

Where:

- χ is the arm angle of the suspended foil;
- β is the angle between the pivot arm and the foil;
- α_o is the zero lift angle of attack;
- $\Delta\alpha_o$ is the zero lift angle of attack correction angle.

The torque acting on the pivot point as a result of the foil forces is given by equation 4.32.

$$T_k = l_a [L_{mf} \cos \chi + D_{mf} \sin \chi] \quad (4.32)$$

Where:

- l_a is the arm length;
- χ is the angle of the pivot arm with the horizontal axis.

To satisfy the calm water trim condition the stiffness of the spring is calculated using equation 4.33.

$$k_{is} = \frac{l_a [L_{mf} \cos \chi + D_{mf} \sin \chi]}{[\theta_{ho} - \chi + \chi_o]} \quad (4.33)$$

Where:

- χ_o is the initial arm displacement;

CHAPTER 4: Hysucat Suspension System Modelling

- k_{ts} is the torsional spring stiffness;
- θ_{ho} is the running trim of the vessel.

The spring stiffness must be chosen to satisfy the calm water conditions as well as damp out vertical accelerations. The stiffness also depends on the initial displacement of the hydrofoil arm.

Most Hysucats are designed so that 40% to 60% lift is achieved from the main hydrofoil at the design speed. The stiffness would thus have to be chosen so that as the velocity of the hydrofoil tends towards the design speed, the angle of the hydrofoil will reach the design calm water angle of attack relative to the hull. This in effect would make it the same as normal Hysucat with rigidly fixed hydrofoils.

The design speed of the model for this Hysucat configuration was 6 m/s (32 knots). If we plot equation 4.33 we obtain the hydrofoil lift as a function of the spring stiffness for various initial angles of attack.

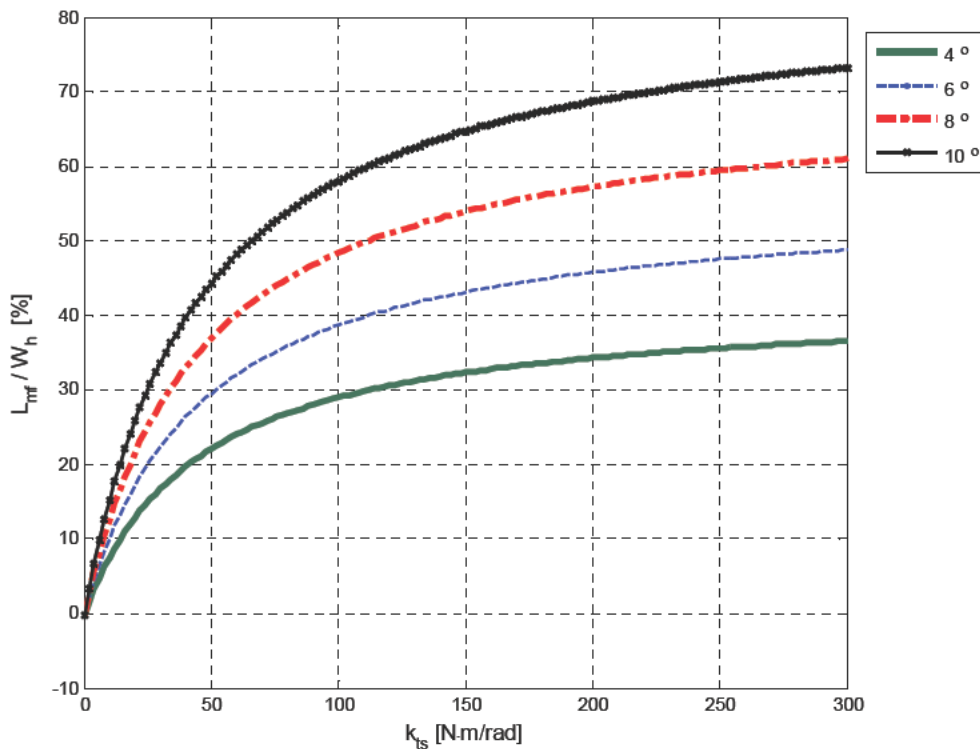


Figure 26: Foil lift for varying spring stiffness ($u_o = 6$ m/s, $\theta_{ho} = 2.023^\circ$, $l_a = 0.75 c$)

It is evident from figure 26 that the stiffer the spring is the less the variation in lift from the main foil. As the stiffness of the spring increases the initial displacement would have to decrease if the calm water conditions are to be satisfied.

The equations of motion for the hull with the torsional suspension system in an orbital velocity wave field are derived in the following section.

CHAPTER 4: Hysucat Suspension System Modelling

4.4.2 Seakeeping Analysis

The up-flow angle of attack is dependent on the orbital wave motion as well as the motion of the hydrofoil itself. Figure 27 shows the variation in angle of attack as a result of the hydrofoil motion around the pivot point in the orbital velocity field.

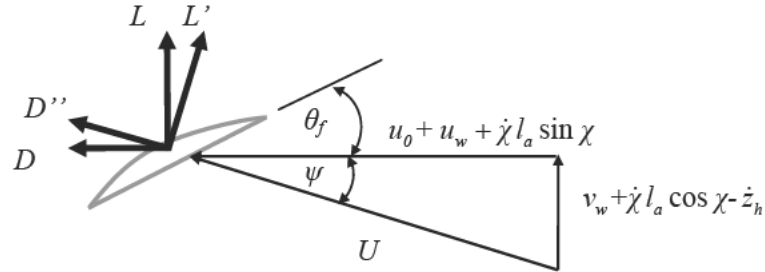


Figure 27: Suspended hydrofoil in orbital velocity field

The up-flow angle is calculated using equation 4.34.

$$\psi = \text{atan} \left(\frac{v_w + \dot{\chi} l_a \cos \chi - \dot{z}_h}{u_o + u_w + \dot{\chi} l_a \sin \chi} \right) \quad (4.34)$$

The resultant velocity is given by equation 4.35.

$$U^2 = (u_o + u_w + \dot{\chi} l_a \sin \chi)^2 + (v_w + \dot{\chi} l_a \cos \chi - \dot{z}_h)^2 \quad (4.35)$$

The lift and drag forces are calculated with equation 4.17 and 4.18 using the up-flow angle and resultant velocity described by equations 4.34 and 4.35 respectively.

The motion for the foil on the support arm rotating around the pivot point is described by equation 4.36.

$$T_k - l_a (L_{mf} \cos \chi + D_{mf} \sin \chi) = \ddot{\chi} (I_{mf} + I_q) \quad (4.36)$$

Where:

- T_k is the torque applied to pivot point by the torsion spring;
- I_{mf} is the moment of inertia of the foil system around the pivot point;
- I_q is the added moment of inertia of the foil system around the pivot point.

According to Payne (1997) the added inertia can be calculated using equations (19) and (20) in Payne (1997).

To calculate the forces transmitted to the hull, an approach similar to Payne (1997) was followed. Equations 4.37 and 4.38 represent the final equations.

CHAPTER 4: Hysucat Suspension System Modelling

$$L_{hull} = \frac{T_k}{l_a} \cos \chi + (L_{mf} - W_w) \sin^2 \chi - D_{mf} \sin \chi \cos \chi - m_{mf} l_a \dot{\chi}^2 \sin \chi \quad (4.37)$$

$$D_{hull} = \frac{T_k}{l_a} \cos \chi - (L_{mf} - W_w) \sin \chi \cos \chi + D_{mf} \cos^2 \chi + m_{mf} l_a \dot{\chi}^2 \cos \chi \quad (4.38)$$

Equations 4.37 and 4.38 were first simulated with the hydrofoils connected to a lumped mass that was free to heave in an orbital velocity wave field. This was used to determine how effective a torsion spring would be in damping out vertical transmitted forces. The lumped mass models were simulated with the same mass as the scale model in 0.04 m sinusoidal waves at 6 m/s. This is the same height that will eventually be tested with the scale hull in the towing tank. The arm length of the pivot was set at 75% of the chord length of the foil.

The stiffness of the torsion spring was chosen using figure 26 using a lift ratio of 43%. Three stiffness values, 44, 66 and 126 N·m/rad were simulated which corresponds to initial angles of attack of 10, 8 and 4° respectively. The results for the simple lumped mass models with and without suspension in an orbital velocity field are shown in figure 28.

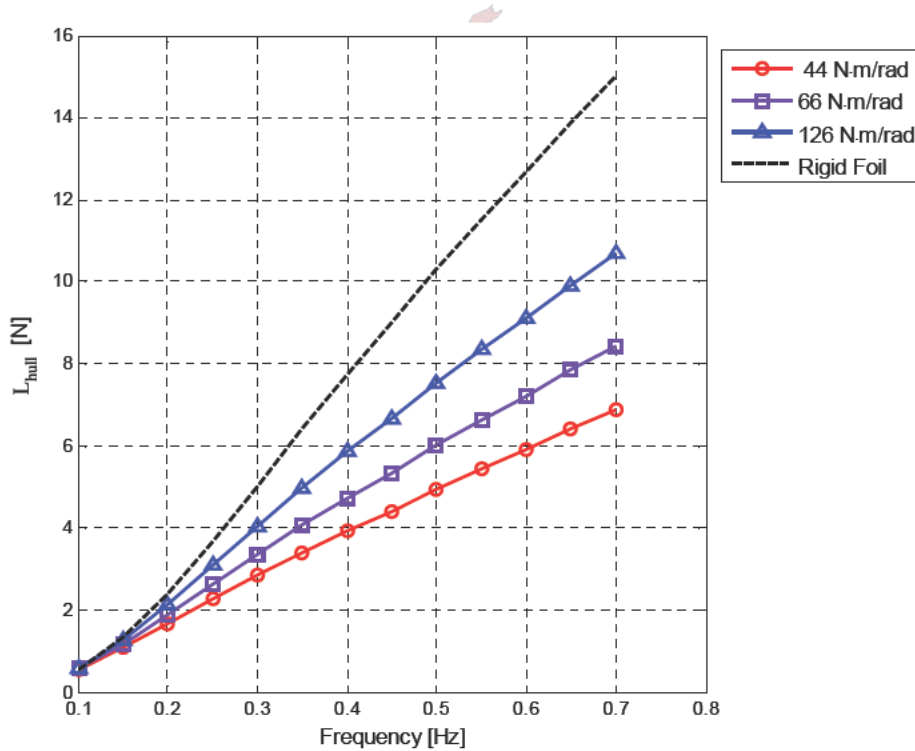


Figure 28: Hydrofoil lift for lumped mass model ($u_o = 6$ m/s, $\zeta_o = 0.04$ m)

The suspended foil was combined with the complete hull model derived in section 4.1 and shown in figure 25.

CHAPTER 4: Hysucat Suspension System Modelling

The equation of motion derived from Newton's second law of motion is given by equation 4.39.

$$F_o \zeta_o \sin(\omega_e t) - k_z z_h - b_h \dot{z}_h + \gamma_{yf} U_{yf}^2 [C_{L_{yf}} \cos \psi_{yf} + C_{D_{yf}} \sin \psi_{yf}] + \frac{k_{ts}(\theta_h - \chi)}{l_a} \cos \chi + (L_{mf} - W_w) \sin^2 \chi - D_{mf} \sin \chi \cos \chi - m_{mf} l_a \dot{\chi}^2 \sin \chi = (m_h + m_a) \ddot{z}_h \quad (4.39)$$

The equation of motion for the pitch of the vessel is given by equation 4.40.

$$M_o \zeta_o \sin(\omega_e t) - b_\theta \dot{\theta}_h - k_\theta \theta_h - \gamma_{yf} U_{yf}^2 l_{yf} [C_{L_{yf}} \cos \psi_{yf} \cos \theta_h + C_{D_{yf}} \sin \psi_{yf} \cos \theta_h] - \gamma_{yf} U_{yf}^2 (l_{yf} \sin \theta_h + l_{VCG} \cos \theta_h) [-C_{L_{yf}} \sin \psi_{yf} + C_{D_{yf}} \cos \psi_{yf}] = (I_h + I_a) \ddot{\theta}_h \quad (4.40)$$

The equation of motion for the pivot arm is represented by equation 4.41.

$$k_{ts}(\theta_h - \chi) - l_a [(L_{mf} - W_w) \cos \chi + D_{mf} \sin \chi] = \ddot{\chi} (I_{mf} + I_q) \quad (4.41)$$

The above non-linear equations were simulated using Simulink. The same inputs as for the other models were used. The results are shown in figure 29.

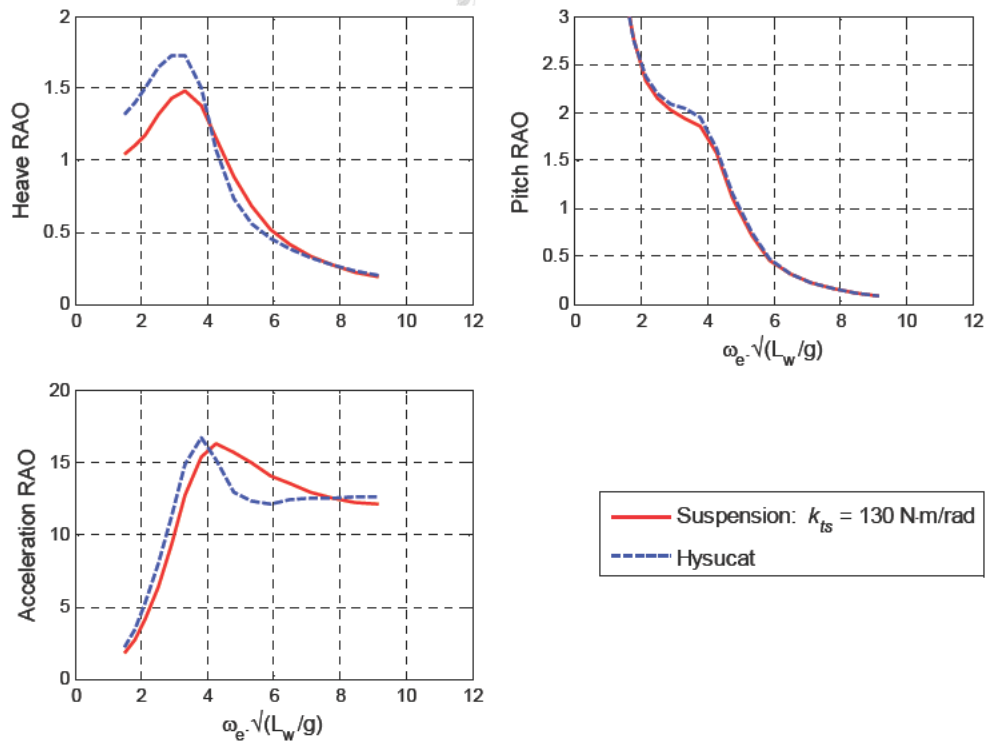


Figure 29: Torsion suspension modelling results ($u_o = 6$ m/s, $I_a = 0.75$ c)

The results show that improvements can be achieved with the torsional suspension system especially for the heave RAO. The pitch RAO does not show much difference

CHAPTER 4: Hysucat Suspension System Modelling

between the Hysucat and the suspended foil. This is due to the arm pivot point being modelled as if it were located on the LCG of the vessel.

At lower frequencies a slight improvement is noticeable on the acceleration RAO, however is considerable worse at the natural frequency of the system. It is evident however from the hull and Hysucat modelling that the acceleration RAO is inaccurate at the higher frequencies. The foil forces at the higher frequencies cannot be modelled that accurately.

The model was also simulated with various torsional damping values. Most of the reduction in transmitted acceleration is achieved through the variation in angle of attack as this is the crucial factor for the concept.

4.5 Discussion and Conclusions

The modelling of the Hysucat and the two concepts was discussed. The models were derived from experimental data using parameter estimation. The model for the planing catamaran demi-hulls was combined with hydrofoil theory to derive the models for the Hysucat and the two concepts using Newton's second law of motion.

The hull and Hysucat simulation models showed good comparison to the experimental data obtained for the Hysucat with and without foils and thus showed that such an experimental based approach can be used to obtain a model for the system. Inaccuracies were obtained for the pitch at low frequencies as well as the acceleration at the higher wave encounter frequencies.

The following conclusions can be made from the suspension system modelling:

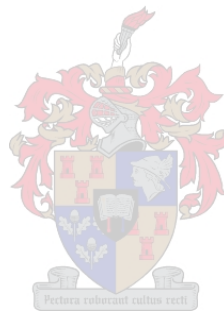
- The simulation results for the vertical suspension system indicate that little reduction is achieved using such a system as the stroke available is limited by the Hysucat configuration as well as the calm water operating limits.
- The acceleration RAO for the vertical suspension system is worse at all the normalised encounter frequencies.
- The torsional suspension system shows that reduction in heave is achievable.
- The torsional suspension system acceleration RAO results show some reduction at low frequencies however shows an increase in accelerations at the natural frequency.
- The simplified models achieved almost identical results as the non-linear models. The simplified models are sufficiently accurate to use for further design and analysis.

The simulation results showed that the vertical suspension concept was not feasible and would not be effective in damping out the transmitted forces. The

CHAPTER 4: Hysucat Suspension System Modelling

torsional suspension system model indicated that reductions in heave would be possible as well as reductions in accelerations at low encounter frequencies. The model showed a worse acceleration response at the higher frequencies. However, the hull and Hysucat model both indicated that the acceleration modelling at high frequencies was unreliable.

It was thus decided that the torsional suspension system concept would be investigated further through experimental testing.



CHAPTER 5: DESIGN AND EXPERIMENTAL TESTING

The modelling of the Hysucat and the two concepts was discussed in the previous chapter. The modelling showed that the torsional suspension system concept was the most effective in improving the seakeeping of the Hysucat. The torsional suspension system would therefore be investigated further through experimental testing. This chapter discusses the experimental procedure and setup that was used to test the torsional suspension system design and the results that were obtained.

The design of the scale suspension system is discussed in the following section.

5.1 Scale Model with Torsional Suspension System

A suspension system for the scale model was manufactured so that the dynamics and hydrodynamics of the Hysucat suspension system could be evaluated and to determine the response for the different suspension configurations. The seakeeping of the full scale hull could be evaluated by analysing the response of the scale model. The model would therefore have to resemble the final design so that the hydrodynamics could be evaluated.

The scale CAD model is shown in figure 30. The figure shows one of the demi-hulls with the fitted hydrofoils. An assembly drawing of the Hysucat with suspension system is included in appendix A.

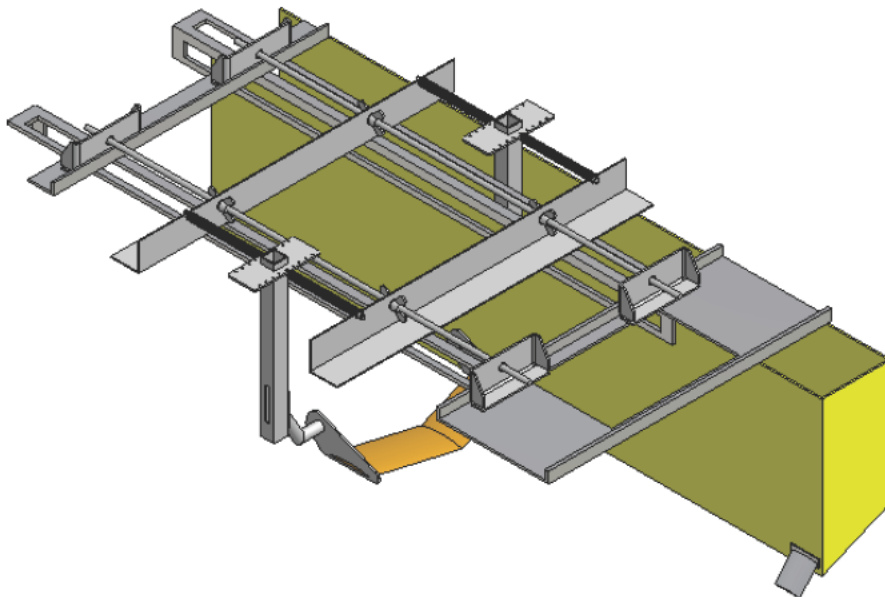


Figure 30: Torsional suspension system for model Hysucat

The suspension system for the scale model was manufactured from aluminium to prevent corrosion and to minimise weight. The mass of the hull with the suspension

Chapter 5: Design and Experimental Testing

system was maintained the same as the Hysucat with and without fitted foils in order to obtain comparable data so that evaluations could be made between the various hull configurations.

The main hydrofoil was mounted on side brackets in the tunnel of the hull. The side brackets guide the flow over the hydrofoil and prevent flow separation which would result in loss of lift and an increase in resistance.

The torsion spring was simulated by using tension coil springs mounted above the hull model. The springs were mounted on adjustable brackets so that the pretension in the springs could be adjusted to meet the calm water requirements. The stiffness was varied by adding and removing the tension springs that were mounted parallel to one another on the adjustable brackets.

The stiffness of the springs was chosen from data obtained using the simulation model developed in chapter 4. The coil springs were designed so that the three torsion spring stiffness values could be simulated with different configurations of the coil springs. The three torsion spring stiffness values were 37, 74 and 148 N·m/rad. The design of the springs is shown in appendix C.

The experimental procedures and setup used to obtain the Hysucat data and to test the suspension system are discussed in the following section.

5.2 Experimental Validation

The experiments were conducted according to the International Towing Tank Convention (ITTC) guidelines: *ITTC – Recommended Procedures, High Speed Marine Vehicles, 7.5-02-05*.

The 90 m towing tank at the University of Stellenbosch was used to conduct the experiments. The tank is 4.2 m wide, 2.7 m deep and is equipped with a self propelled trolley that is used to tow the scale models. The maximum speed of the trolley is 8.2 m/s which makes it ideally suited for testing hulls at planing Froude numbers. Figure 31 shows the towing tank and the trolley.

The models were towed at 4, 5 and 6 m/s, corresponding to the desired Froude numbers of 2.4, 3 and 3.6 respectively. The trolley is equipped with 5 sensors that are used to record the experimental data. The sensor specifications are listed in table 4.

Chapter 5: Design and Experimental Testing



Figure 31: Towing tank and trolley used for testing

Table 5: Measurement sensor specifications

Measured Value	Variable	Sensor	Specifications
Velocity	V	Tachometer	Telemecanique XCC HF7B50
Model Resistance	R_T	Load cell	HBM Inc RSCM-50kg-25152
Bow Trim	h_b	Coil displacement sensor	Micro-Epsilon WPS-750-Mk30-P
Stern Trim	h_s	Coil displacement sensor	Micro-Epsilon WPS-750-Mk30-P
Wave Height	ζ	Ultrasonic distance sensor	Senix TS-30S
Temperature	T	Analogue Thermometer	Germanow-Simon Co Tel-TRM

The trolley is fitted with spotlights to increase visibility during testing as well as a wind shield to reduce wind resistance effects on the model. The trim sensors, load cell and wave height sensor were calibrated before each series of tests commenced or when there were large changes in ambient temperature in the towing tank. The wave height sensor was very sensitive to temperature variations and had to be continuously recalibrated.

The trim sensors were calibrated by measuring the output voltages at 0 and 0.3 m extensions. The sensors showed a linear voltage output for the desired operating range. The zero offset of the calm water trim was measured when the vessel was stationary in calm water. The load cell was calibrated by attaching a 10 kg mass to the load cell and measuring the output voltages with and without load. The wave height calibration values were determined in a similar manner to the trim sensor by measuring the voltages at predetermined distances. The tachometers on the trolley wheels are pre-calibrated and thus did not require calibration before each series of tests.

The sensors are part of a data acquisition (DAQ) system. The signals from the sensors are fed to a signal conditioning box on the trolley which provides 0-10 V analogue outputs. A laptop was used to capture the data and to perform calibration conversions as well as initial post processing of the raw data. The laptop was fitted with a National

Chapter 5: Design and Experimental Testing

Instruments PCMCIA card. (NI DAQcard 6024-E). A LabVIEW program was written to capture the data as well as perform the initial post processing after each test run. The program is also being used for commercial work in the towing tank.

5.2.1 Towing Setup

Figure 32 shows the Hysucat scale model that was used for the tests. The model dimensions and parameters are shown in appendix A. The figure shows the model in 0.04 m waves at 5 m/s with the fitted torsional suspension system.

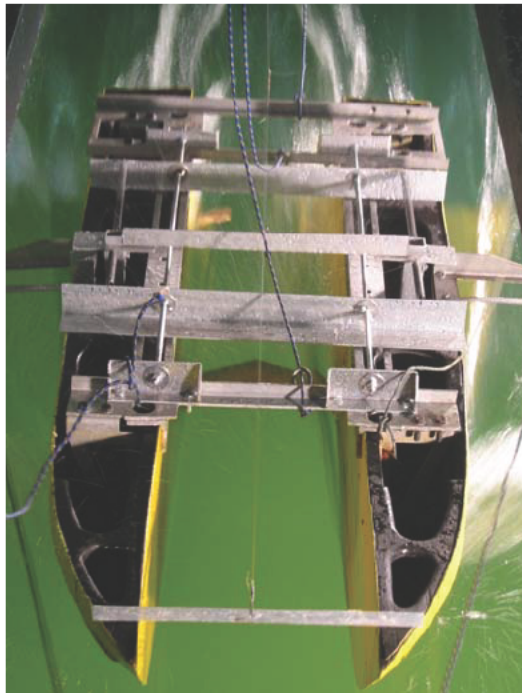


Figure 32: Scale model – Hys 1

Figure 33 shows the setup of all the apparatus and sensors for the towing tank tests.

The setup was the same for all the tests in order to obtain comparable data between the various hull configurations.

The model was towed with a towing point slightly forward and above the centre of gravity with a towing angle of 0 degrees. The towing position creates a forward moment around the LCG which simulates the moment created by the propeller uplift force. The wave height sensor is located forward of the bow. The model is towed with rope harness connected to a load cell. The ultrasonic wave height sensor is located in front of the model and records the wave height during each test.

Chapter 5: Design and Experimental Testing

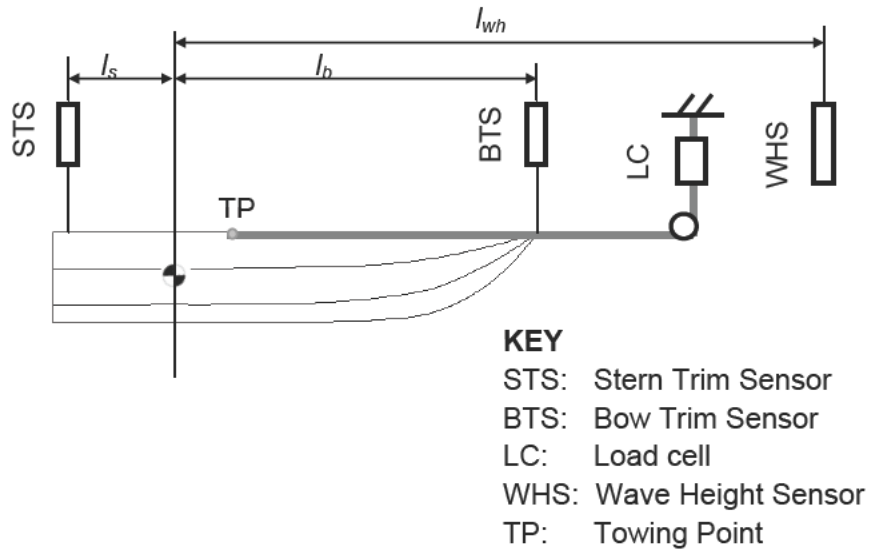


Figure 33: Towing setup

5.2.2 Wave Generation

The towing tank is equipped with a wave generator at the far end of the tank that is able to generate regular sinusoidal head waves. The wave generator produces waves by means of cyclical air pressure on the water surface controlled by a rotating choke valve. The wave generator is shown in figure 34.



Figure 34: Wave generator

Chapter 5: Design and Experimental Testing

The range of frequencies available in the tank ranges from 0.2 Hz to 1 Hz. The wave frequencies used to determine the frequency response curves were derived from the wave height sensor. The method used to determine the wave frequencies is discussed in section 5.3.

A shortcoming of the wave generator is that the wave height is frequency dependent and cannot be independently controlled. This made it difficult to investigate the linearity of the hull response in waves. The highest waves are generated at the mid frequency range. The frequency of the waves cannot be set accurately which limits the repeatability of the results.

5.3 Post Processing

For each test run the following steps were followed to process the experimental data.

1. The data from all 5 sensors was measured for each run. The towing trolley accelerates to the set velocity and maintains the required velocity until the trolley is stopped by the operator upon which it decelerates to a standstill. After each run the measured voltages are converted with the calibration values and the steady-state data is cropped as the data from the acceleration and deceleration phase is not required.
2. The velocity was obtained by averaging the velocity data obtained for each test run.
3. The wave height sensor is located in front of the bow of the hull therefore the wave height measured was not that experienced by the LCG of the hull. The wave height data was shifted with a time delay calculated using equation 5.1.

$$t_d = l_{wh} / u_o \quad (5.1)$$

4. The measured bow and stern displacements were then used to calculate the heave and pitch of the hull at the LCG. The heave and pitch were calculated using equation 5.2 and 5.3 respectively.

$$z_h = \left(\frac{h_b l_s}{l_b + l_s} \right) + \left(\frac{h_s l_b}{l_b + l_s} \right) - h_o \quad (5.2)$$

$$\theta_h = \text{asin} \left(\frac{h_b - h_s}{l_b + l_s} \right) \quad (5.3)$$

5. The RMS values of the measured pitch and heave as well as the wave height were obtained from a Power Spectral Density (PSD) calculation on the experimental data. The PSD was performed using a single Hanning window with no overlap and a 95% confidence level. The PSD gave the energy per

Chapter 5: Design and Experimental Testing

measured frequency of the recorded data. Figure 35 shows a PSD of the measured wave height, heave and pitch.

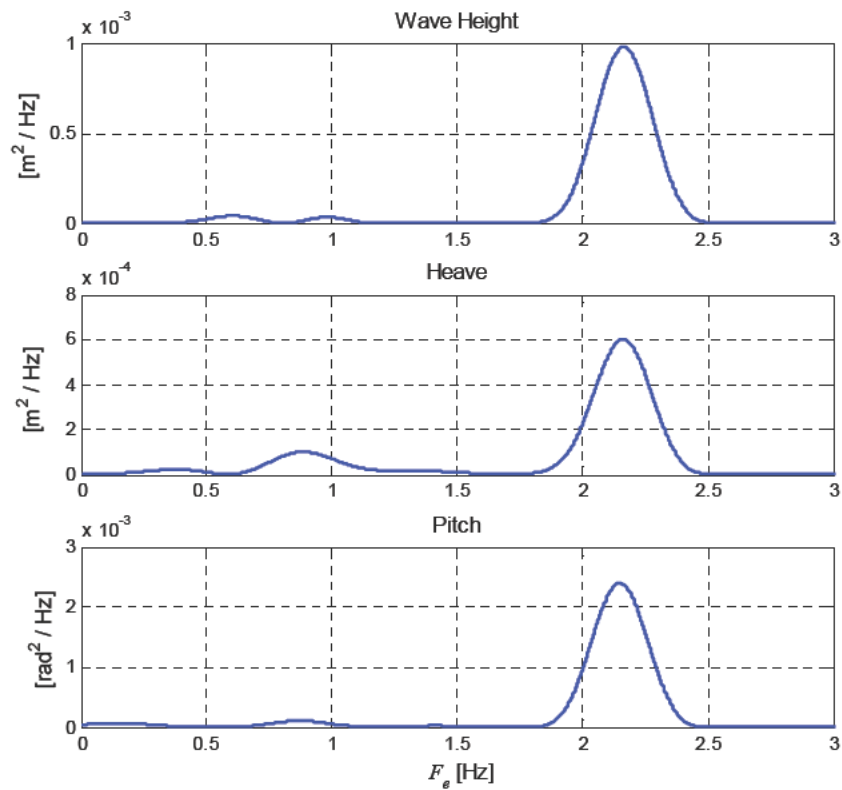


Figure 35: PSD of experimental data

The RMS values were obtained from the PSD data by measuring the area of the dominant frequency in the system corresponding to the encounter frequency of the wave height data. The PSD was also used to obtain the frequency of the waves as they were not able to be set accurately.

6. The pitch and heave RAOs were calculated by dividing the heave and pitch RMS values with the wave height RMS value at each encounter frequency. The encounter frequencies were normalised by multiplying with $\sqrt{L_w/g}$.
7. The resistance for each test run was measured. The added resistance was measured by subtracting the calm water resistance from the mean resistance in waves.

The above steps were done for the Hysucat with and without rigidly attached hydrofoils and the suspension system with various setup configurations. Over 100 test runs were performed in the towing tank.

Chapter 5: Design and Experimental Testing

5.4 Limitations

The experimental facilities limited the scope of the experimental testing. The limitations are listed below.

- Tests were only performed in regular sinusoidal head waves.
- The temperature in the towing tank could not be maintained constant and varied between tests.
- The wave height could not be set independently of frequency thus the linearity of the results could not be investigated.
- The wave frequency, as well as the trolley speed, could not be set accurately therefore the repeatability of the results could not be investigated.

The results however still gave a good indication of the seakeeping response of the suspension system. The following section discusses the experimental results that were obtained for the Hysucat with the torsional suspension system.

5.5 Experimental Results

5.5.1 Suspension System with Different Stiffness Configurations

The model suspension system was tested with various configurations of the tension springs with the help of the simulation model.

The experiments were run at 4, 5 and 6 m/s, the same velocities as the tests done to investigate the Hysucat seakeeping, in order to obtain comparable data. The pre-tension in the springs was set by towing the model in calm water until the hydrofoil was in the desired calm water position. The calm water simulation results are given in appendix C.

Three different stiffness values were tested namely 37, 74 and 148 N·m/rad. This corresponds to initial angles of attack of 11.8, 7.4 and 4.1° respectively. The experimental results for the tested stiffness values are shown in figures 36 to 39.

The heave RAO shows the same tendencies as was achieved when the Hysucat with and without foils was tested. The response for the spring stiffness equal to 148 N·m/rad levels out at the lower frequencies and does not tend to 1 which indicates that it increases the heave motion at the lower frequencies. The results are also very close to each other. The 74 N·m/rad stiffness gave the best results at all three tested velocities.

Chapter 5: Design and Experimental Testing

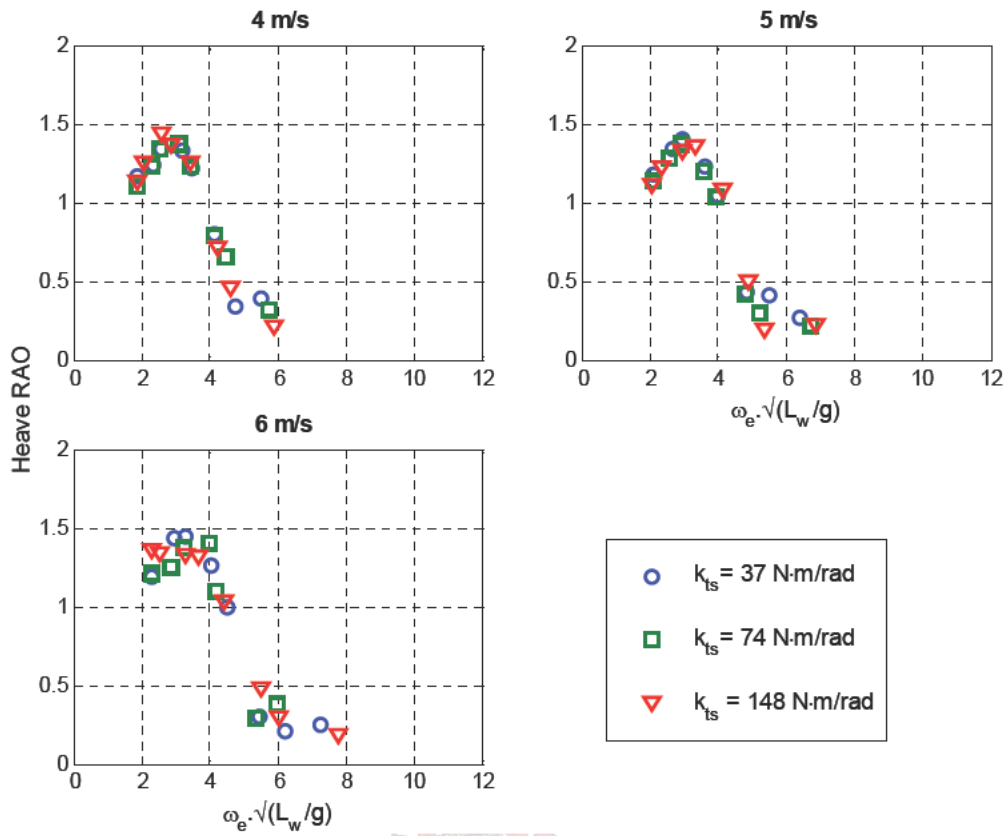


Figure 36: Heave RAO

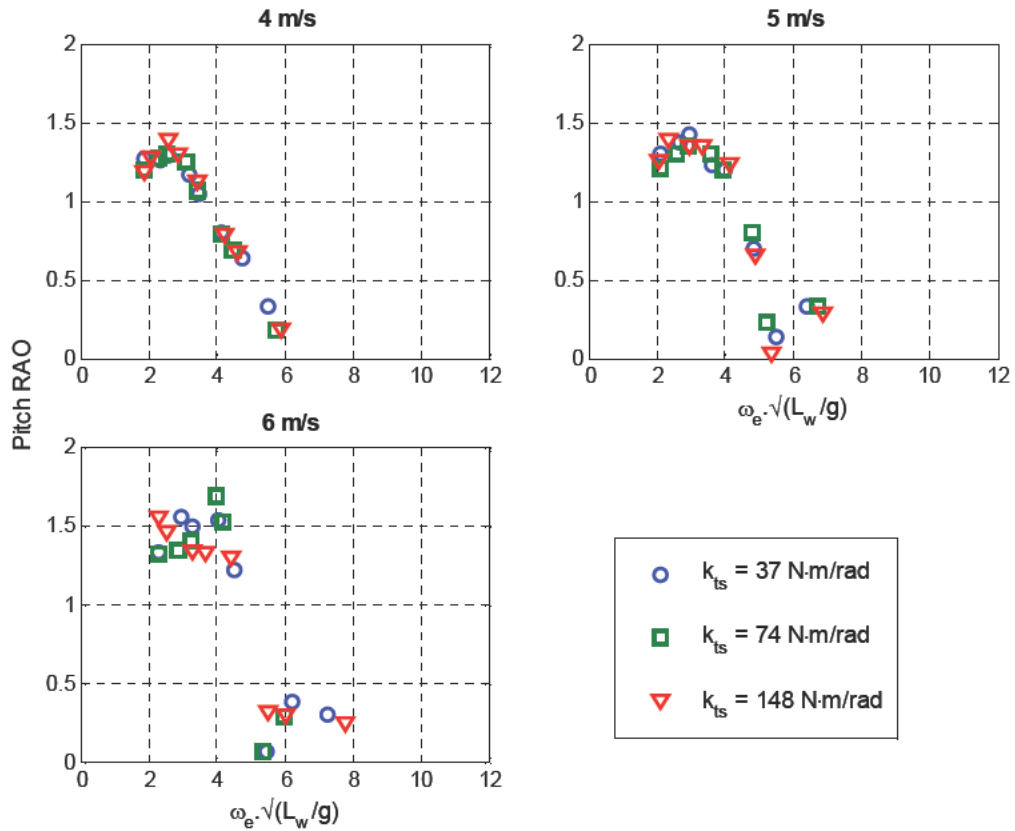


Figure 37: Pitch RAO

Chapter 5: Design and Experimental Testing

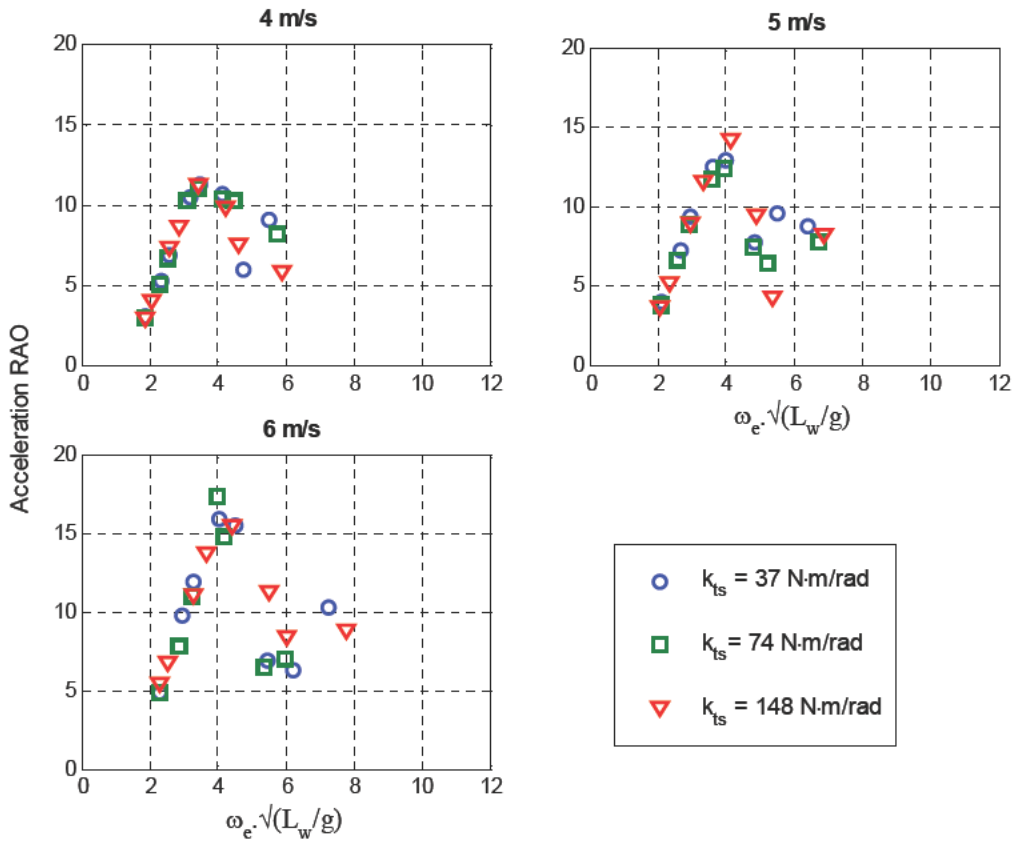


Figure 38: Acceleration RAO

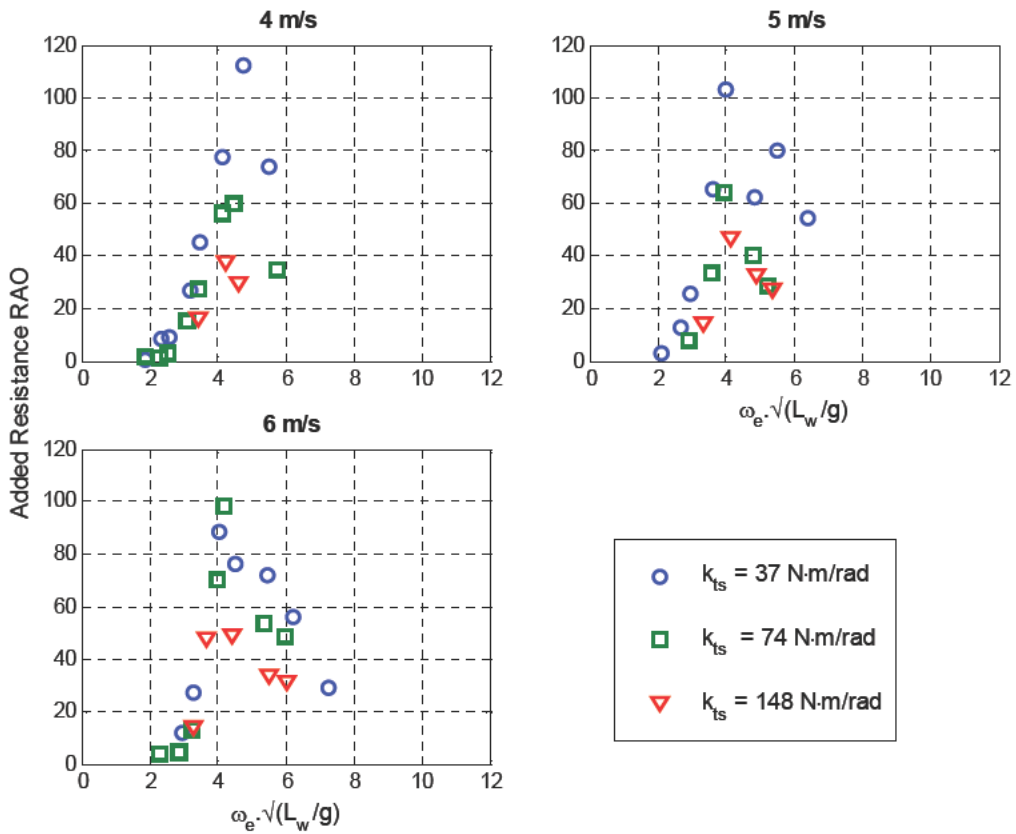


Figure 39: Added resistance RAO

Chapter 5: Design and Experimental Testing

Figure 37 shows the pitch RAO experimental results. The pitch RAO shows the same tendencies as the heave RAO. However, at the design velocity of 6 m/s, the pitch is worse with the stiffness of 74 N·m/rad. The experimental data for 148 N·m/rad also shows a tendency to increase towards infinity instead of unity.

The acceleration RAO experimental results show that the best reduction in acceleration is achieved with 74 N·m/rad at 5 and 6 m/s but is the worse at 4 m/s. The stiffness of 74 N·m/rad also gives the worst peak response at the natural frequency.

The added resistance RAO shows a clear trend in that the 37 N·m/rad shows the worst added resistance with 148 N·m/rad being 40% better. This is due to the less stiff spring being more susceptible to variations in the wave orbital velocity. As the stiffness of the springs increases the added resistance becomes less at all the measured velocities.

The next step was to compare the above experimental results with the experimental results obtained for the Hysucat with and without foils that was presented in chapter 3 as part of the specification development.

5.5.2 Comparison with Hysucat with and without Foils

The comparison of the RAOs for the suspension system with spring stiffness of 74 N·m/rad are shown in figures 40-43.

The heave RAO indicates that the suspension system shows the same response as the Hysucat at 4 m/s. At 6 m/s an improvement of 27% over the hull without foils was achieved and 15% improvement over the Hysucat with rigidly attached foils.

The pitch RAO also shows an improvement over the hull and Hysucat although the improvement is less than the heave RAO. This was also evident from the simulation models obtained in chapter 4. An improvement of 16% is achieved at 6 m/s over the Hysucat without foils.

The acceleration RAO comparison is shown in figure 42. The results indicate that the suspension system damped out the vertical transmitted accelerations. Improvements of 10-22% are achieved at the higher frequencies at 4 and 5 m/s. The response at 6 m/s is not as good as what was anticipated at the resonant frequency however the results show an improvement at the higher encounter frequencies.

Chapter 5: Design and Experimental Testing

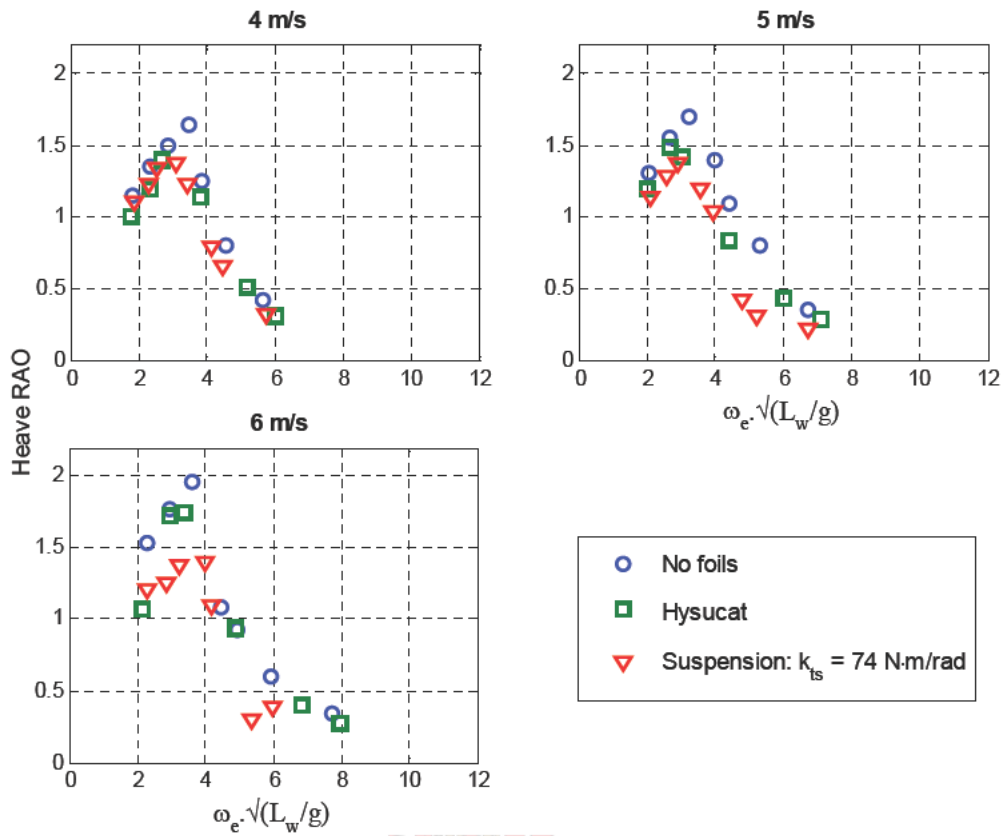


Figure 40: Heave RAO comparison

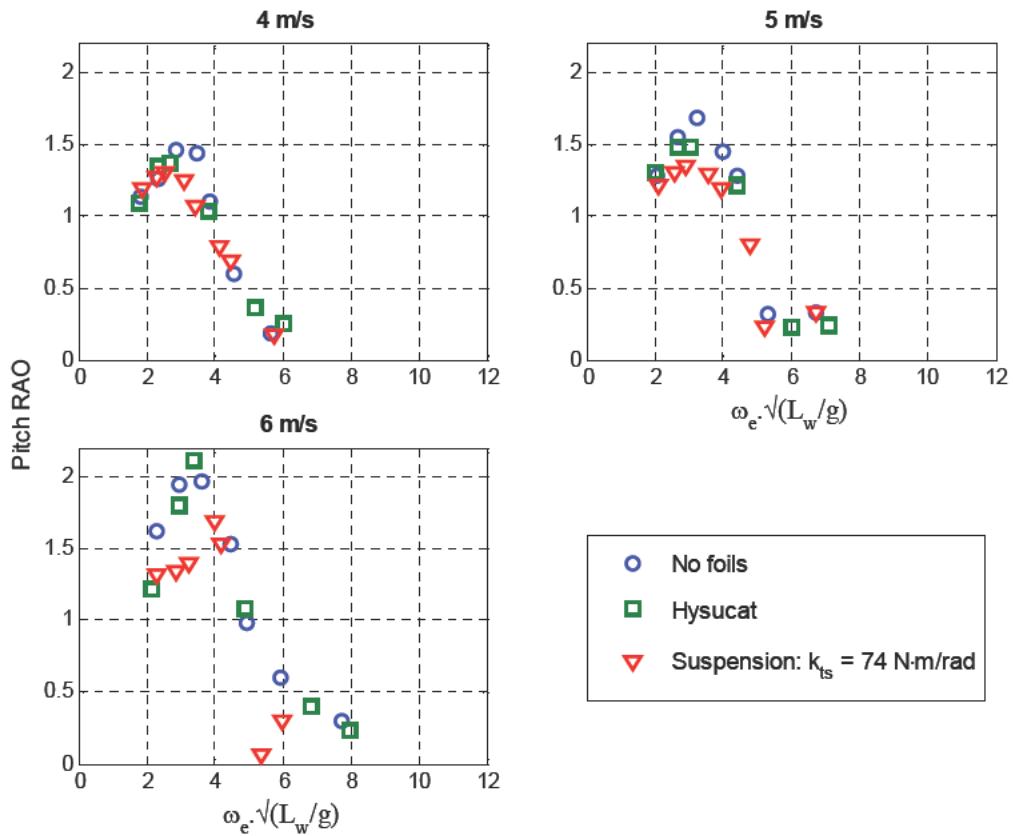


Figure 41: Pitch RAO comparison

Chapter 5: Design and Experimental Testing

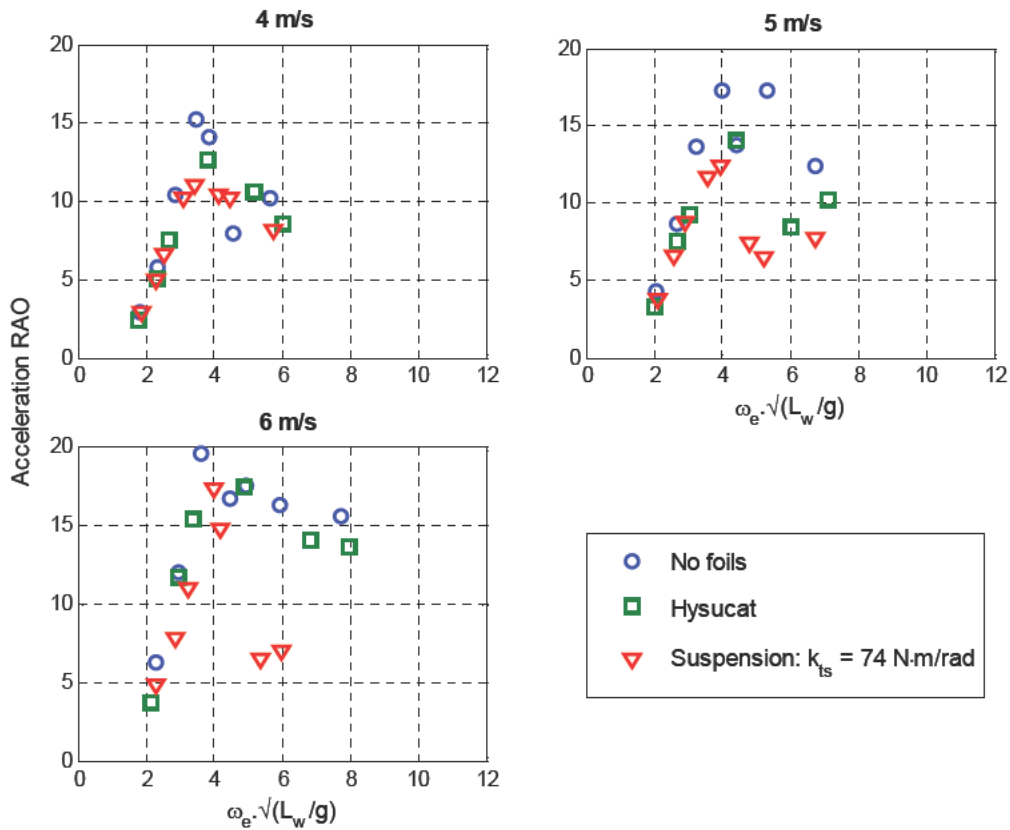


Figure 42: Acceleration RAO comparison

The added resistance RAO response shows that there is an increase in the resistance of the hull with suspension system over the hull without foils but is still less than the added resistance that was achieved with the Hysucat. At 4 and 5 m/s there is a decrease in the added resistance.

Figure 44 shows the calm water resistance that was measured for the hull without foils, Hysucat and Hysucat with suspension system. The results show that the resistance of the suspended Hysucat resistance lies between the results obtained for hull without foils and the Hysucat. The resistance at 6 m/s increased by 16% over the Hysucat with rigidly attached hydrofoils. The results are similar at the other tested velocities.

The increased calm water resistance is to be expected as appendages have had to be added to the side of the hydrofoils. The angle of attack also varies with the forward velocity of the vessel. No effort was made to optimise the calm water resistance of the hull. Methods to minimise the resistance of the added appendages would have to be investigated for future designs.

Chapter 5: Design and Experimental Testing

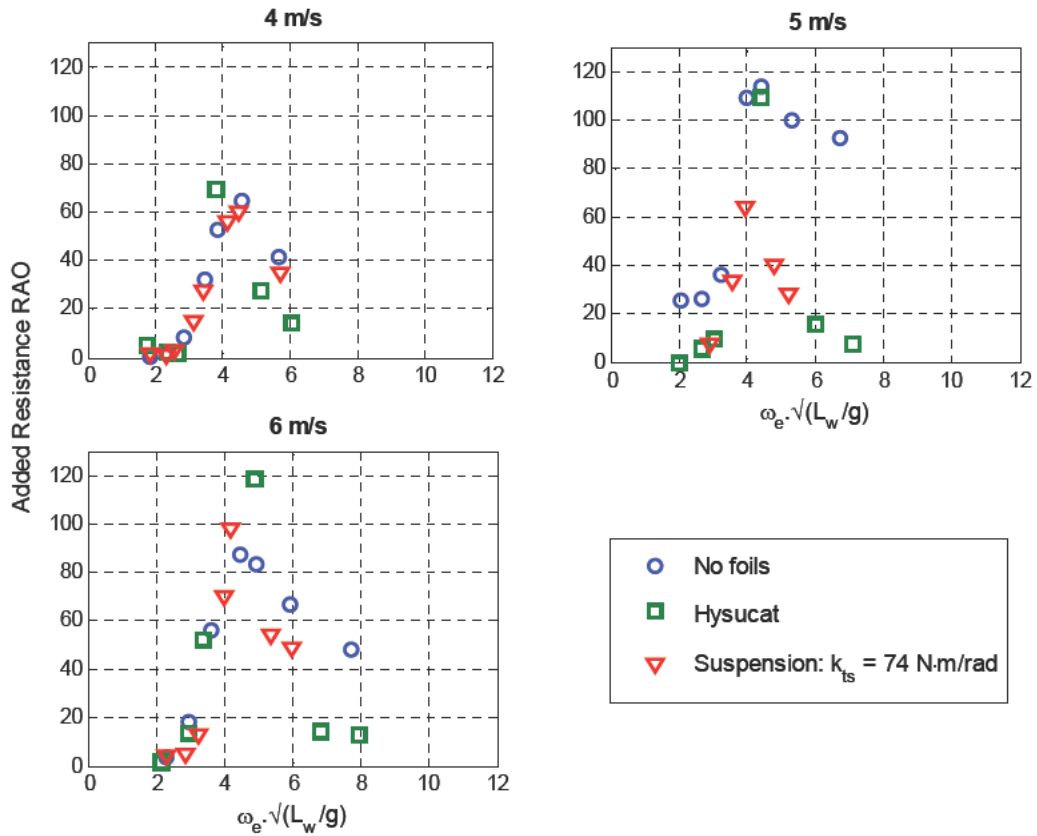


Figure 43: Added resistance RAO comparison

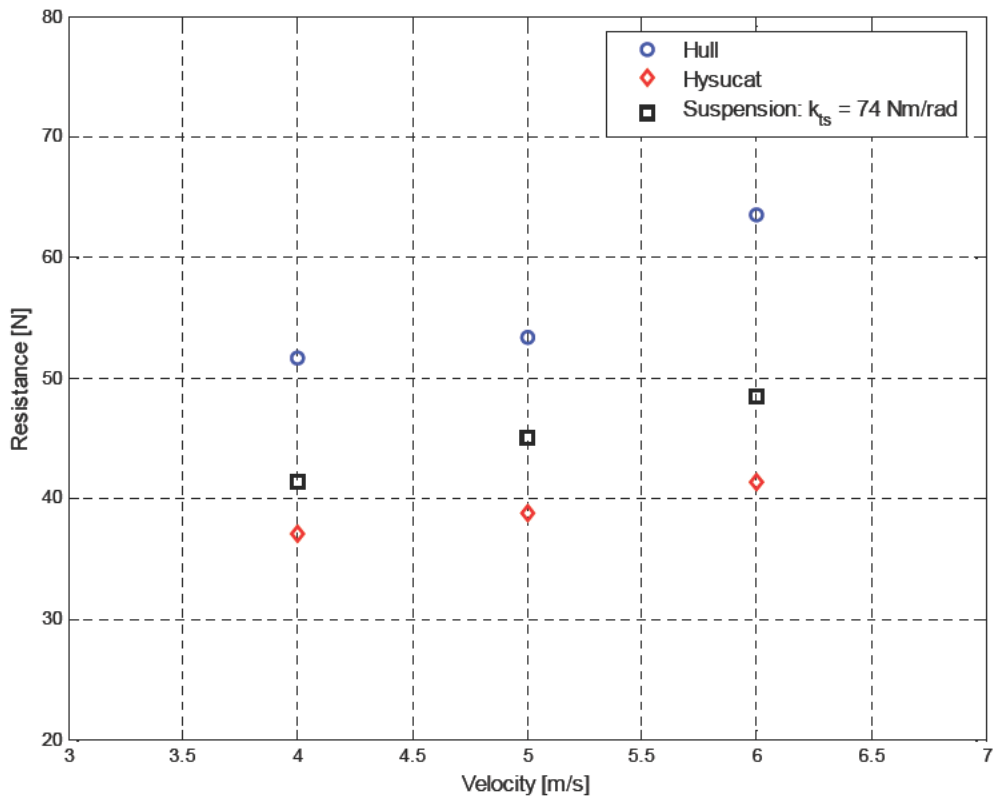


Figure 44: Calm water resistance comparison

Chapter 5: Design and Experimental Testing

5.6 Full Scale Implementation

The experimental results were compared to the customer requirements and engineering specifications to determine the feasibility of implementing the system on a full scale Hysucat. The benefits of the system have to be evaluated against the added complexity of the overall system.

The dimensions and parameters for the full size and 1/8 scale hull and hydrofoils are given in appendix A.

5.6.1 Environmental Conditions

An important aspect is the environmental conditions that the suspension system would operate in. The towing tank tests were performed in regular sinusoidal head waves which are far removed from the conditions found in an ocean seaway. The seakeeping response for displacement craft in irregular waves can be determined by multiplying the regular wave results with an appropriate ocean energy spectrum. However, the seakeeping of planing hulls can only be analysed through towing tank tests in irregular waves or analytically using strip methods as the response is non-linear with wave height.

From the ITTC 1978 spectrum for the Atlantic Ocean, presented in chapter 3, it is evident that the modal frequency increases with an increase in vessel velocity. The total energy is also spread over a wider range of frequencies as the velocity increases. At the design speed of 16.6 m/s (32 knots) the modal frequency for the Atlantic Ocean in wave state 4 is 0.25 Hz. The modal frequency increases as the velocity of the hull increases however the energy at the frequency decreases.

The experimental results indicate that the resonant frequency for the full scale Hysucat is 0.6 Hz. This is higher than the modal frequency for the Atlantic Ocean calculated in chapter 3. According to Savitsky and Koelbel (1993) resonance on ocean vessels can be avoided by changing the vessel speed or changing the direction of the hull relative to the encountered waves. Therefore resonance is not a major design consideration for the suspension system. The experimental results also showed a reduction in the heave RAO at the resonant frequency of the system.

The experimental results showed that there was an improvement with the transmitted acceleration RAO of 18% at resonance and up to 50% at the higher encounter frequencies. The results are only valid for regular head waves and tests in irregular waves would have to be performed to make a proper evaluation. The experiments did however indicate that an improvement is achievable with the passive torsional suspension system.

The wave-height velocity envelope (figure 7) indicates that at 16.6 m/s the maximum height that passenger vessels and small leisure craft could operate in to be within safe operating limits, as determined by ISO 2631:1982, is 0.21 and 0.3 m respectively. The highest wave height that can be negotiated without physical injuries occurring is 0.48

Chapter 5: Design and Experimental Testing

m. The suspension system would allow the vessel to operate in higher sea states at higher encounter frequencies. At low frequencies there is not much improvement in the seakeeping of the vessel.

5.6.2 Vessel Efficiency

Figure 44 indicated that there was an increase in calm water resistance of the Hysucat with suspension system of approximately 12%. However, this is still an improvement of 24% over the Hysucat without foils.

The increase in power thus has to be compared to the increase in speed at which higher sea states can be negotiated. Many HSC never attain their top speed due to the continuous rough water that they have to negotiate negating the positive effects of the increased calm water efficiency. The vessel would be able to handle rougher water at higher velocities than the hull on its own or the Hysucat with rigidly attached hydrofoils due to the reduction of vertical accelerations and a decrease in added resistance at the higher encounter frequencies. Figure 43 indicates that the extra power required to negotiate the waves is less than the Hysucat even though there was an increase in the calm water resistance.

5.6.3 Structural Considerations

Only a scale model of the Hysucat was tested where structural considerations were not considered. The expected lifetime of the design is 20 years with a planned annual maintenance.

The QFD (figure 5) indicated that reliability is an important requirement for all the customers. The suspension system cannot therefore fail under normal operating conditions. A major factor in the structural design of the suspension system is fatigue induced failures as the Hysucat experiences cyclical loading during normal operation. Another factor is that the suspension system is located beneath the hull and water surface where visibility is limited and damage cannot be easily detected.

The forces acting on the suspension system in waves would be difficult to determine accurately. Aspects such as slamming and broaching are difficult to calculate analytically. The safety factors generally employed on hydrofoil assisted craft is 3 for foils located near the bow due to slamming impacts and 2 for foils located near the stern. However, due to the foil being located on a pivot arm a higher safety factor would have to be used to account for the extra loading on the hydrofoil. This would especially be required with new designs to account for unknowns in the system. As the design became more mature lower safety factors could be used.

The model suspension system torsional spring stiffness values were tested with tension coil springs attached to an arm that pivoted as the hydrofoil moved in the waves. The suspension system on the full scale model could be implemented differently. Torsion springs or similar products could be used with the same effect. Variations in the arm length were not investigated however the length was kept as

Chapter 5: Design and Experimental Testing

short as possible to keep the hydrofoil in the same position as the Hysucat with rigidly attached hydrofoils.

The suspension system would have to be manufactured from a corrosive resistant material, such as stainless steel that could withstand the cyclical loads and slamming impacts experienced by the hydrofoil and hull. The suspension system would be located inside the tunnel of the Hysucat to minimise exposure to corrosive sea water. The hydrofoil would operate near the free surface and thus would not be subjected to high water pressure. The seals would not be subject to high pressures but would operate in a highly corrosive environment and would have to be checked during the annual maintenance to avoid any corrosion induced failures.

5.7 Discussion and Conclusions

The model design, experimental setup, data processing and feasibility of implementing the design on a full scale Hysucat were discussed. The results of the experimental testing showed that an improvement is obtained with the suspended hydrofoil system.

The results show that there is not much variation in the results obtained for the three spring stiffness values that were tested. In hindsight it would have been beneficial to measure the displacement angle of the hydrofoil. The angles were never measured physically on the experimental setup however the simulation models indicated that the hydrofoil angle of attack would not vary by more than 2 degrees.

Figure 45 shows a comparison of the results that were obtained at the model design velocity of 6 m/s. The results are compared to the hull without hydrofoils. The results are for the low encounter frequencies, natural frequency and high encounter frequencies. A negative value shows an improvement in the seakeeping over the hull without foils.

Figure 45 indicates that improvement with most seakeeping parameters was achieved except for the pitch and added resistance at the natural frequency. At frequencies higher than the resonant frequency, improvements with the acceleration and added resistance of up to 45% were achieved. No significant difference was noticeable in the acceleration and added resistance results at the low encounter frequencies.

Figure 46 shows the calm water comparison of the Hysucat and Hysucat with suspension system for the three tested velocities. The calm water resistance increases with the fitment of the suspension system, however there is still an overall decrease in resistance. The suspension system was not optimised to reduce calm water resistance therefore the results could be improved by focusing on the calm water design.

Chapter 5: Design and Experimental Testing

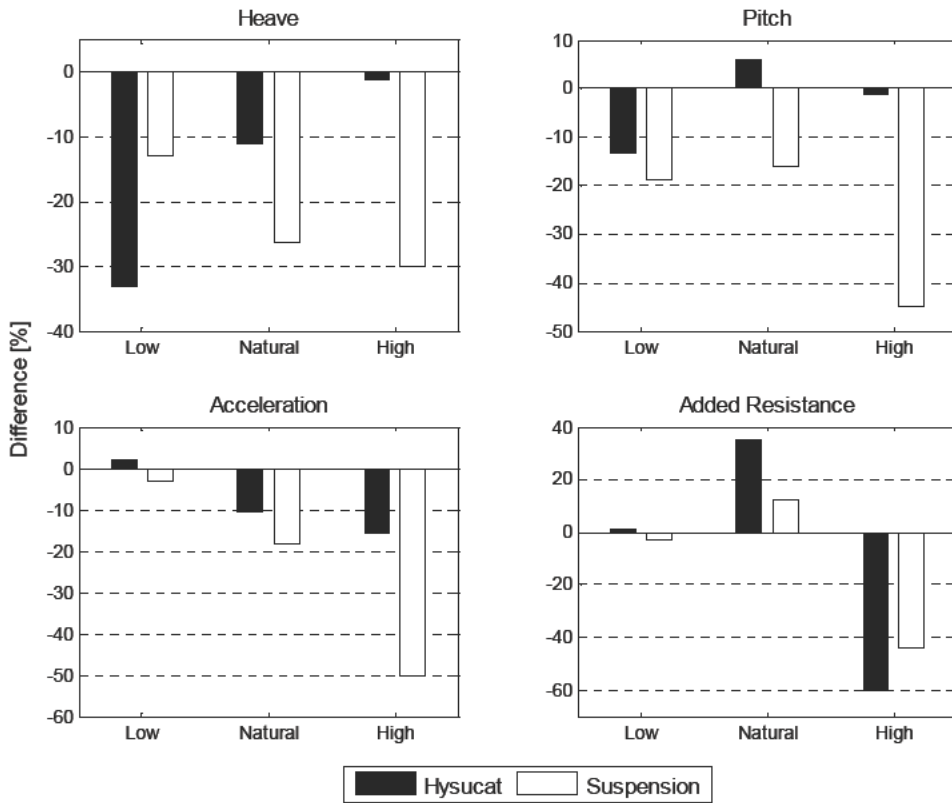


Figure 45: Seakeeping comparison to hull without foils

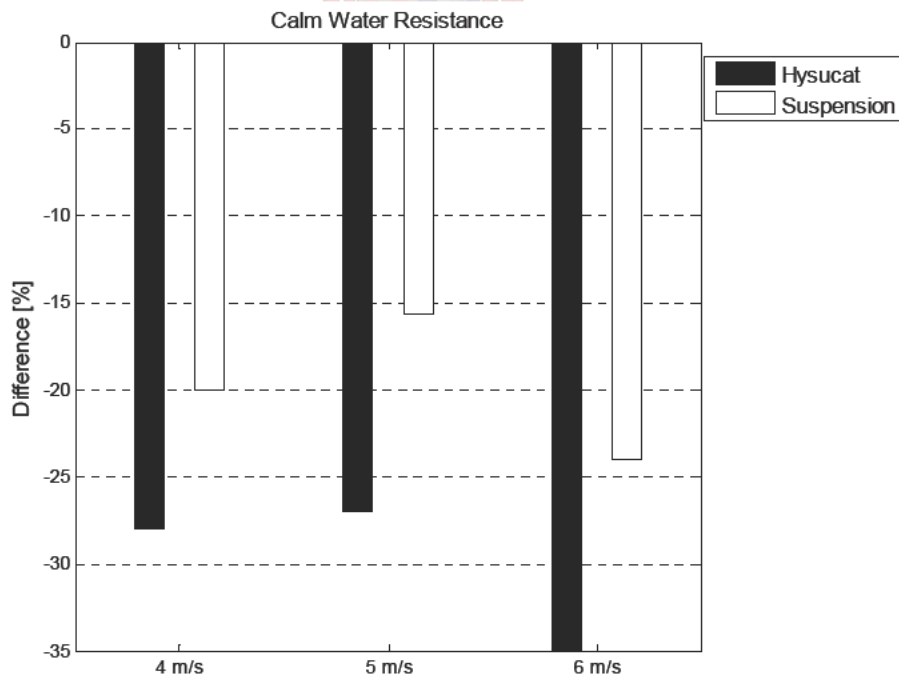
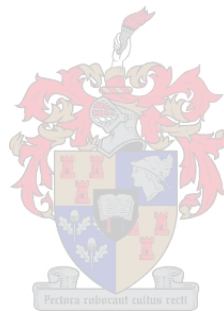


Figure 46: Calm water resistance comparison

Chapter 5: Design and Experimental Testing

The feasibility analysis showed that resonance would not be a major design issue on a full scale hull. The main concern would be structural failures due to unknown forces that cannot be determined analytically. The benefit of fitting a suspension system to the main hydrofoil of a Hysucat would have to be evaluated against the extra complexity that is added to the overall system.



CHAPTER 6: CONCLUSIONS

The design of a passive suspension system for the main hydrofoil of the Hysucat was discussed in the preceding chapters. A design process, proposed by Ullman (1997), was followed for the design. Engineering specifications were compiled and numerous concepts were generated. The two most feasible concepts were the vertical suspension system and torsional suspension system. The concepts were investigated further through the development of numerical simulation models and one was tested experimentally. The main conclusions from the research are as follows:

The Hysucat with rigidly attached hydrofoils improves the seakeeping of the vessel when compared to the hull without foils. The seakeeping of the Hysucat was investigated in section 3.3.3. Hoppe (1989) discussed the improvements in Hysucat seakeeping over conventional catamarans but his analysis was based on perceptions from sea trials. The seakeeping improvement was investigated experimentally for the first time in this research. The results indicated that heave was improved by 11% but the pitch RAO increased by 6% at the resonant frequency. Improvements by up to 15% were achieved with the acceleration RAO at the higher frequencies whilst added resistance showed improvements by up to 60%. The results are summarised in figure 45.

A useful simulation model for the vertical motions of the Hysucat and Hysucat with suspension system can be developed using experimental system identification techniques. A LTI simulation model for the catamaran hull was developed and combined with a theoretical hydrofoil model to simulate the Hysucat and the two concepts. The unknown parameters for the hull model were determined using parameter estimation. The models were validated through experimental testing and represented the experimental data to varying degrees. The results showed that the heave and acceleration of the Hysucat could be modelled accurately at the lower frequencies. The modelling of the pitch RAO at low frequencies was inaccurate due to the wave number tending to zero quicker than the numerator when calculating the pitch RAO. The modelling of the Hysucat with passive suspension system is discussed in chapter 4.

Simulation models indicated that the torsional suspension system was the most feasible and experimental results showed improvements in the seakeeping of the Hysucat fitted with the suspension system. Scale model towing tanks tests were performed to investigate the effectiveness of the torsional suspension system. The experimental results indicated that improvements with certain parameters could be achieved. An improvement of 27% was achieved with the heave RAO at the resonant frequency at the scale design velocity of 6 m/s (32 knots). At the higher frequencies reductions in accelerations by up to 50% were achieved.

The calm water operating limits placed restrictions on the design parameters that were available. The Hysucat seakeeping had to be improved whilst minimising the effect on the calm water operating conditions of the vessel. The initial angle of attack had to be

CHAPTER 6: Conclusions

carefully chosen to prevent hydrofoil stall as well as reduce the calm water resistance of the design.

Figure 44 indicated that there was an increase in calm water resistance of the Hysucat with the suspension system of approximately 12%. However, this is still an improvement of 24% over the Hysucat with no foils. This was due to the appendages that were added to the Hydrofoil. The design could be further refined to minimise the calm water resistance.

The following section discusses further research that can be done in this field.

6.1 Further Work

This was the first attempt at the design and modelling of a passive suspension system for a Hysucat and there is much scope for further research. Some suggestions for further work in terms of modelling are:

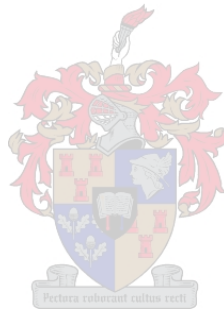
- Develop a Hysucat model using 2-D strip methods as developed by Zarnick (1978). This would eliminate the need for parameter estimation to determine the unknown parameters of the LTI model. Milandri (2006) attempted to combine a hydrofoil model with strip methods and obtained inaccurate results. The results could be improved with the incorporation of a more accurate hydrofoil model. (Milandri, 2006)
- Investigate the accuracy of the Payne (1997) hydrofoil model in an orbital velocity wave field using experimental techniques. Payne (1997) never tested the model experimentally to determine its accuracy.
- Investigate the effect of interference between the hull and the hydrofoils on the seakeeping of the Hysucat. Dyachkov and Makov (2005) developed a model for catamarans with fin stabilisers that was valid for fast displacement craft. Their model took hull interferences into account however they never validated their results at semi-planing and planing Froude numbers.
- This study only investigated concepts for the main hydrofoil of the Hysucat. Concepts that combine the dynamics of the trim foils with the main foil could be investigated.

For the practical implementation of such a passive suspension system the following is recommended.

- Implement the suspension system on a full scale prototype. This could only be done after more research work had been completed and extensive towing tank tests had been performed. The benefits of a passive suspension system would only be evident once sea trials had been completed.

CHAPTER 6: Conclusions

- Perform experimental towing tank tests in irregular waves in order to determine the effectiveness of the suspension system in irregular waves. Experimental testing would be the only way to accurately determine the seakeeping of the Hysucat.
- Perform tests on different Hysucat models with different hydrofoil configurations.



REFERENCES

- Akers, RH, 1999, *Dynamic Analysis of Planing Hulls in the Vertical Plane*, Presented at the meeting of the New England section of The Society of Naval Architects and Marine Engineers, New England.
- Bertram, V, 1999, *Practical Ship Hydrodynamics*, Butterworth Heinemann, Oxford.
- Bhattacharyya, R, 1978, *Dynamics of Marine Vehicles*, John Wiley and Sons, New York.
- Chapman, LB (ed.), 1967, *Principles of Naval Architecture*, Society of Naval Architects and Marine Engineers, Jersey City, New York.
- Couser, P, undated, *Seakeeping Analysis for Preliminary Design*, Formation Design Systems.
- Daskovsky, M, 2000, The Hydrofoil in Surface Proximity, Theory and Experiment, *Ocean Engineering*, Vol. 27, pp. 1129-1159.
- Du Cane, P, 1972, *High Speed Small Craft*, David & Charles, Newton Abbot.
- Dyachkov, V and Makov, J, 2005, Seakeeping of Fast Displacement Catamaran, *Transport*, Vol. XX, No. 1, pp. 14-22.
- Egorov, IT and Sokolov, VT, 1965, *Hydrodynamics of Fast Craft*, In Russian (English translation: NTIS AD A032120, 1976).
- Fang, CC, Chan, HS and Incecik, A, 1996, Investigation of Motions of Catamarans in Regular Waves –I, *Ocean Engineering*, Vol. 23, No. 1, pp. 89-105.
- Fang, CC, Chan, HS and Incecik, A, 1997, Investigation of Motions of Catamarans in Regular Waves –II, *Ocean Engineering*, Vol. 24, No. 10, pp. 949-966.
- Griffin, MJ, 1990, *Handbook of Human Vibration*, Academic Press Ltd, London.
- Haddara, MR, Xu, J, 1999, On the Identification of Ship Coupled Heave-Pitch Motions Using Neural Networks, *Ocean Engineering*, Vol. 26, pp. 381-400.
- Hoerner, SF, 1965, *Fluid Dynamic Drag*, Hoerner Fluid Dynamics, Bricktown, New Jersey.
- Hoppe, KG, 1989, *The Hysucat Development*, Internal Report, Department of Mechanical Engineering, University of Stellenbosch, South Africa.

REFERENCES

- Hoppe, KG, 1995, Optimisation of Hydrofoil-Supported-Planing Catamarans, *In Fast '95, 3rd International Conference of Fast Sea Transportation*, pp.307-317, Lübeck, Trauemünde, Germany.
- Hoppe, KG, 2001, Recent Applications of Hydrofoil-Supported-Catamarans, *Fast Ferry International*, pp. 30-36.
- Hoppe, KG, undated, *Hysucat Principles*, [Online]. Available: <http://www.fastcc.hysucraft.com>, [2006, September 20].
- Hoppe, KG, 1990, *Performance Evaluation of High Speed Surface Craft with Reference to the Hysucat Development*, Research Report, Department of Mechanical Engineering, University of Stellenbosch, South Africa.
- Kim, S-H and Yamoto, H, 2004, An Experimental Study of the Longitudinal Motion Control of a Fully Submerged Hydrofoil Model in Following Seas, *Ocean Engineering*, Vol. 31, pp. 523 -537.
- Kim, S-H and Yamoto, H, 2004a, On the Design of a Longitudinal Motion Control System of a Fully- Submerged Hydrofoil craft based on the Optimal Preview System, *Ocean Engineering*, Vol. 31, pp. 1637 -1657.
- Kim, S-H and Yamoto, H, 2005, The Estimation of Wave Elevation and Wave Disturbance Caused by the Wave Orbital Motion of a Fully Submerged Hydrofoil Craft, *Marine Science and Technology*, Vol. 10, pp. 22-31.
- Köpke, MW, 2006, *A Suspension System for a Hydrofoil Assisted Catamaran*, Project Proposal, Department of Mechanical and Mechatronic Engineering, University of Stellenbosch, South Africa.
- Lewis, E (ed.), 1988, *Principles of Naval Architecture*, Volume 2, The Society of Naval Architects and Marine Engineers, Jersey City, New York.
- Maine, RE and Iliff, KW, 1986, *Application of Parameter Estimation to Aircraft Stability and Control: The Output Error Approach*, Reference publication, NASA.
- Matveev, K and Duncan, R, 2006, Development of the Tool for Predicting Hydrofoil System Performance and Simulating Motion of Hydrofoil-Assisted Boats, In: *Proceedings of the ASNE Symposium for High Speed / High Performance Craft*.
- Matveev, K, 2006, Correspondence, July, South Africa.
- Meirovitch, L, 2001, *Fundamentals of Vibrations*, McGraw Hill International Series, New York.
- Michel, WH, 1999, Sea Spectra Revisited, *Marine Technology*, Vol. 36, No. 4, pp. 211-227.

REFERENCES

- Migeotte, G, 1997, *Development of Hydrofoil Supported Catamarans with Semi-Displacement Hulls*, Master's thesis, University of Stellenbosch, Stellenbosch, South Africa.
- Migeotte, G, 2002, *Design and Optimisation of Hydrofoil Assisted Catamarans*, Ph.D thesis, University of Stellenbosch, Stellenbosch, South Africa.
- Migeotte, G, 2007, Correspondence, South Africa.
- Milandri, GS, 2006, *Seakeeping Control of HYSUCATs*, Masters Thesis, University of Stellenbosch, Stellenbosch, South Africa.
- Milne, GW, 2000, *MMLE-3 Identification Toolbox for State-Space System Identification using Matlab*, Version 1.3 and 1.4.
- O' Hanlon, JF and McCauley. ME, 1974, Motion Sickness Incidence as a Function of the Frequency and Acceleration of Vertical Sinusoidal Motions, *Aerospace Medicine*, Vol. 45, No. 4, pp. 366-369.
- Payne, PR, 1988, *Design of High Speed Boats*, Volume 1, Fishergate Inc, Maryland.
- Payne, PR, 1997, The Response of a Hydrofoil to Wave Orbital Velocity Fields, *Ocean Engineering*, Vol. 24, No. 3, pp. 235 – 263.
- Pienaar, LdV and Roos, H, 1991, *Ship Model Tests*, Final year project, Department of Mechanical Engineering, University of Stellenbosch, Stellenbosch, South Africa.
- Riegels, FW, 1961, *Aerofoil Sections*, Butterworths, London.
- Rosén, A, 2004, *Loads and Responses for Planing Craft in Waves*, Aeronautical and Vehicle Engineering, Division of Naval Systems, Stockholm, Sweden.
- Savitsky, D, 1964, Hydrodynamic Design of Planing Hulls, *Marine Technology*, pp.71-95.
- Savitsky, D and Koelbel, JG, 1993, *Seakeeping of Hard Chine Planing Hulls*, Society of Naval Architects and Marine Engineers, Technical and Research Bulletin, No. R-42.
- Söding, H, 2001, Global Seaway Statistics, *Ship Technology Research*, Vol. 48, pp. 147-153.
- Taunton, DJ, 2001, *Methods for Assessing the Seakeeping Performance of High Speed Displacement Monohulls and Catamarans*, Phd Thesis, Faculty of Engineering and Applied Science, University of Southampton, United Kingdom.

REFERENCES

Ullman, DG, 1997, *The Mechanical Design Process*, 2nd Edition, McGraw-Hill, New York.

Vorus, WS, 1996, A Flat Cylinder Theory for Vessel Impact and Steady Planing Resistance, *Journal of Ship Research*, Vol. 40, 2, 100.

Welnicki, W, 1998, The Influence of Fixed Foils on Seakeeping Qualities of Fast Catamaran, In: *Proceedings of the 7th International Symposium on Practical Design of Ships and Mobile Units*, The Haque, The Netherlands.

Welnicki, W, 1998a, The Enhancement of Seakeeping Qualities of Fast Catamarans by Means of Stabilising Foils, *Polish Maritime Research*, Vol. 5, No. 3, pp. 10-13.

Xu, J and Haddara, MR, 1999, Estimation of Wave-induced Hull Bending Moment from Ship Motion Measurements, *Marine Structures*, Vol. 14, pp. 593-610.

Zarnick, E, 1978, *A Nonlinear Mathematical Model of Motions of a Planing Boat in Regular Waves*, David W. Taylor Naval Ship Research and Development Center, Bethesda, DTNSRDC-78/032.

Zarnick, EE and Turner, CR, 1981, *Rough Water Performance of High Length to Beam Ratio Planing Hulls*, David W. Taylor Naval Ship R&D Center, Ship Performance Department, Bethesda, DTNSRDC/SPD-0973-01.





APPENDIX A: HULL AND HYDROFOIL DIMENSIONS AND PARAMETERS

A.1 Model Hull Dimensions

The model Hysucat utilised in the design was the same used by Milandri (2006). The measured points are given in table A.1. A measuring table with height gauge was used to obtain the required measurements at each station.

Table A.1: Hull model dimensions

st	x	Keel		Chine	
		y	z	y	z
0	0.000	0.000	0.000	0.129	0.053
1	0.165	0.000	0.000	0.129	0.053
2	0.330	0.000	0.000	0.129	0.055
3	0.495	0.000	0.000	0.128	0.056
4	0.660	0.000	0.000	0.128	0.059
5	0.825	0.000	0.000	0.127	0.064
6	0.904	0.000	0.000	0.126	0.071
7	0.996	0.000	0.003	0.122	0.089
8	1.163	0.000	0.013	0.102	0.118
9	1.240	0.000	0.440	0.084	0.138
10	1.330	0.000	0.135	0.048	0.164

The above measurements were used to generate a CAD model of the hull. The model layout view is given in figure A.1.

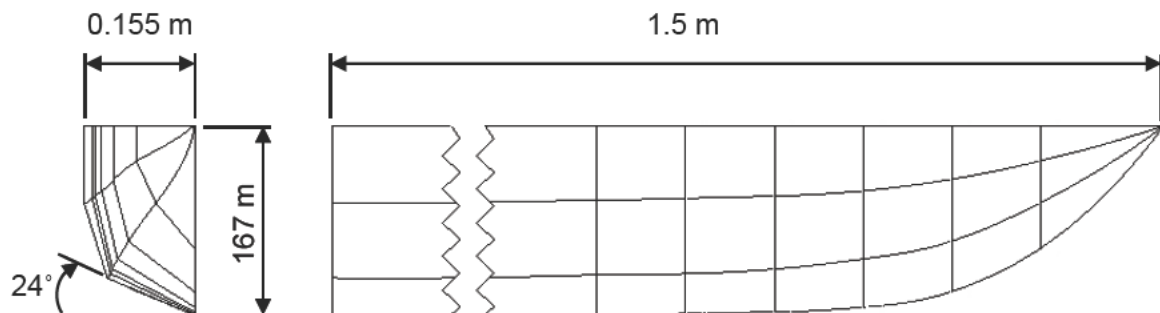


Figure A.1: Model dimensions - Hys 1

APPENDIX A: Hull and Hydrofoil Dimensions and Parameters**A.2 Calculation of Moment of Inertia and Radius of Gyration**

Simple pendulum experiments were used to determine the radius of gyration of the model hull. This approach is similar to that used by Zarnick and Turner (1981) and Milandri (2006)

The radius of gyration is obtained by swinging the hull at its natural frequency and assuming pendulum behaviour so that the radius of gyration can be determined.

The natural frequency of a pendulum around its pivot point is calculated using equation A.1

$$\omega_n = \sqrt{\frac{l m_h g}{I_{oo}}} \quad (\text{A.1})$$

Where:

- l is the length from the LCG to the pivot point;
- I_{oo} is the mass moment of inertia around the pivot point.

The natural frequency of the system was obtained by swinging the hull around the pivot point. The moment of inertia around the centre of gravity is then obtained using Steiner's theorem given in equation A.2.

$$I_{cg} = I_{oo} - m_h l^2 \quad (\text{A.2})$$

The radius of gyration can then be obtained using equation A.3.

$$r_g = \sqrt{\frac{I_{cg}}{m_h}} \quad (\text{A.3})$$

The radius of gyration was calculated to be 0.402 m.

A.3 Hydrofoil Dimensions and Parameters

Existing hydrofoils were used with the suspension system design. The hydrofoil specifications for the main and trim hydrofoils are given in table A.2.

APPENDIX A: Hull and Hydrofoil Dimensions and Parameters

Table A.2: Hydrofoil specifications

Parameter	Unit	Main Foil		Trim Foil (each)	
		Model	Full scale	Model	Full scale
Chord [c]	[m]	0.0735	0.588	0.045	0.36
Thickness [t]	[m]	0.005	0.04	0.003	0.024
Thickness/Chord [t/c]	[-]	0.068	0.068	0.067	0.067
Span [d]	[m]	0.26	2.08	0.07	0.56
Sweep Angle [A]	[degrees]	25.21	25.21	24.6	24.6
Planform Area [S]	[m ²]	0.021	1.351	0.00315	0.2016
Camber Ratio [f]	[-]	0.0347	0.0347	0.03417	0.03417
Aspect ratio [AR]	[-]	3.53	3.53	1.556	1.556
Dihedral angle [Γ]	[degrees]	-	-	-	-



APPENDIX A: Hull and Hydrofoil Dimensions and Parameters

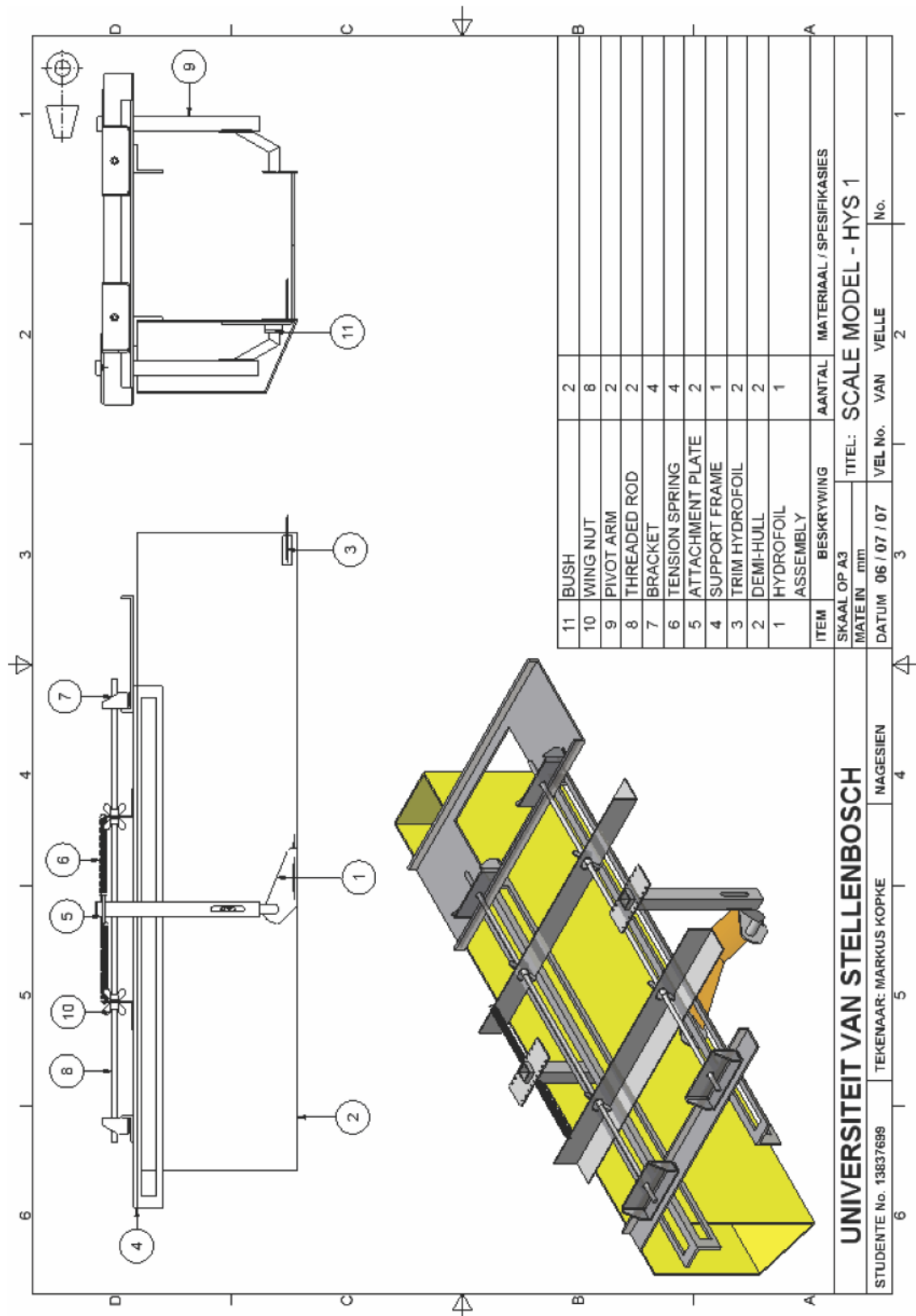


Figure A.2: Hysucat with suspension system model assembly

APPENDIX B: HYDROFOIL CALCULATIONS

B.1 Calm Water Hydrofoil Theory

The equations below were used to calculate the lift and drag coefficients for the modelling of the Hysucat as well as the suspension system concepts.

Hydrofoil lift is calculated using equation B.1.

$$L = \frac{1}{2} \rho u_o^2 S C_L \quad (\text{B.1})$$

In the sub-cavitating region, lift and drag forces can be calculated using aeronautical theory with corrections for the free surface. The three-dimensional lift coefficient is calculated using equation B.2.

$$C_L = C_{L\alpha} (\alpha - \alpha_o + \Delta\alpha_o) \quad (\text{B.2})$$

Where:

- $C_{L\alpha}$ is the lift curve slope;
- α the angle of attack;
- α_o the zero lift angle of attack;
- $\Delta\alpha_o$ is the correction for the zero lift angle of attack.

The zero-lift angle of attack correction factor, from Egrov and Sokolov (1965), is calculated using equation B.3.

$$\Delta\alpha_o = \frac{t_f/c}{2} \left(\frac{1}{k_\phi} - 1 \right) \quad (\text{B.3})$$

Where:

- t_f is the maximum hydrofoil thickness.
- c the hydrofoil chord length.

and

$$k_\phi = 1 - \left(0.5 + \frac{t}{c} \right) e^{-2(h/c)^{0.6}} \quad (\text{B.4})$$

Where:

- h is the submergence below free surface measured from quarter chord.

The zero lift angle of attack can be calculated using two dimensional aerofoil theory. Hoerner (1965) presents the following equation for circular arc profiles.

$$\alpha_o = -1.15 \left(\frac{f}{c} \right) \% \quad (\text{B.5})$$

Where:

APPENDIX B: Hydrofoil Calculations

- f is the foil camber.

The three dimensional lift-curve slope was calculated using theory presented by Du Cane (1972).

The main difference between hydrofoils and aerofoils is the presence of free surface effects. The low pressure above the hydrofoil causes a distortion of the water surface which decreases the lift of the foil. This effect becomes more negligible the deeper the hydrofoil is submerged. Du Cane (1972) explains that this effect is relatively complex but approximations can be made by including the following:

- The lift loss due to pressure relief as a function of foil depth calculated at an infinite Froude number;
- The change in angle of the lift vector due to the wave effect.

The lift loss due to pressure relief is approximated by equation B.6.

$$K = \frac{\left(\frac{4h}{c}\right)^2 + 1}{\left(\frac{4h}{c}\right)^2 + 2} \quad (\text{B.6})$$

The free surface wave effects lift as well as drag and can be approximated using equation B.7.

$$\begin{aligned} \Omega &= \frac{\alpha_w}{C_L} = \frac{C_{Di}}{C_L^2} = \frac{I + \sigma}{\pi A} \\ &= \frac{I}{2F_c^2} \exp\left(\frac{-2h}{cF_c^2}\right) \end{aligned} \quad (\text{B.7})$$

Where:

- F_c is the chord Froude number defined by equation B.8.

$$F_c = \frac{u_o}{g c} \quad (\text{B.8})$$

The finite span of the foil results in a further decrease in the lift curve slope due to the trailing vortices at the wing tips which induces an increased drag. A hydrofoil with aspect ratio AR has an induced lift and drag component given by equation B.9.

$$\frac{\alpha_l}{C_L} = \frac{I + \sigma}{\pi AR} \quad (\text{B.9})$$

Where:

- σ is Prandtl's finite-span biplane factor defined by

APPENDIX B: Hydrofoil Calculations

$$\sigma = \frac{AR}{AR + \frac{12h}{c}} \quad (\text{B.10})$$

Where:

- AR is the hydrofoil aspect ratio.

Modest aspect ratios must be multiplied with an empirical correction factor. The planform correction factor is given by equation B.11.

$$E = 1 + \frac{2}{AR^2} \quad (\text{B.11})$$

The lift curve slope, from Du Cane (1972), is therefore calculated using equation B.12.

$$C_{La} = \left[\frac{\frac{1}{K} + \frac{2}{AR^2}}{2\pi \cos \lambda \cos \Gamma} + \Omega + \frac{1 + \sigma}{\pi AR} \right] \quad (\text{B.12})$$

Where:

- Γ is the dihedral angle;
- λ is the sweep angle.

The drag force acting on a hydrofoil when moving through a liquid medium is similar to lift and is given by equation B.13.

$$D = \frac{1}{2} \rho u_0^2 S C_D \quad (\text{B.13})$$

Where:

- C_D is the drag coefficient.

Most of the drag acting on the hydrofoil is parasitic drag as a result of fluid viscosity. The various drag components are shown below

$$C_D = C_{DP} + \delta C_{DP} + C_{Di} + C_{Dw} + C_{Ds} + C_{Dsep} \quad (\text{B.14})$$

Where:

- C_{DP} is the skin friction coefficient;
- δC_{DP} is the profile drag increment due to the angle of attack;
- C_{Di} is the induced drag;
- C_{Dw} is the wave drag;
- C_{Ds} is the surface piercing strut drag;
- C_{Dsep} is the separation drag.

The skin friction, C_{DP} , was determined using equation B.15 from Migeotte (2001) which takes the free surface into account.

APPENDIX B: Hydrofoil Calculations

$$C_{DP} = C_F \left[1 + C_L \left[(m_p + 0.5) \frac{\kappa}{k_\phi} - 0.5 \right] \right] \quad (\text{B.15})$$

C_F is the frictional coefficient of the hydrofoil and is determined using the ITTC 1957 formula.

$$C_F = \frac{0.075}{(\log_{10} Rn - 2)^2} \quad (\text{B.16})$$

m_p is an empirical correction factor which is given by equation B.17.

$$m_p = \frac{2C_L}{3} + 0.3833 \quad (\text{B.17})$$

κ is the free surface correction factor.

$$\kappa = 1 - \exp \left[-2 \left(\frac{h}{c} \right)^{0.6} \right] \quad (\text{B.18})$$

k_ϕ is the lift curve slope correction factor.

$$k_\phi = 1 - \left(0.5 + \frac{t_f}{c} \right) \exp \left[-2 \left(\frac{h}{c} \right)^{0.6} \right] \quad (\text{B.19})$$

The profile drag increment due to angle of attack is approximated using Lewis (1988).

$$\delta C_{DP} = 0.005 C_L^2 \quad (\text{B.20})$$

The wave drag (C_{Dw}) is caused by the wave formation as the hydrofoil approaches the water surface. The waves disturb the water surface and in effect transfer momentum to the water.

Riegels (1961) presented the following equation for determining the wave drag.

$$C_{Dw} = \frac{0.5 C_L^2}{\frac{u_o^2}{gh} \exp \left(\frac{2gh}{u_o^2} \right)} \quad (\text{B.21})$$

Where:

- h is the submergence of the quarter chord.

The induced drag is caused by the downward velocity including the bi-plane interference effect.

APPENDIX B: Hydrofoil Calculations

$$C_{Di} = \frac{C_L^2}{\pi ARP \cos \lambda \cos^2 \Gamma} (I + \sigma)(I + E) \quad (\text{B.22})$$

Where:

$$P = \frac{16 (h/c)^2 + 1}{16 (h/c)^2 + 2} \quad (\text{B.23})$$

The separation drag has to be included in the analysis. The separation drag is due to thin aerofoil stall because thin aerofoil theory assumes potential flow. The following equation from Migeotte (1997) is used to calculate the separation drag

$$C_{Dsep} = \frac{\sin^2 \alpha}{0.222 \sin \alpha + 0.283} - \frac{\left(\frac{\sin \alpha \cos \alpha}{0.222 \sin \alpha + 0.283} \right)^2}{\pi AR} \quad (\text{B.24})$$



APPENDIX B: Hydrofoil Calculations

B.2 Hysucat Calm Water Calculation

The Hysucat configuration was analysed by Migeotte (2007) using proprietary software. The results were used in the calm water analysis of the vertical suspension system as well as the torsional suspension system. The results are shown in table B.1.

Table B.1 Hysucat calm water analysis

Speed:	32 [knots]	Fn	3.493 [-]
Displacement:	11.88 [t]		
Foil Weight	0.00001 [t]	0.0 [%]	
Vessel Main Parameters			
Hulls			
L _{CHINE} :	10.32 [m]	Trim:	2.0 [deg]
B _{chine} :	2.06 [m]	L _K :	12.36 [m]
LCG:	4.35 [m] 42.17 [%]	L _C :	4.099 [m]
VCG:	0.5 [m]	Transom subm.	0.4373 [m]
Deadrise:	24 [deg]	COP:	4.958 [m]
Frontal Area:	0.001 [m ²]	roughness addition:	0.0003 [-]
Front Foil		Rear Foil	
chord:	0.588 [m]	chord:	0.36 [m]
thickness ratio:	0.068 [-]	thickness ratio:	0.067 [-]
camber ratio:	0.0347 [-]	camber ratio:	0.03417 [-]
nose radius:	n/a [m]	nose radius:	n/a [m]
span:	2.08 [m]	span:	0.56 [m]
sweep angle:	25.21 [deg]	sweep angle:	25.21 [deg]
dihedral angle:	-	dihedral angle:	-
AR:	3.2 [-]	AR:	1.556 [-]
α:	0 [deg]	α:	2 [deg]
α _{effective} :	2.027 [deg]	α _{effective} :	2.358 [deg]
L _{quarter chord} :	5.084 [m]	L _{quarter chord} :	0.496 [m]
submergence:	0.23 [m]	submergence:	0.02598 [m]
subm. ratio:	0.3835 [-]	subm. ratio:	0.07216 [-]
plan form area:	1.352 [m ²]	plan form area:	0.2016 [m ²]
height relative to baseline:	0.032 [m]	height relative to baseline:	0.144 [m]
		free surface height reduction:	-0.2498 [m]
	LIFT	LIFT [%]	DRAG DRAG[%] L/D D/L
Hull:	5.667 [t]	47.71 [%]	1.359 [t] 76.77 [%] 6.541 [-] 0.2399
Front Foil:	5.183 [t]	43.64 [%]	0.30 [t] 16.69 [%] 17.54
Front Struts:	-	-	0.00 [t] 0.00 [%] -
Rear Foil:	0.97 [t]	8.129 [%]	0.09 [t] 5.23 [%] 10.43 0.0
Rear Struts:	-	-	0.00 [t] 0.00 [%] -
Air:	-	-	0.00 [t] 0.00 [%] -
Appendage:	-	-	0.02 [t] 1.31 [%] -
Thrust:	0.062 [t]	0.53 [%]	- - -
TOTAL:	11.88 [t]	100.0 [%]	1.771 [t] 100.0 [%] 6.708 0.1491
Power Requirements			
Thrust:	17.38 [kN]		
P _{effective} :	288.1 [kW] 383.7 [hp]	OPC:	0.57
P _{brake} :	502 [kW] 673.1 [hp]	% MCR:	100
P _{installed} :	502 [kW] 673.1 [hp]	TF:	3.821

APPENDIX C: Spring Design

APPENDIX C: SPRING DESIGN

The springs for the scale model were designed using Design Accelerator for Autodesk Inventor. The results are shown below.

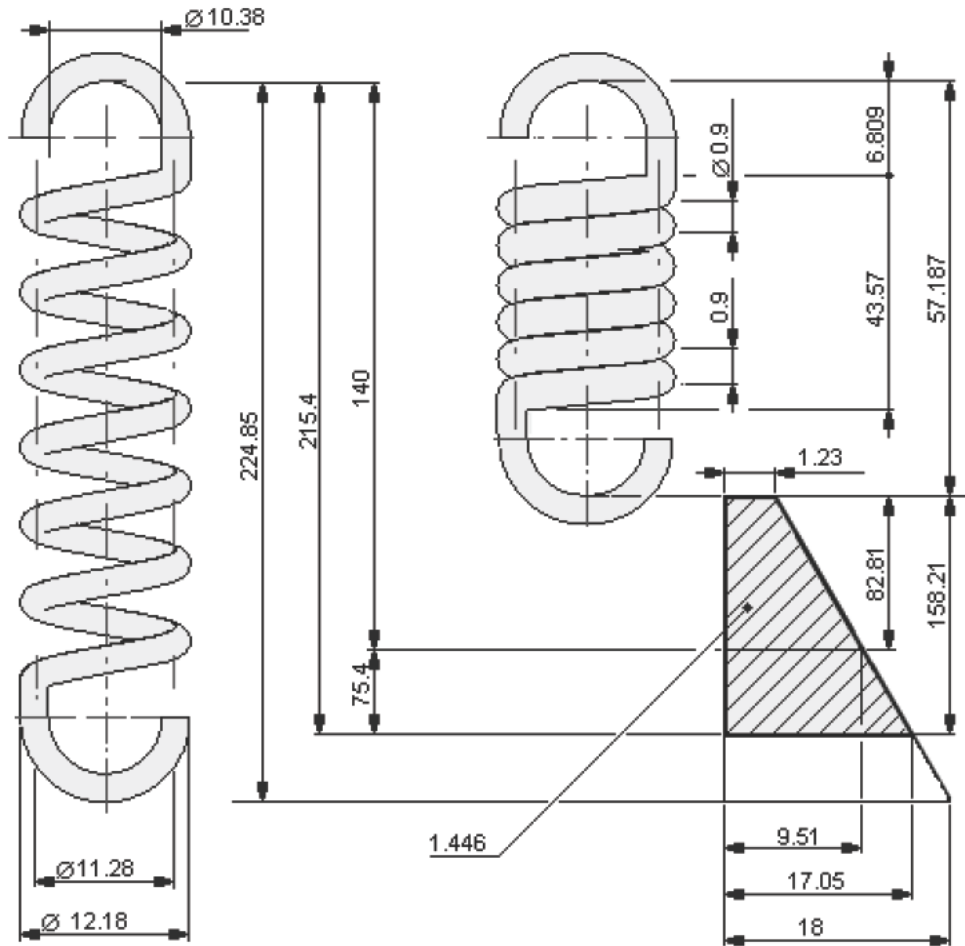


Figure C.1: Tension springs

APPENDIX C: Spring Design

Table C.1: Tension spring calculation results

Spring Load		
Min. working force	9.51	N
Max. working force	17.05	N
Working force	12.81	N
Spring Dimensions		
Loose spring length	0.0572	m
Wire Diameter	0.0009	m
Outside diameter	0.0128	m
Mean diameter	0.01128	m
Inside diameter	0.0138	m
Spring index	12.53	
Spring coils		
Total no. of coils	46	
Coiling direction	right	
Spring Hook		
Spring hook height	0.00681	m
Hook height factor	0.656	
Assembly directions		
Preloaded spring length	0.14	m
Fully loaded spring length	0.215	m
Working stroke	0.0754	m
Working spring length	0.173	m
Spring Prestress		
Initial tension	1.23	N
Free state stress	53.94	Mpa
Spring Material		
	Music wire	
Calculation Results		
Wahl correction factor	1.114	
Spring constant	100	N/m
Length of coiled part	0.04357	m
Limit spring length	0.22486	m
Preloaded spring deflection	0.07971	m
Spring limit force	18	N
Preload stress	417.47	Mpa
Full load stress	748.46	Mpa
Natural frequency	55.4	Hz
Deformation energy	1.442	J
Spring mass	0.009	kg

APPENDIX D: DATA**D.1 Atlantic Ocean Data**

The wave height envelope and ITTC 1978 sea spectrum was determined using the data presented in table D.1.

Table D.1: Atlantic Ocean seaway data

Atlantic Ocean Data					
Sea State Number	Significant Wave Height (m)		Probability of sea state	Modal Wave Period (sec)	
	Range	Mean		Range	Mean
0-1	0 - 0.1	0.05	0.7		
2	0.1 - 0.5	0.3	6.8	3.3 - 12.8	7.5
3	0.5 - 1.25	0.88	23.7	5 - 14.8	7.5
4	1.25 - 2.5	1.88	27.8	6.1 - 15.2	8.8
5	2.5 - 4	3.25	20.64	8.3 - 15.5	9.7
6	4.1 - 6	5	13.15	9.8 - 16.2	12.4
7		7.5	6.05	11.8 - 18.5	15
8		11.5	1.11	14.2 - 18.6	16.4

